Theses and Dissertations   1. Thesis and Dissertation Collection, all items

1975-03

Velocity measurements in a transonic compressor using a calibrated pressure probe.

Anderson, Dennis Jay

Monterey, California. Naval Postgraduate School

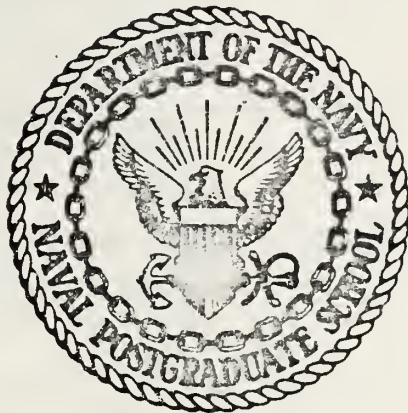https://hdl.handle.net/10945/21116

VELOCITY MEASUREMENTS IN A TRANSONIC COMPRESSOR USING A CALIBRATED PRESSURE PROBE

Dennis Jay Anderson

NAVAL POSTGRADUATE SCHOOL
Monterey, California

THESIS

Velocity Measurements in a Transonic
Compressor Using a Calibrated Pressure
Probe

by

Dennis Jay Anderson

Thesis Advisor   R. P. Shreeve

T166570

REPORT DOCUMENTATION PAGE		READ INSTRUCTIONS BEFORE COMPLETING FORM
1. REPORT NUMBER	**2. GOVT ACCESSION NO.**	**3. RECIPIENT'S CATALOG NUMBER**
4. TITLE (and Subtitle) Velocity Measurements in a Transonic Compressor Using a Calibrated Pressure Probe		**5. TYPE OF REPORT & PERIOD COVERED** Master's Thesis: March 1975
		6. PERFORMING ORG. REPORT NUMBER
7. AUTHOR(s) Dennis Jay Anderson		**8. CONTRACT OR GRANT NUMBER(s)**
9. PERFORMING ORGANIZATION NAME AND ADDRESS Naval Postgraduate School Monterey, California 93940		**10. PROGRAM ELEMENT, PROJECT, TASK AREA & WORK UNIT NUMBERS**
11. CONTROLLING OFFICE NAME AND ADDRESS Naval Postgraduate School Monterey, California 93940		**12. REPORT DATE** March 1975
		13. NUMBER OF PAGES
14. MONITORING AGENCY NAME & ADDRESS(if different from Controlling Office) Naval Postgraduate School Monterey, California 93940		**15. SECURITY CLASS. (of this report)** Unclassified
		15a. DECLASSIFICATION/DOWNGRADING SCHEDULE

16. DISTRIBUTION STATEMENT (of this Report)

Approved for public release: distribution unlimited.

17. DISTRIBUTION STATEMENT (of the abstract entered in Block 20, if different from Report)

18. SUPPLEMENTARY NOTES

19. KEY WORDS (Continue on reverse side if necessary and identify by block number)

Pressure probe calibration
Transonic compressor
Velocity and angle distribution ·
Rotor inlet and exit

20. ABSTRACT (Continue on reverse side if necessary and identify by block number)

The application is reported of a United Sensor Corporation 5-hole pressure probe to determine the flow field upstream and downstream of the rotor of a transonic compressor operating to near sonic speeds. Calibration of the probe was reduced to a set of equations to allow off-line data reduction and presentation using a Hewlett-Packard Model 9830A Calculator system. The flow velocities and angles measured upstream of the rotor were

compared with results of compressible flow calculations.
Blockage factors were determined which related analytical
approximations of the flow incident at the rotor to the
measured flow rate. The measurements downstream of the rotor
were compared with those of a second probe of different design.
Both probes required corrections to their calibrations which
were established in an axial annular flow of similar geometric
cross section. It is shown that the results derived from the
corrected calibration of the 5-hole probe were the more accur-
ate.

Velocity Measurements in a Transonic
Compressor Using a Calibrated Pressure Probe

by

Dennis Jay Anderson
Lieutenant, United States Navy
B.S., Purdue University, 1968

Submitted in partial fulfillment of the
requirements for the degree of

MASTER OF SCIENCE IN AERONAUTICAL ENGINEERING

from the

NAVAL POSTGRADUATE SCHOOL
March 1975

ABSTRACT

The application is reported of a United Sensor Corporation 5-hole pressure probe to determine the flow field upstream and downstream of the rotor of a transonic compressor operating to near sonic speeds. Calibration of the probe was reduced to a set of equations to allow off-line data reduction and presentation using a Hewlett-Packard Model 9830A Calculator system. The flow velocities and angles measured upstream of the rotor were compared with results of compressible flow calculations. Blockage factors were determined which related analytical approximations of the flow incident at the rotor to the measured flow rate. The measurements downstream of the rotor were compared with those of a second probe of different design. Both probes required corrections to their calibrations which were established in an axial annular flow of similar geometric cross section. It is shown that the results derived from the corrected calibration of the 5-hole probe were the more accurate.

ACKNOWLEDGEMENT

TABLE OF CONTENTS

LIST OF TABLES

ILLUSTRATIONS

ILLUSTRATIONS

TABLE OF SYMBOLS

Latin

c_p	Constant pressure specific heat	$(BTU/lbm\text{-}^{O}R)$
F_{ϕ}	5-hole probe calibration factor	(-)
$F_{\phi}^{'}$	5-hole probe calibration function	(-)
F_{θ}	5-hole probe calibration factor	(-)
$F_{\theta}^{'}$	5-hole probe calibration function	(-)
$F_{\lambda}^{'}$	5-hole probe calibration function$(F_{\phi}^{'}/F_{\theta}^{'})$	(-)
H	Normalized distance (y/h)	(-)
h	Distance from hub to outer wall	(in)
K	Constant	(-)
$\overline{K}_{\phi}$	Pitch angle correction constant	(-)
$\overline{K}_{x}$	Velocity correction constant	(-)
M	Mach number	(-)
p	Pressure	$(lbf/in.^{2})$
p_1	Pressure port 1	$(in.H_2O)$
p_2	Pressure port 2	$(in.H_2O)$
p_3	Pressure port 3	$(in.H_2O)$
p_4	Pressure port 4	$(in.H_2O)$
p_5	Pressure port 5	$(in.H_2O)$
p_{23}	Average of pressure ports 2 and 3	$(in.H_2O)$
r	Distance from compressor centerline	(in.)
R	Normalized distance (r/r_o)	(-)
R_G	Gas constant	$(ft\text{-}lbf/lbm\text{-}^{O}R)$
V	Velocity	(ft/sec)
$\dot{w}$	Mass flow rate	(lbm/sec)
$\overline{W}$	$\dot{w}/\rho_t V_t \pi r_o^2$	(-)

| X | Non-dimensional velocity (V/V_t) | (-) |
| y | Distance from hub | (in.) |

Greek

Δ	Finite difference	(-)
ε	Convergence limit for iteration	(-)
γ	Ratio of specific heats	(-)
λ	Flow pitch angle	(rad.)
ϕ	Flow pitch angle	(deg.)
Φ	Flow function	
$\bar{\Phi}$	Normalized flow function (Φ/Φ_o)	(-)
ρ	Density	(lbm/ft^3)
ξ	Ratio of total non-dimensional flow rate	(-)
	to flow function at the compressor outer wall	

Subscripts

B	Blockage
i	The ith value
j	The jth value
m	Measured
o	Outer wall
r	Reference
s	Static
t	Total (or stagnation)
1	Station 1 (rotor inlet)

14

I.   INTRODUCTION

The study reported here is an initial part of a program
to obtain a full understanding of the flow within a tran-
sonic compressor stage, with the ultimate object of obtaining
improved designs. Toward this goal, a transonic compressor
of the "impulse" type was designed and built by Dr. M.H.
Vavra in the Turbopropulsion Laboratories at the Naval
Postgraduate School. The work was sponsored by Naval Air
Systems Command, Code 310 through the office of Mr. H.J.
Mueller. The so-called TRANSX compressor has been operated
to 65% of design speed.

The inlet of the TRANSX compressor is designed to con-
tract and to rapidly accelerate the flow in order to gener-
ate near uniform conditions. with thin boundary layers, at
the rotor face. It is necessary to determine the radial dis-
tributions of the flow velocity and angle in order to estab-
lish the operating condition and to evaluate the performance
of the rotor blading. At or near design speeds, the possibil-
ity that wakes in the flow might induce vibrations in the
highly stressed rotor blades, prohibits the use of probes
just upstream of the rotor. Therefore it is necessary to be
able to predict velocity and pitch angle distributions at
high speeds from data gathered at lower speeds. Reference 1
gives analytical approximations of the rotor face flow velo-
city and angle distributions which were obtained from com-
pressible flow calculations. The first goal of the present
study was to determine the flow into the rotor by measurement,
and to compare the results with the analytical predictions.

15

A United Sensor 5-hole cylindrical pressure probe was selec-
ted for its ability to measure pitch angle and for ease of
mounting. The probe calibration was first established in a
uniform jet. Following a description of the TRANSX compress-
or in Section II, the investigation upstream of the rotor is
described in Section III of this report.

Measurement of the flow downstream of the rotor is
necessary in order to establish blade element performance.
The calibrated United Sensor 5-hole probe and a NASA combin-
ation probe [Ref. 2] were used simultaneously to conduct
radial surveys of the flow downstream of the rotor. In this
manner redundant measurements of Mach number and flow angle
were obtained using two completely independent probes and
their respective calibrations. It was found that the Mach
numbers evaluated by the two probes disagreed by as much as
10% when the calibrations, established in the uniform jet,
were applied to the probe measurements made downstream of
the rotor. Methods were devised for correcting the calibra-
tions established in the uniform jet for application of the
probes in the smaller compressor annulus. Following the
application of corrections, which were greatest for the NASA
probe, the disagreement in Mach number profiles was greatly
reduced; in some cases to less than 1%. The measurements
carried out downstream of the rotor using the 5-hole probe
are described in Section IV.

The calibration of the 5-hole probe and the method de-
vised for correcting the calibration for application in the
compressor annulus are described fully in Appendix A.

Inter-related non-linear calibration relations are therein represented by analytic functions which allow computer reduction of probe survey measurements. The methods described in Appendix A can be adapted to other probes and to measurements with the same probe in passages of different geometry.

II.   THE TRANSONIC COMPRESSOR

A.   DESCRIPTION

A schematic of the compressor test rig is shown in Fig. 1. The test rig consists of an air-turbine drive unit and an induction section containing a filter, a throttle, a settling chamber and a flow measuring nozzle. The air turbine is designed to deliver 450 H.P. at 30,000 RPM. The transonic compressor is designed to operate at 30,460 RPM with a relative tip Mach number of 1.5. The compressor flow rate is controlled by a rotating throttle plate [Fig. 1]. The test rig, located in an explosion proof cell, is controlled by an operator at a remote console. A complete description of the laboratory facilities are given in Ref. 3, and the details of the test rig design is given in Ref. 4. Figure 2 shows the compressor assembly and identifies the instrumentation stations 0 through 3 referred to in the following discussion. As indicated in view J of Fig. 2, peripheral surveys were made by rotating the outer casing.

B.   INSTRUMENTATION

The transonic compressor is equipped with stationary probes to provide routine performance data. The measurement of torque was not available at any time during this

investigation, since the honeycomb flow straightener (Fig. 3) was removed to allow higher flow rates. The fixed instrumentation is not discussed in this report.

The results presented here were obtained using a United Sensor DA-125 three dimensional pressure probe. The probe calibration is reported in detail in Appendix A. The probe mounting arrangement is shown in Fig. 3. Radial surveys were taken at a fixed peripheral angle by manually positioning the probe using a traverse unit. Peripheral surveys were made by manually rotating the outer casing, causing the probe to move through an arc at a fixed radius. All pressures were measured by a calibrated transducer in a scanivalve arrangement. Predetermined angular and radial positions were input into the data logging system on thumb wheels.

C. DATA ACQUISITION AND REDUCTION

A data logging system [Ref. 3] was used to scan and record pressure, temperature and position data. The recorded output was on punched paper tape. Reduction of data was carried out using a Hewlett-Packard Model 9830A Calculator system, shown schematically in Fig. 4.

A program, designated TCR Reduction (Station 1), was written to reduce data from rotor inlet flow measurements. Data were input from the punched tapes. The program calculated and printed the non-dimensional radial probe position, compressor case angle, flow pitch and yaw angles, non-dimensional velocity, velocity and Mach number. These results

18

were stored on digital magnetic tape and the radial distri-
butions were graphed using the X-Y plotter (Fig. 4).

A program entitled TCR Reduction (Station 2) was
written to calculate the flow downstream of the rotor from
probe measurements. The program accepted data from magnetic
tape, rather than punched paper tape. The paper tape data
were therefore transferred to magnetic tape before beginning
data reduction. This procedure was selected because data
from two different probes were required to be in the same
form to allow distribution plots to be made on a common
graph. When data had been reduced, the calculated results
were stored on magnetic tape and the radial profiles were
produced on the X-Y plotter.

III. FLOW INTO THE ROTOR

A. DESCRIPTION OF TESTS

The purpose of these surveys was to measure the flow
properties at the rotor inlet and to compare the results
with analytical distributions reported in Ref. 1. Prelimin-
ary impact pressure surveys were made prior to this investi-
gation, and as a result, a bellmouth inlet fairing was added
(Fig. 2) to improve inlet profiles.

The 5-hole probe was positioned ahead of the rotor at
station 1. The flow profiles were measured in two separate
runs (numbered 33 and 39). All surveys were radial, from
hub-to-tip. The speed was set at 50% of design speed in run
33, and varied from 65% to 40% of design speed in run 39.

Throttle settings corresponded to fully open, near surge, or design point for each speed of a given survey. The case angle, or peripheral location of the probe, was not considered to be significant for measurements at this station.

The surveys began with the sensing holes 0.27 inch from the rotor hub. The probe was then withdrawn in 0.1 inch intervals until the total pressure sensing port was flush with the inner surface of the casing. At each point, pressure, temperature and position data were recorded on punched tape. These data were reduced to velocities, angles and non-dimensional position.

B. RESULTS

Radial distributions of the pitch angle and Mach number derived from probe measurements are shown in Fig. 5 to Fig. 11. The measured data were reduced using the probe calibration described in Appendix A, section A2. The radial distribution of pitch angle, derived in Ref. 1, is also shown on the plots. The data were taken in two separate tests. Results from run 33 in Figs. 5-7 show good agreement with the derived profile except at the upper and lower 20% of the distribution. Note the wall effect on pitch angles for radial positions greater than R=0.85. Within the measurement accuracy, distribution of pitch angle is independent of flow rate for all surveys taken in a given test. The results of run 39 (Figs. 9-12) show an overall reduced level of pitch angle, but also shows no dependence upon throttle position or speed. The reason for the reduced levels is not known and should first be confirmed by further measurements.

In order to plot the analytical Mach number distribution as a comparison with the measurements plotted in Fig. 5 to Fig. 11, the area blockage factor must first be determined. Therefore the measured distribution of the mass flux compared with the analytical distribution was chosen to represent the same information, and is presented in the following section.

The calibration correction for application in the compressor annulus does not apply to measurements at the rotor inlet. However, this correction was applied to the profile in Fig. 6, and the results displayed in Fig. 8. The correction applied near the outer wall causes the profile to better match the analytical distribution at the wall. Since the wall angle at the inlet is the same as that in the calibration annulus, the effect brought about by applying the correction supports its validity for this region.

C. DETERMINATION OF BLOCKAGE FACTOR

Details of blockage factor calculations are given in Appendix B. Reference 1 determined a viscous blockage factor, K_{B_1} =0.989, which accounted for wall boundary layer displacement thickness. Figures 13 and 14 show distributions of the non-dimensional mass flux, or flow function obtained from probe measurements and a comparison with the analytical distribution given in Ref. 1 and Appendix B. It is shown in Appendix B that by equating the integral of the measured mass flux, over the region for which the probe measurements are free of wall effects, to the integral of the analytical mass

flux distribution, a blockage factor can be defined. The blockage factors listed in Figures 13 and 14 were obtained in this manner and the analytical distributions are consistent with these values.

The prediction that the mass flux increases with increasing radius is supported by the measurements, but the measured variation is larger than anticipated. This could be the result of the inlet bellmouth velocity profile which has yet to be measured.

The mass flux profiles are quite similar in shape, but considerable variation occurs in the blockage factors deduced from the measurements (.963 to .984). This is possibly due to the measurement of the total mass flow rate, which was observed to vary during the surveys. As shown in Appendix B, an attempt was made to eliminate this effect; however insufficient data was taken to make the process statistically accurate. It is observed that the smallest blockage factors were obtained at the lowest flow rates, for which the measurements are least accurate. However, it is also noted that at highly reduced throttle settings, greater distortion appears in the profiles near the rotor tip, suggesting that an increase in blockage does indeed occur. This question may be resolved by collecting more data with the objective of determining how blockage varies with RPM and throttling conditions.

Figures 15 and 16 show calculated flow distributions into the rotor using the method of Ref. 1 with a blockage factor of 0.98. Note, in Fig. 15, that choking of the inlet

occurs at slightly greater than 21 lb/sec. As blockage in-creases (decreasing effective cross sectional inlet area) choking occurs at lower flow rates. Figure 16 shows that the rotor blade relative Mach number is subsonic everywhere at the speeds encountered thus far. At design speed (30,460 RPM) 80% of the blading will see supersonic relative veloci-ties, assuming a blockage factor of approximately 0.98.

IV. FLOW DOWNSTREAM OF THE ROTOR

A. DESCRIPTION OF TESTS

The United Sensor probe and a NASA combination probe [Ref. 2] were mounted at station 2, separated peripherally by a 45° angle. There was a 1.5^o difference in the position of each probe with respect to a stator blade leading edge. Peripheral surveys were plotted such that peripheral angle displacement of each probe was measured with a stator blade leading edge as reference. During radial surveys the two probes were moved outwards and data from both were taken simultaneously.

Three separate runs, numbered 43, 44 and 45 are re-ported. The tests consisted of one radial survey and one peripheral survey at the passage centerline for each of the three runs. Runs 43 and 44 were conducted at the same RPM, but at different throttle settings. Runs 44 and 45 were con-ducted at the same throttle setting, but at different speeds.

The purpose of these surveys was to verify measurements

through redundancy and to calculate rotor performance.
Agreement was obtained only after probe calibrations were
corrected, as described in Appendix A. The verification of
the measurements themselves is described in this section, and
the procedure for calibration, correction and application to
the 5-hole pressure probe is described in Appendix A. The
evaluation of rotor blade element performance will be re-
ported separately.

B. RESULTS

Figure 17 shows a comparison of Mach numbers for run 45,
point 3, evaluated from 5-hole and NASA probe measurements
using calibrations established in a uniform jet. Approxi-
mately 10% disagreement between the measured Mach numbers
was observed. Since neither the static pressure distribu-
tions calculated from the 5-hole probe calibration nor that
from the NASA probe calibration were consistent with the
measured compressor hub and tip wall pressures, the Mach
number distributions shown in Fig. 17 were not acceptable.
It had also been observed from surveys of the uniform jet,
described in Appendix A, that the probes indicated uniform
flow profiles over different regions of the flow. In parti-
cular, the NASA probe failed to indicate uniform conditions
until it was traversed radially more than 3 inches into the
flow. The effect of "immersion" or "wall effect" on the
calibration of the two probes was the probable cause of the
observed disagreement exhibited in Fig. 17. Since the magni-
tude of the immersion effect, in the uniform jet, was quite

different for each probe, the approach taken was to first
devise separate corrections to the calibrations of the two
probes. Agreement between the corrected survey measurements
with both probes, and consistency of the calculated static
pressure distributions with the measurements at the hub and
tip walls were sought. The corrections were based upon sur-
vey measurements made in an annular axial flow passage which
was similar in size to the compressor annulus downstream of
the rotor. The procedure for correcting the 5-hole probe
calibration is described in Section A3 of Appendix A.

The results shown in Fig. 18 to Fig. 29 were obtained
following the application of corrections to the measurements
of both probes. The upper sections of Figs. 18-23 show the
impact pressure (to the right) and indicated static press-
ure (dashed lines) measured by the probes. The solid lines
toward the left are the distributions of static pressure
evaluated from the probe measurements after the annulus
corrections were applied. The lower sections of Fig. 18 to
Fig. 23 compare Mach number and flow angles derived from the
probe measurements. Figures 24 to 29 show pitch angle dis-
tributions from the 5-hole probe measurements.

The results shown in Figs. 18 to 29 were from the three
tests mentioned above. Figures 18, 19 and 20 show radial
surveys at 50% of design speed and design incidence (deter-
mined from Fig. 15), 50% speed near surge and 65% speed near
design incidence, respectively. Figures 21, 22 and 23 show
peripheral surveys of the centerline of the channel at the

25

same test conditions. Figures 24 to 29 show the resulting
pitch angle distributions corresponding to tests shown in
Figs. 18 to 23.

C. DISCUSSION

   1. Radial Surveys

      The radial surveys are shown in Figs. 18 to 20. The
Mach number comparison between the two probes is in much
better agreement than the uncorrected results of Fig. 17.
The differences close to the hub are a result of the static
pressure, rather than total pressure measurements. It was
noted that corrected static pressure measurements for the
5-hole probe tended toward measured hub and tip wall press-
ures, whereas the NASA probe corrected static pressure tend-
ed to values that were too high. As an example, for the test
shown in Fig. 20, the measured hub and tip wall pressures
were -5.3 and 23.1 inches of water respectively. Therefore,
the Mach number calculated from the 5-hole probe measurements
is considered to be more accurate than that given by the NASA
probe.

      Yaw angle measurements of flow behind the rotor are in
agreement to better than one degree. The reason for the resi-
dual disagreement is not clear. It was noticed that the
largest and most consistent disagreement occurred at the
highest speed and flow rate (Fig. 20). In Fig. 21 the flow
angle at the rotor tip is large; corresponding to a low axial
velocity component. This suggests a stalled condition at the
rotor tips.

      Total pressure measurements do not agree as well as in

the steady flow in which the probes were calibrated (Appendix A). Leaks were thought to have been eliminated from the scanivalve and pressure transducer data system. There is a possibility that the total pressure differences were caused by the unsteady nature of the flow. This argument is supported by Fig. 19, corresponding to a near stall condition, for which additional unsteadiness might be expected. However, at the higher frequencies associated with the higher RPM in Fig. 20, the disagreement is greater. Such would not be the case if the increased differences were caused by the unsteady response of the probes.

2. Peripheral Surveys

Figures 21 to 23 show the results of peripheral surveys taken at the passage centerline, corresponding to test conditions shown in Figs. 18 to 20. In Figs. 21 and 23, the impact pressure difference is small and uniform with respect to angular position. (For these tests, profiles hub-to-tip, were also similar).At the near stall condition in Fig. 22, a variation in impact pressure with peripheral position is evident. The two measurements agree only over a small portion of a blade space.

The peripheral variation in corrected static pressure, as indicated by both probes, was quite pronounced. With the stagnation pressures being relatively constant, a variation in Mach number proportional to the probe static pressure differences was measured. Inspection of these figures leads to the conclusion that the stator blades were affecting the flow upstream. The minimum Mach number and flow angle

(Fig. 22) was measured in line with the leading edge of a stator blade, at a case angle of approximately 363°. That angle is consistent with the geometry of the flow into the stator. It is clear that peripheral variations in flow properties must be taken into account for specification of rotor performance from probe measurements at station 2. This is particularly true at reduced throttle settings, as in Fig. 22.

The distribution of static pressure from the NASA probe shown in Fig. 22 is similar in shape to those from both probes in Figs. 21 and 23. The more uniform distribution of the 5-hole probe static pressure is a marked departure from the distributions of Figs. 21 and 23. Since the probes were separated by 3 stator blade passages, it is possible that the stator passage downstream of the 5-hole probe contained a separation, or local stalled condition, whereas the passage downstream of the NASA probe was unaffected.

3. Pitch Angle Measurement

The pitch angle distributions measured downstream of the rotor are shown in Figs. 24 to 29 and correspond to the surveys of Figs. 18 to 23. The variation of pitch angle with radius was nearly linear at design throttle settings (Figs. 24 and 26). The pitch angle is indicated to be approximately -1° close to the outer wall, as might be expected due to boundary layer effects. These measurements, which rely upon the annulus corrections described in Appendix A, are remarkably consistent with the expected distribution. At the point where probe measurements were taken, the hub wall angle was

+12°. Extrapolation of the angle distribution to the wall, in Figs. 24 and 26, is consistent with this value. The results in Fig. 25, for the near surge condition, shows a region of nearly constant pitch angle near the inner wall and a tendency to increase rapidly toward the 12° hub wall angle. This is consistent with rake measurements of impact pressure taken at the stator exit, which indicated a region of separated flow at the hub wall. This would have the effect of creating a large pitch angle gradient near the hub. The larger region of negative pitch angle near the tip would be consistent with an increase in wall boundary layer thickness. This region also exhibits a large pitch angle gradient when compared to the center 50% of the distribution.

Peripheral variations in pitch angle, shown in Figs. 27 to 29 indicate little change at or near design conditions. However, near surge(Fig. 28) the flow angle increased on one side of the stator blade and decreased on the other side. Though it appears to be a significant effect, the variation is no more than one degree either side of the mean line and would not be significant in rotor performance calculations.

V. CONCLUSION

In this study a 5-hole pressure probe was used success-
fully to determine the distribution of velocity and flow
angle upstream of a compressor rotor. Blockage factors were
determined from measurements, which allow the use of analyti-
cal expressions to relate the measured flow rate to the in-
cident flow properties at the rotor.

The same probe was applied downstream of the rotor.
The measurements were compared to those of a NASA probe,
which did not provide a measurement of pitch angle. Part of
the differences in the Mach number distributions, seen near
the hub, was probably for this reason. The 5-hole probe
gave more accurate Mach number distributions mainly because
the static pressure corrections for passage effects were
smaller than those for the NASA probe.

The differences in the radial distributions of impact
pressure were partially the effect of the difference in the
location of the probes with respect to the nearest stator
blade leading edge. Although that difference was only 1.5^Q,
at decreased throttle settings the peripheral variations in
the indicated flow profiles became significant. In future
tests radial surveys should be conducted with both probes in
the flow simultaneously, at fixed speed and throttle setting;
then the probes should be interchanged and the surveys re-
peated without changing conditions. The resulting plots would
differ only as they are affected by the slight peripheral
displacement of the probes. Peripheral survey variations must

be accounted for if probe measurements at station 2 are to be used for derivation of rotor performance.

The effects of unsteady response on probe measurements should also be examined. It is reported that the average indicated total pressure in unsteady flow can be greater than the time average of the total pressure [Ref. 6]. This implies that two different probes in the same steady flow could measure identical total pressures, and when placed in unsteady flow might disagree as a function of speed and throttle setting. While using Reference 6, this effect was calculated to be small for the probes and conditions in the present study. The differences in the measurements suggest that this conclusion should be re-examined.

The correction devised to compensate for wall effect on the 5-hole probe pitch angle measurements was very effective judging from the plotted pitch angle distributions at station 2. The overall effect of correcting the 5-hole probe calibration for application to the specific flow geometry of the transonic compressor, points out the necessity of careful calibration of pressure probes used for making measurements of internal flows.
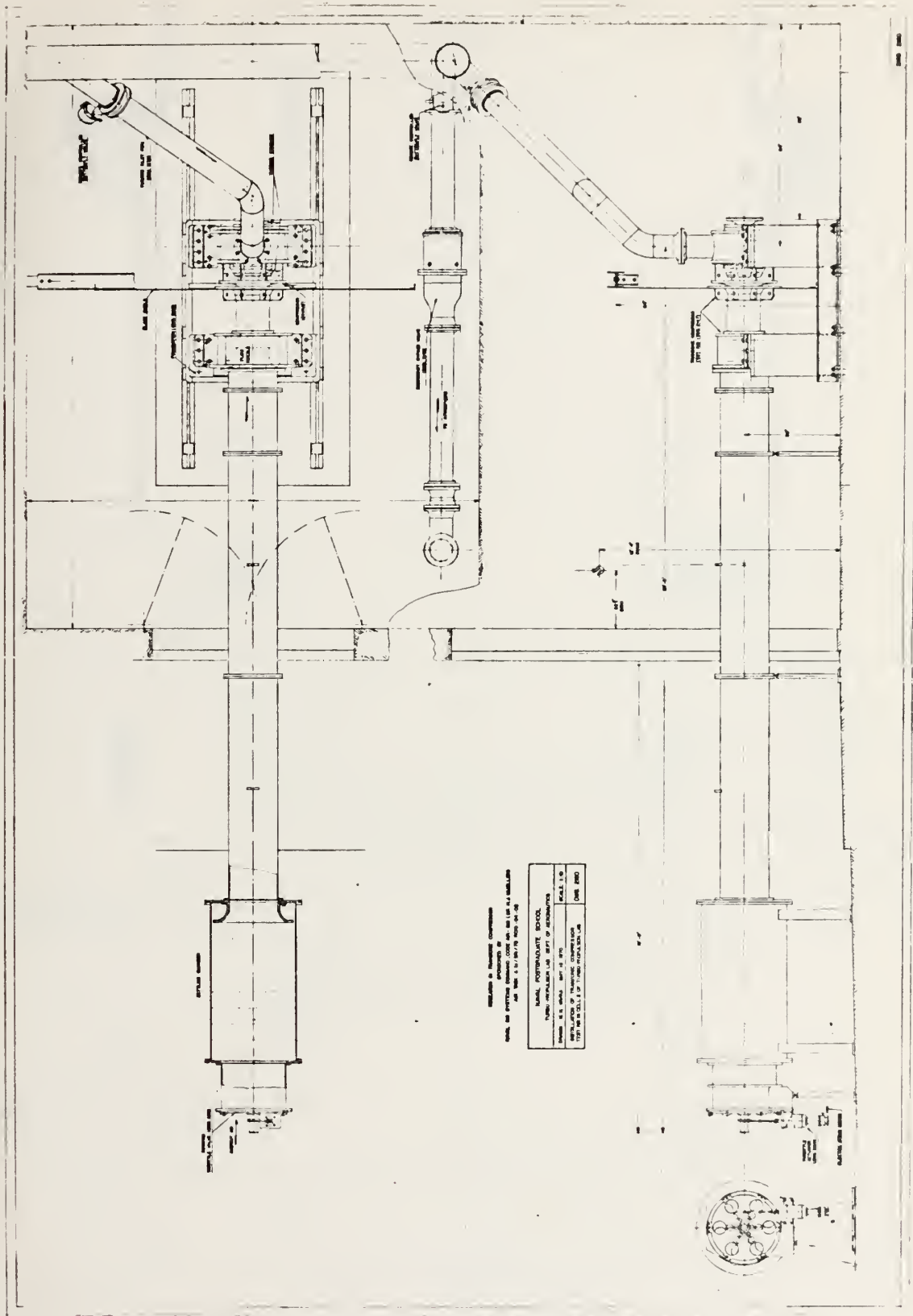
Figure 1. The Compressor Test Rig
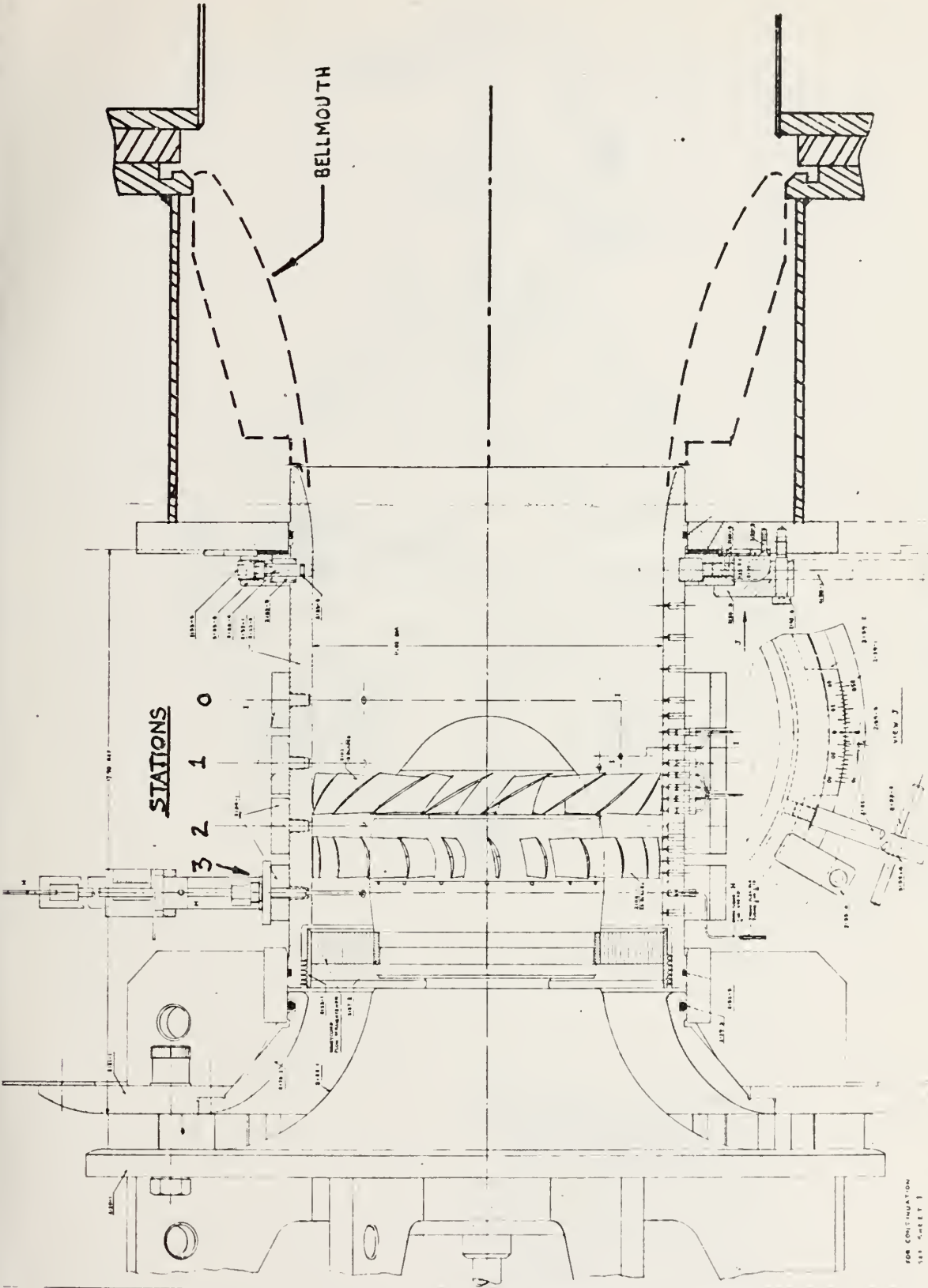
Figure 2. The Compressor Assembly
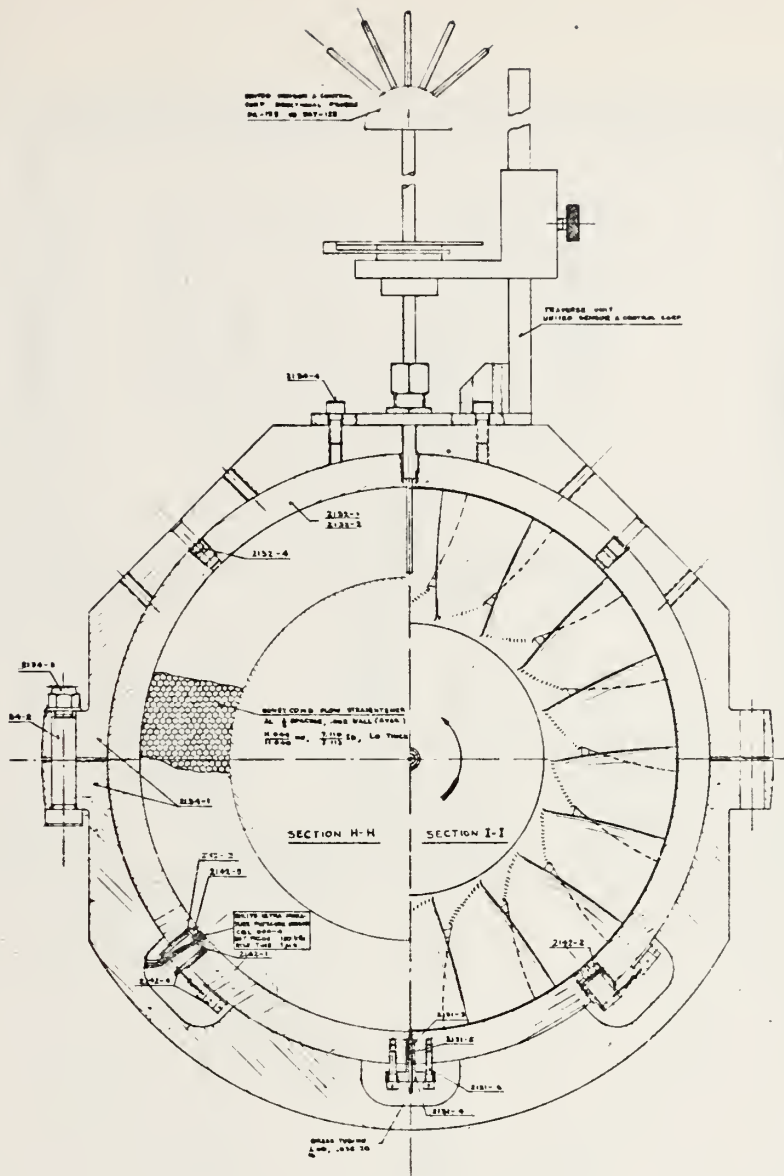
BELLMOUTH

STATIONS

3 2 1 0

33

NAVAL POSTGRADUATE SCHOOL		
DEPT OF AERONAUTICS, TURBO-PROPULSION LABORATORY		
DRAWN M H VAVRA, DEC 10, 1969	SCALE FULL	
ASSEMBLY OF TRANSONIC COMPRESSOR TEST RIG	DWG NO 2147-2	SHEET 2 of 2

Figure 3. End View of Compressor Assembly
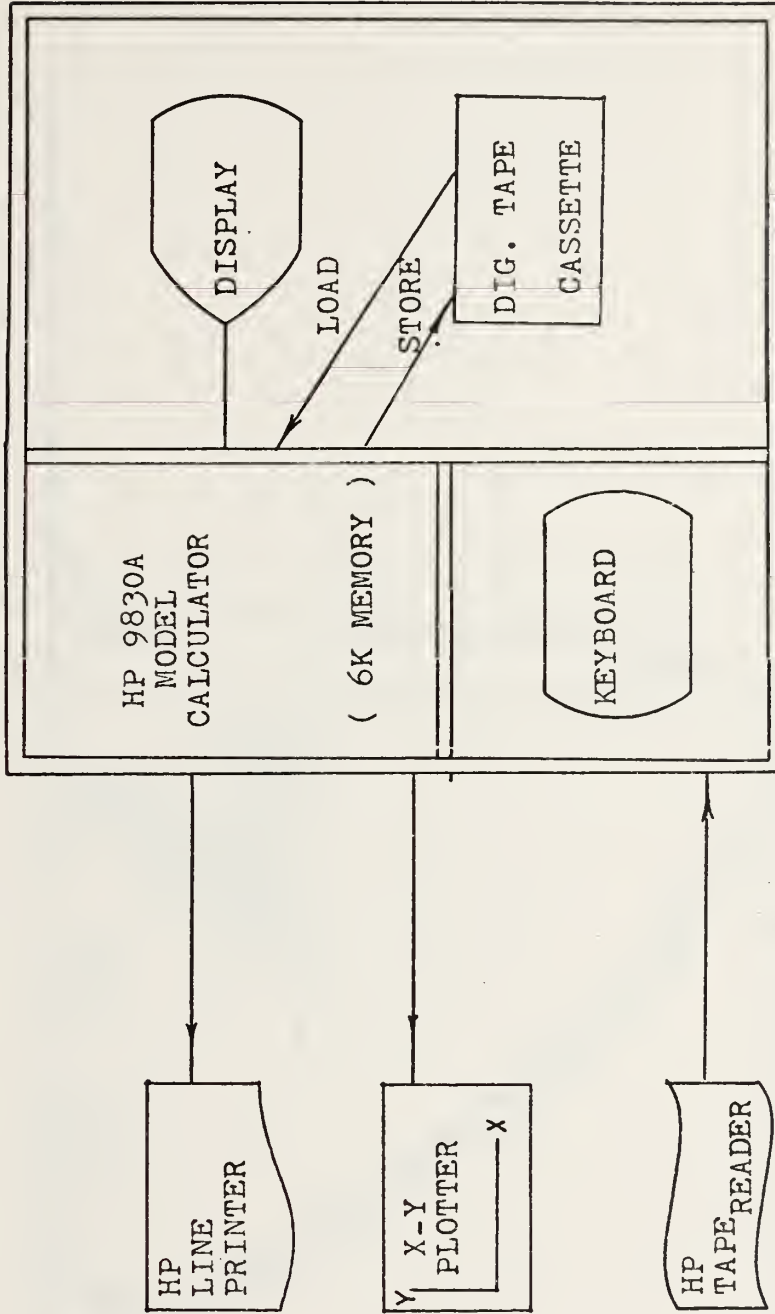
Figure 4. Schematic of the Hewlett-Packard
Model 9830A Calculator System
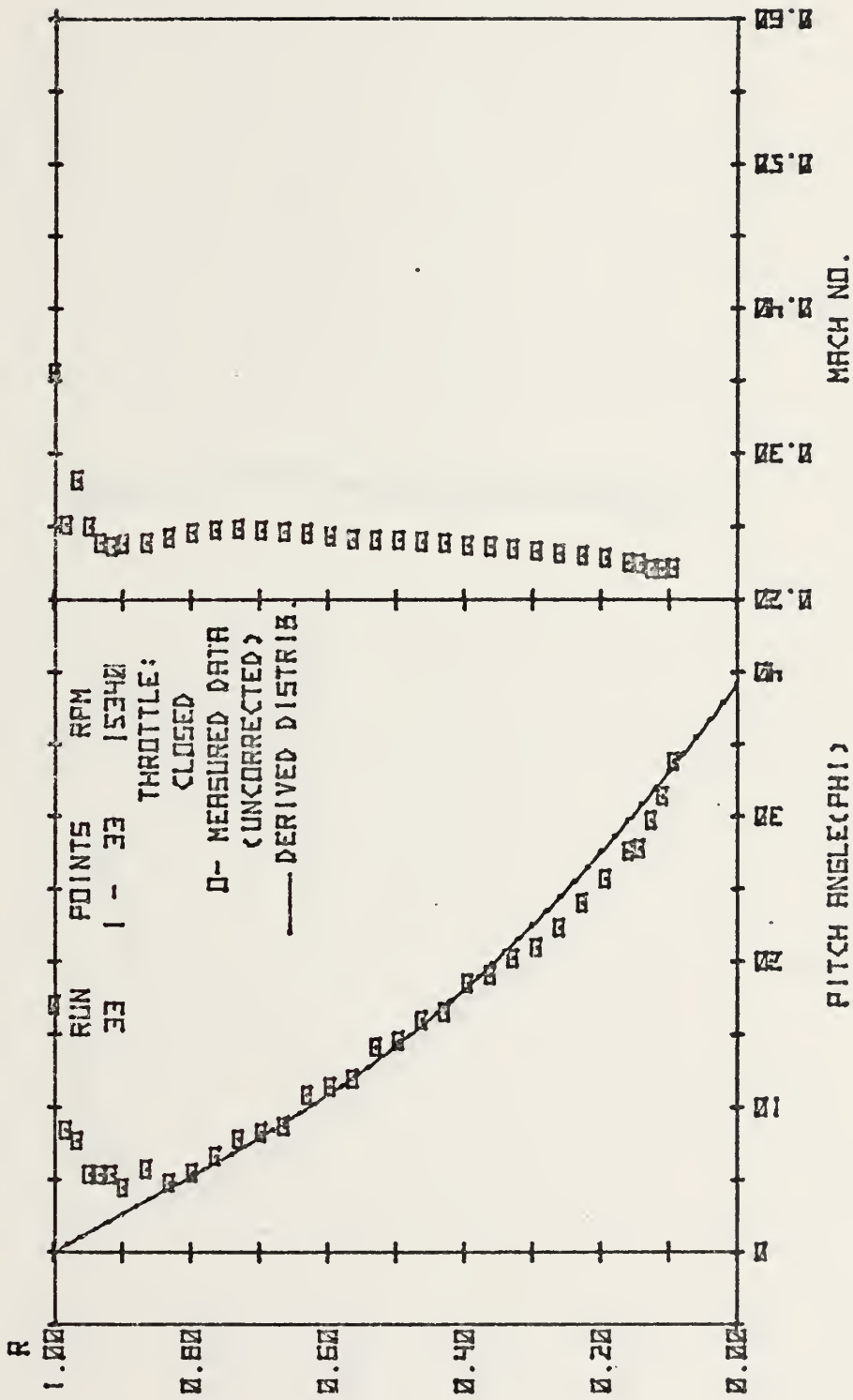
FIGURE 5. PITCH ANGLE AND MACH NO. DISTRIBUTION AT STATION 1.
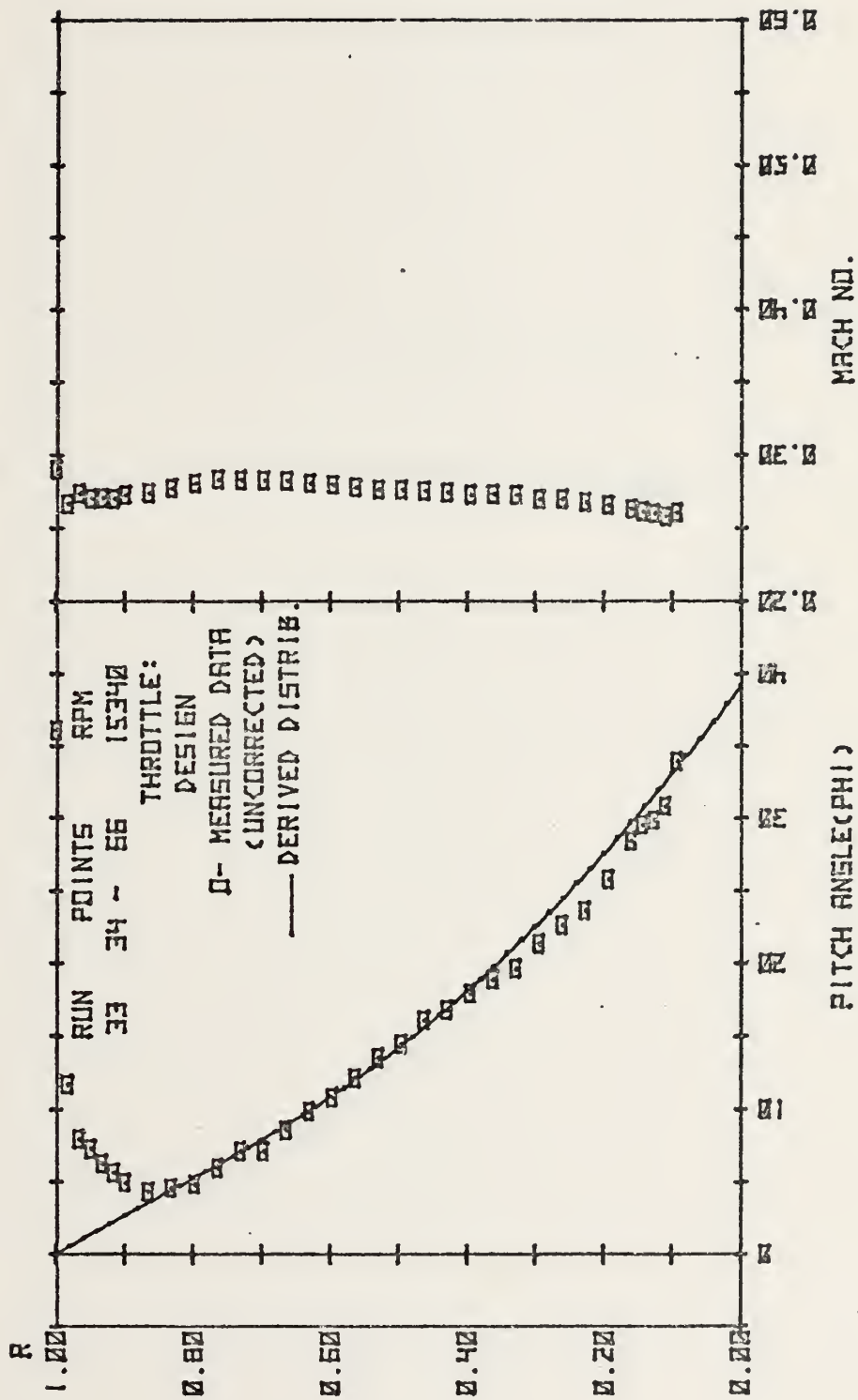
FIGURE 6. PITCH ANGLE AND MACH NO. DISTRIBUTION AT STATION 1.
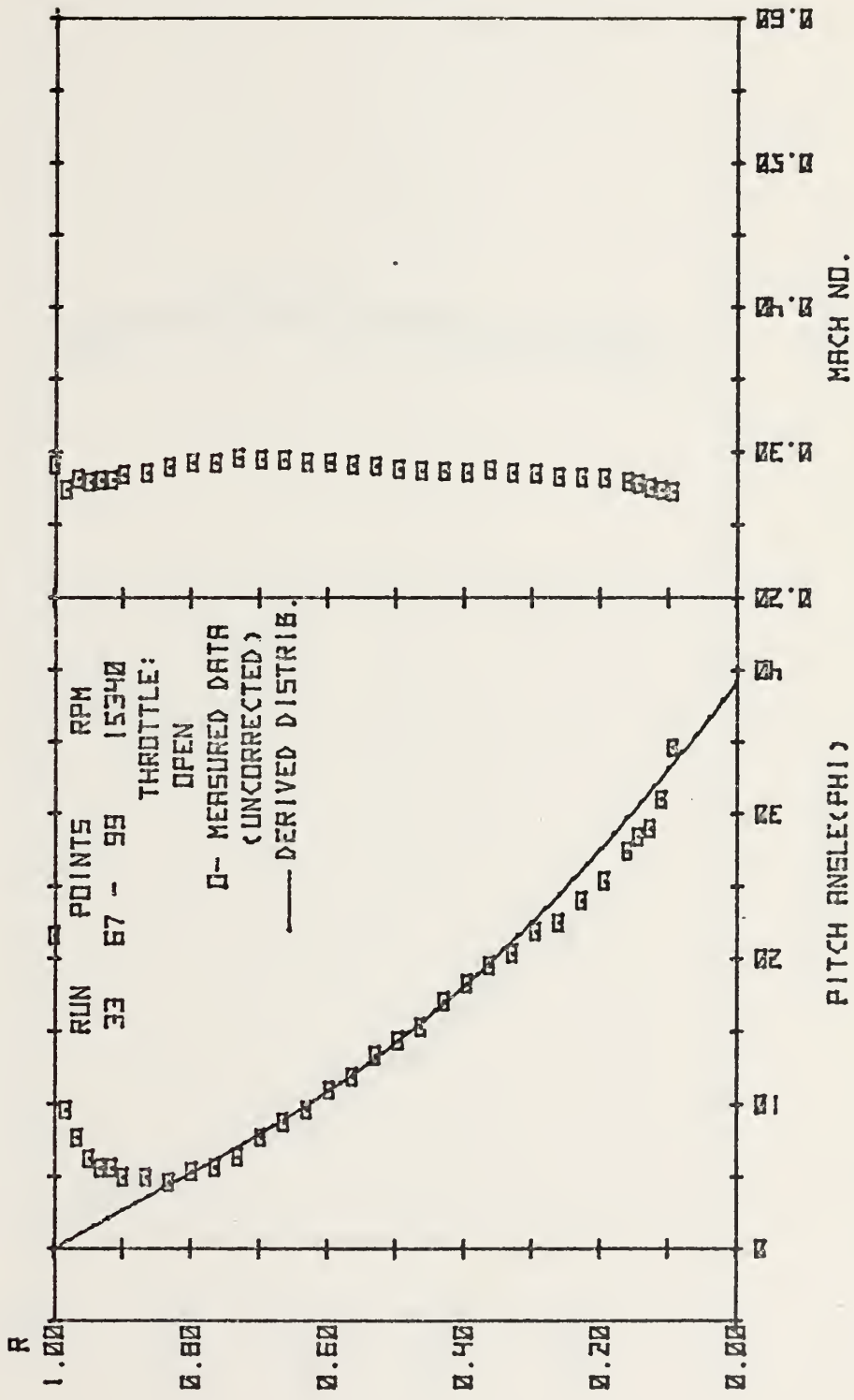
FIGURE 7. PITCH ANGLE AND MACH NO. DISTRIBUTION AT STATION 1.
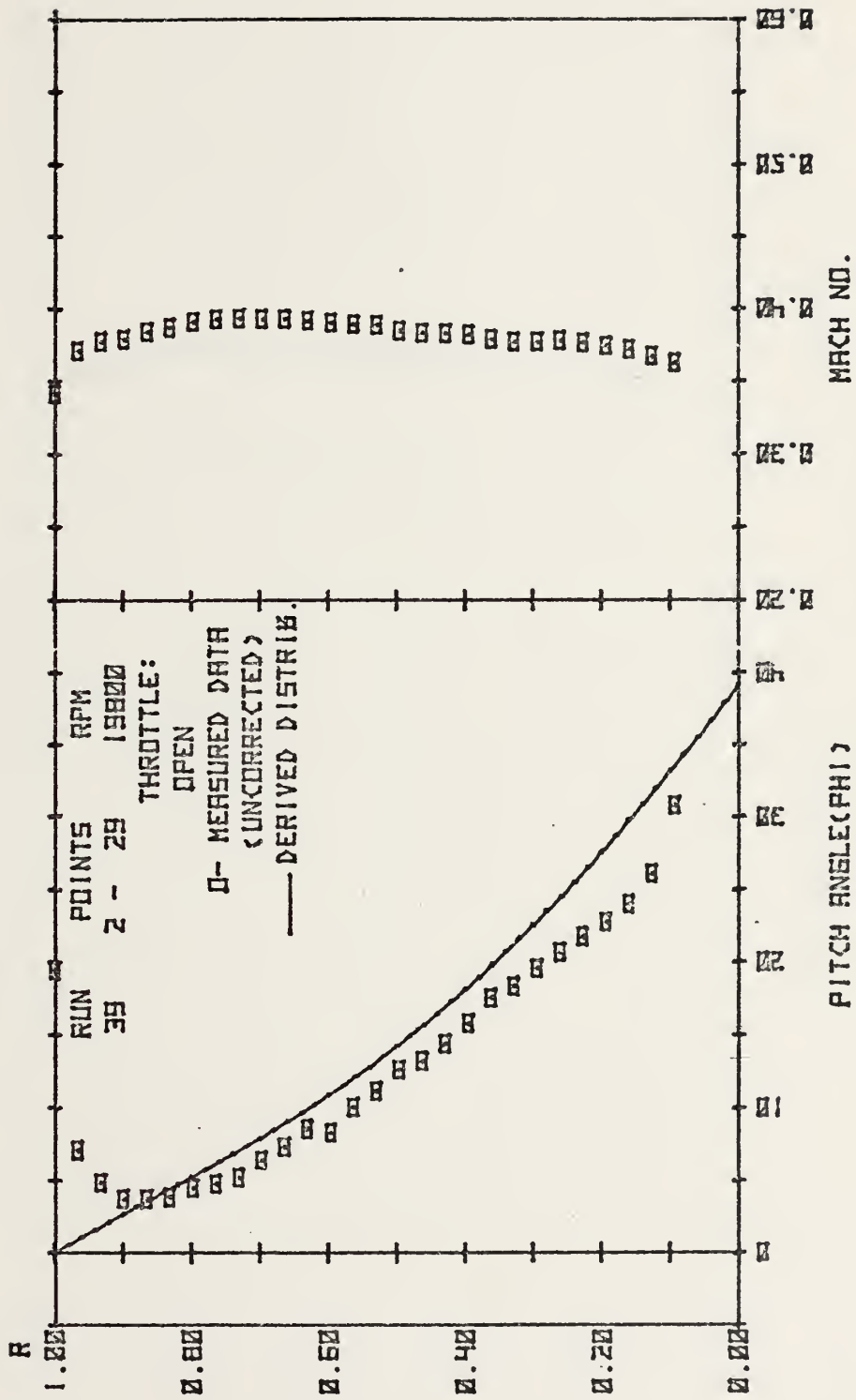
FIGURE 8. PITCH ANGLE AND MACH NO. DISTRIBUTION AT STATION 1.
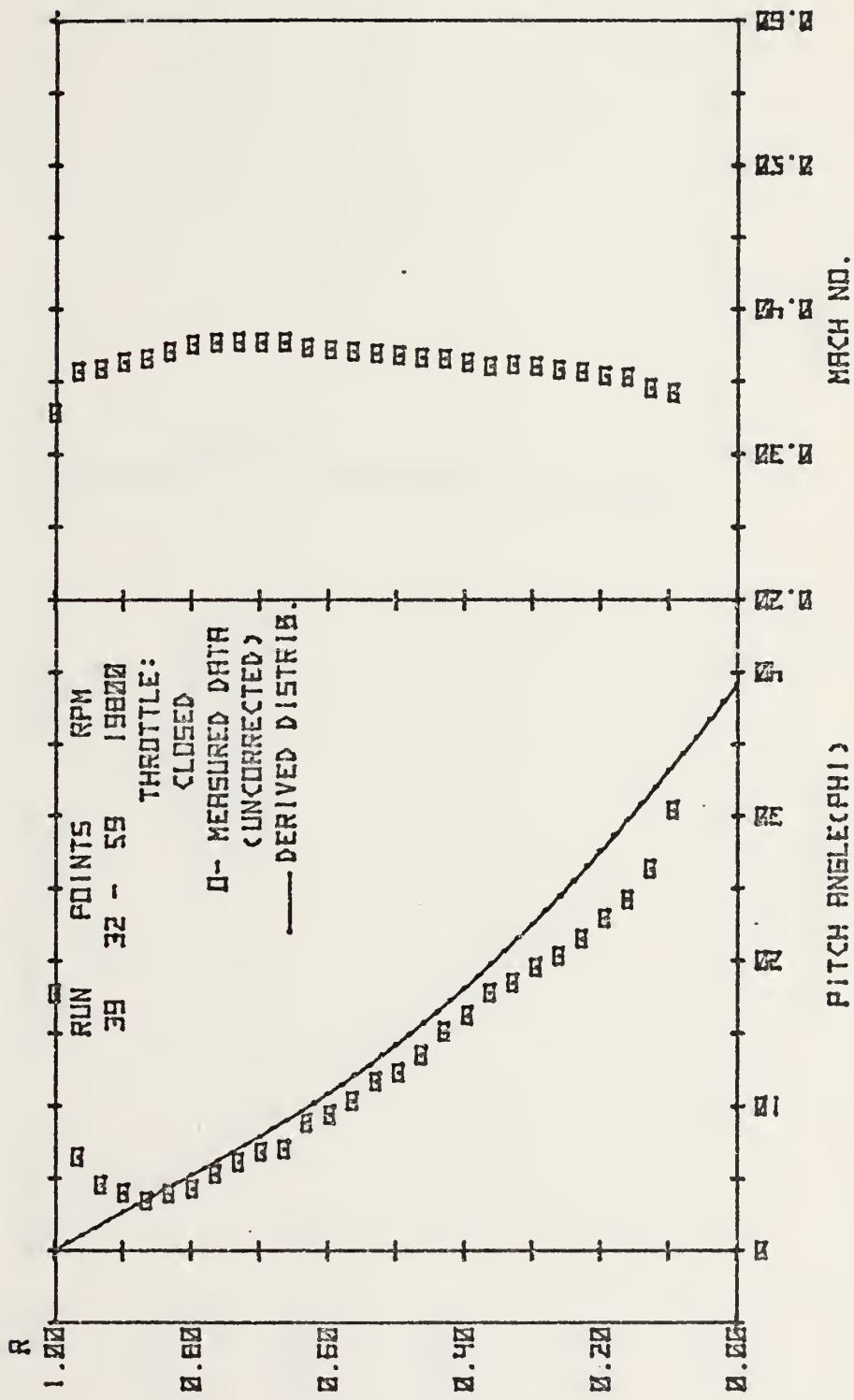
FIGURE 9. PITCH ANGLE AND MACH NO. DISTRIBUTION AT STATION 1.
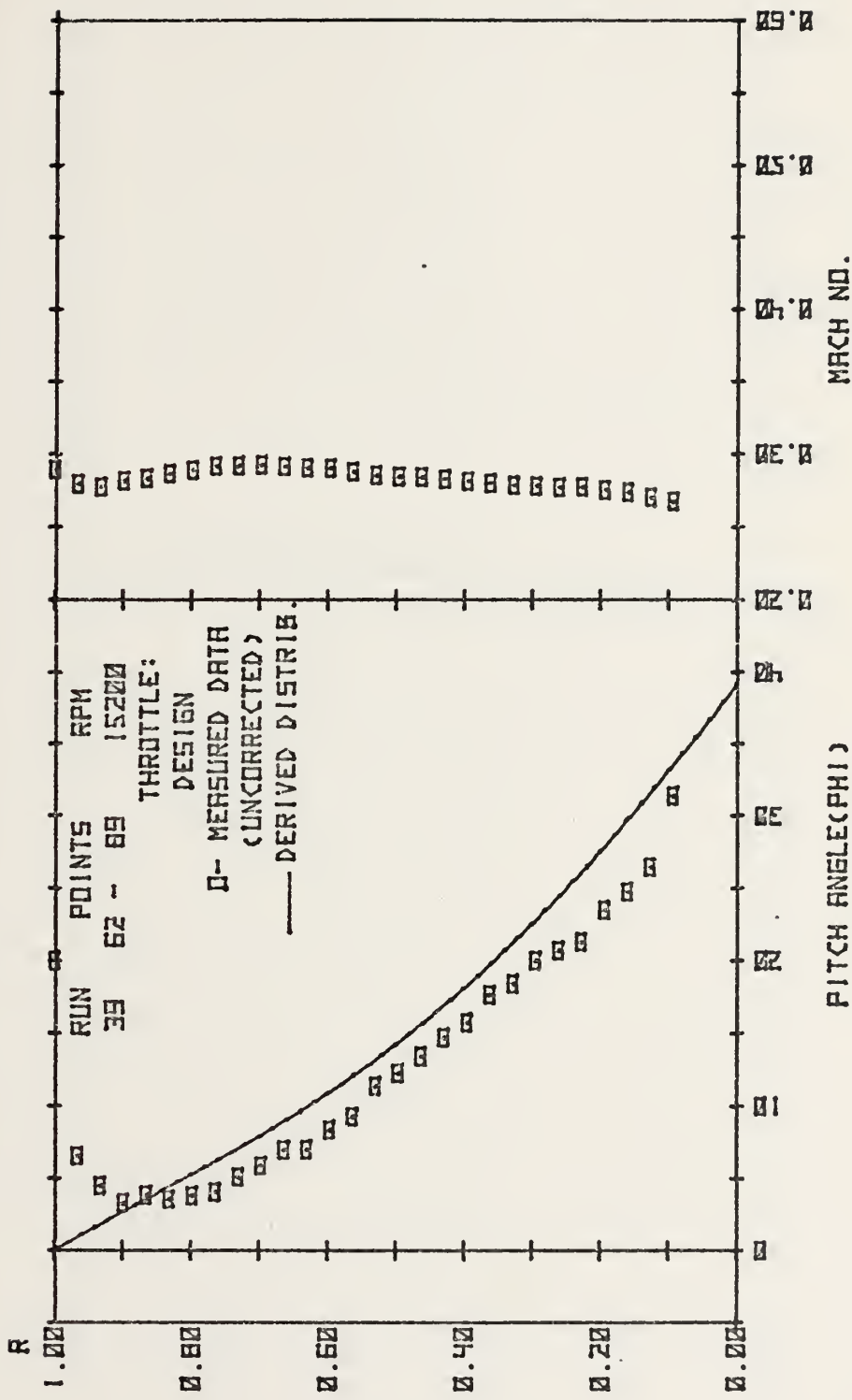
FIGURE 10.PITCH ANGLE AND MACH NO. DISTRIBUTION AT STATION 1.
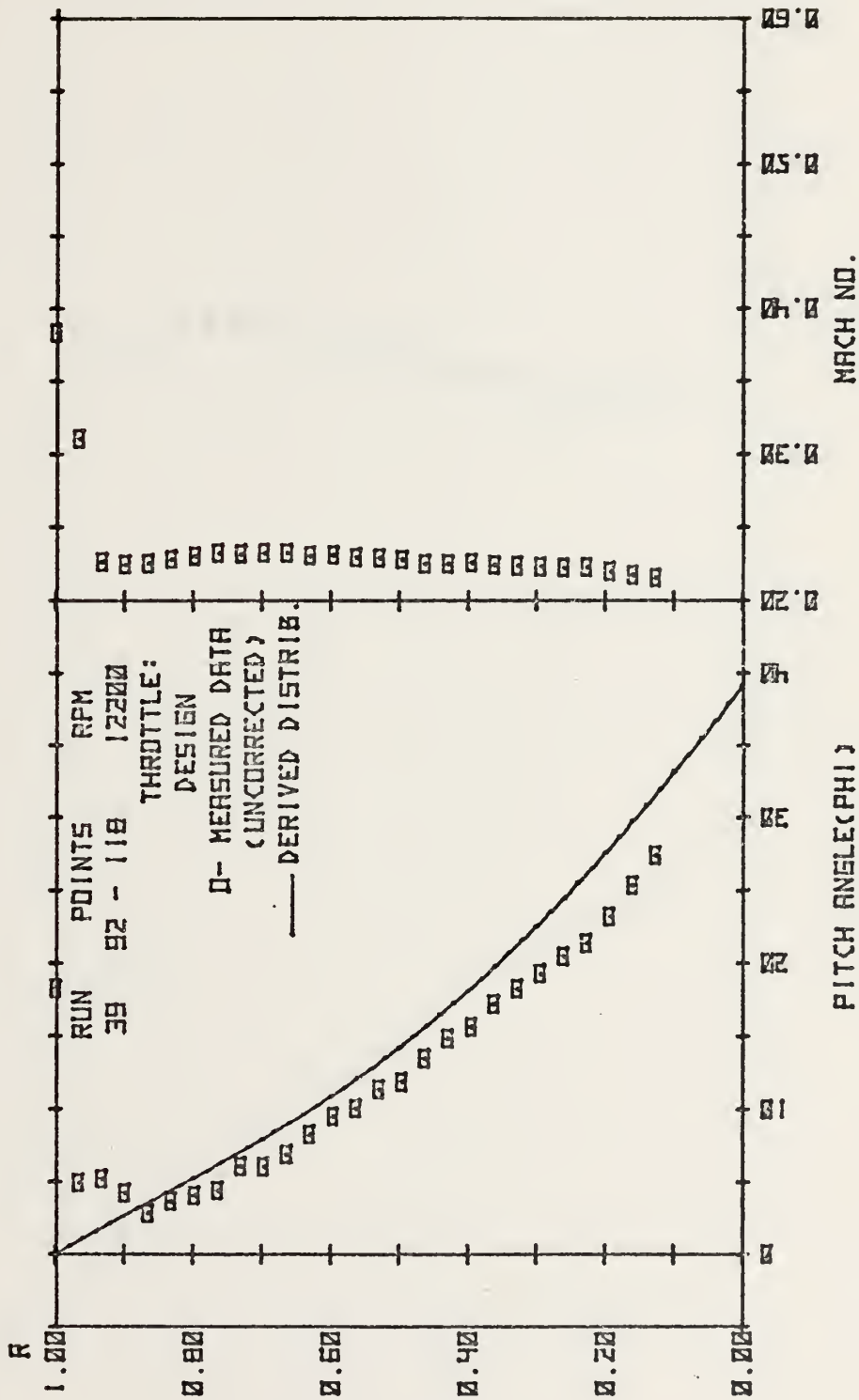
FIGURE 11. PITCH ANGLE AND MACH NO. DISTRIBUTION AT STATION 1.
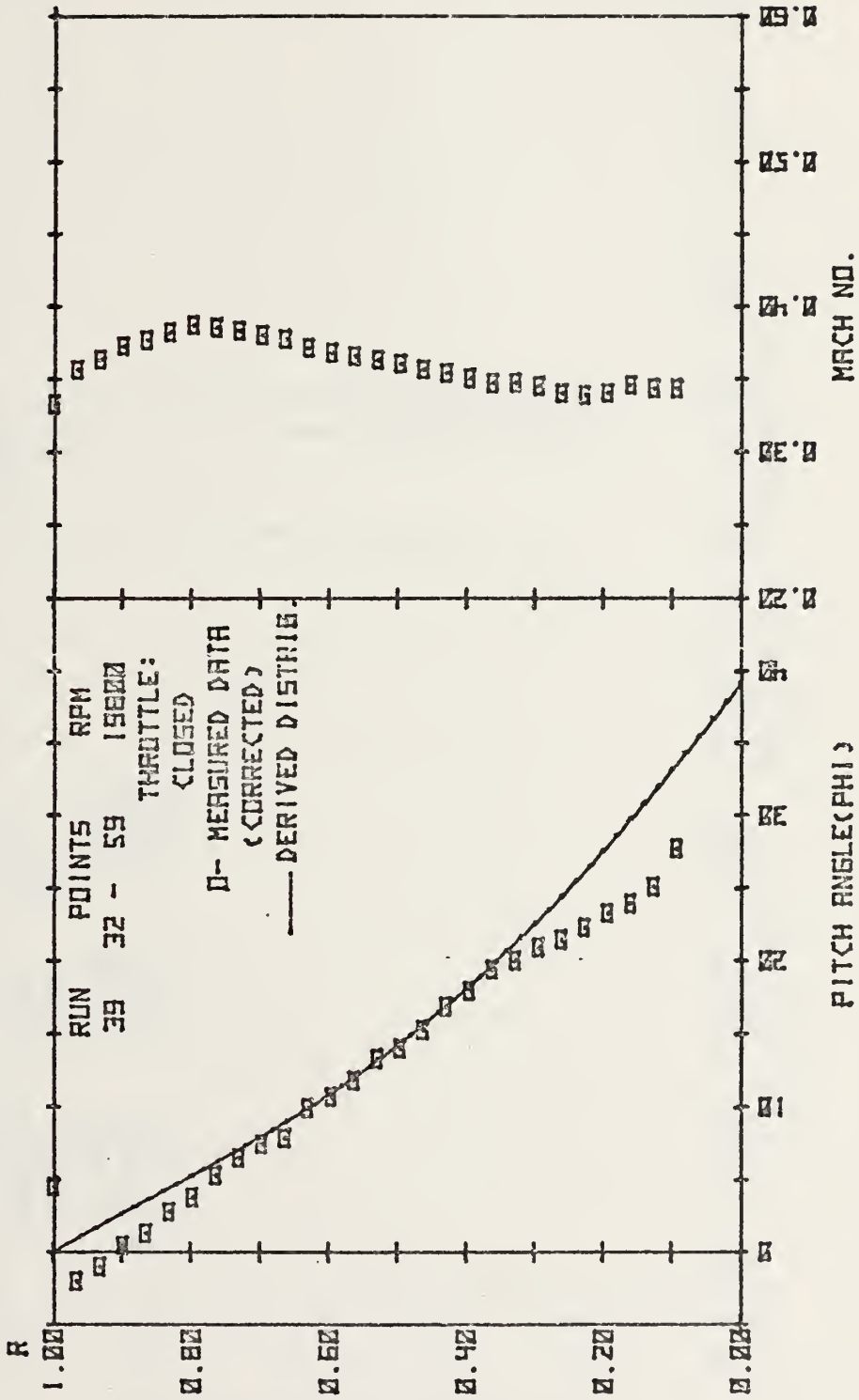
FIGURE 12. PITCH ANGLE AND MACH NO. DISTRIBUTION AT STATION 1.
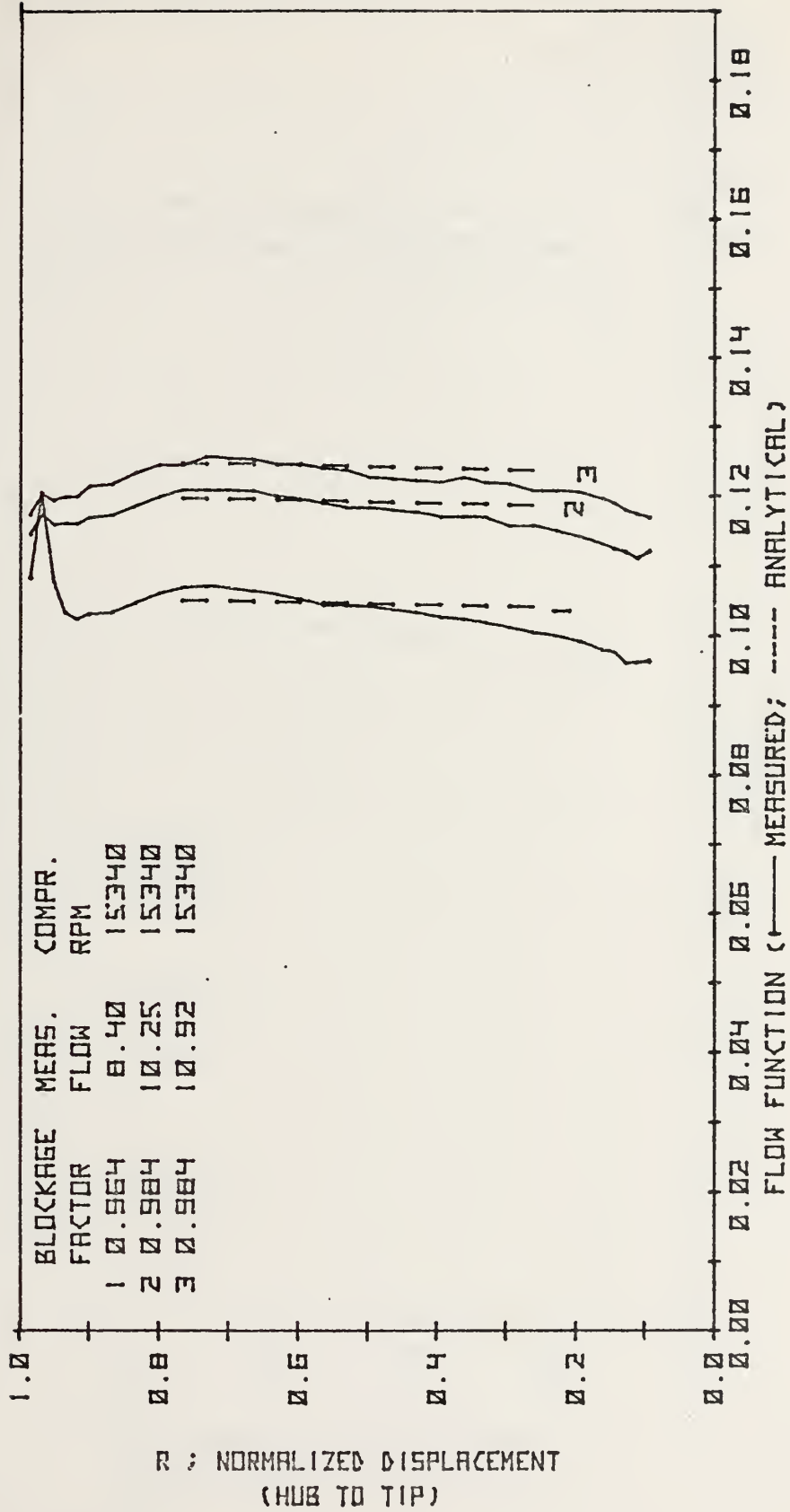
FIG.13. DISTRIBUTION OF FLOW FUNCTION AHEAD OF THE ROTOR.

44
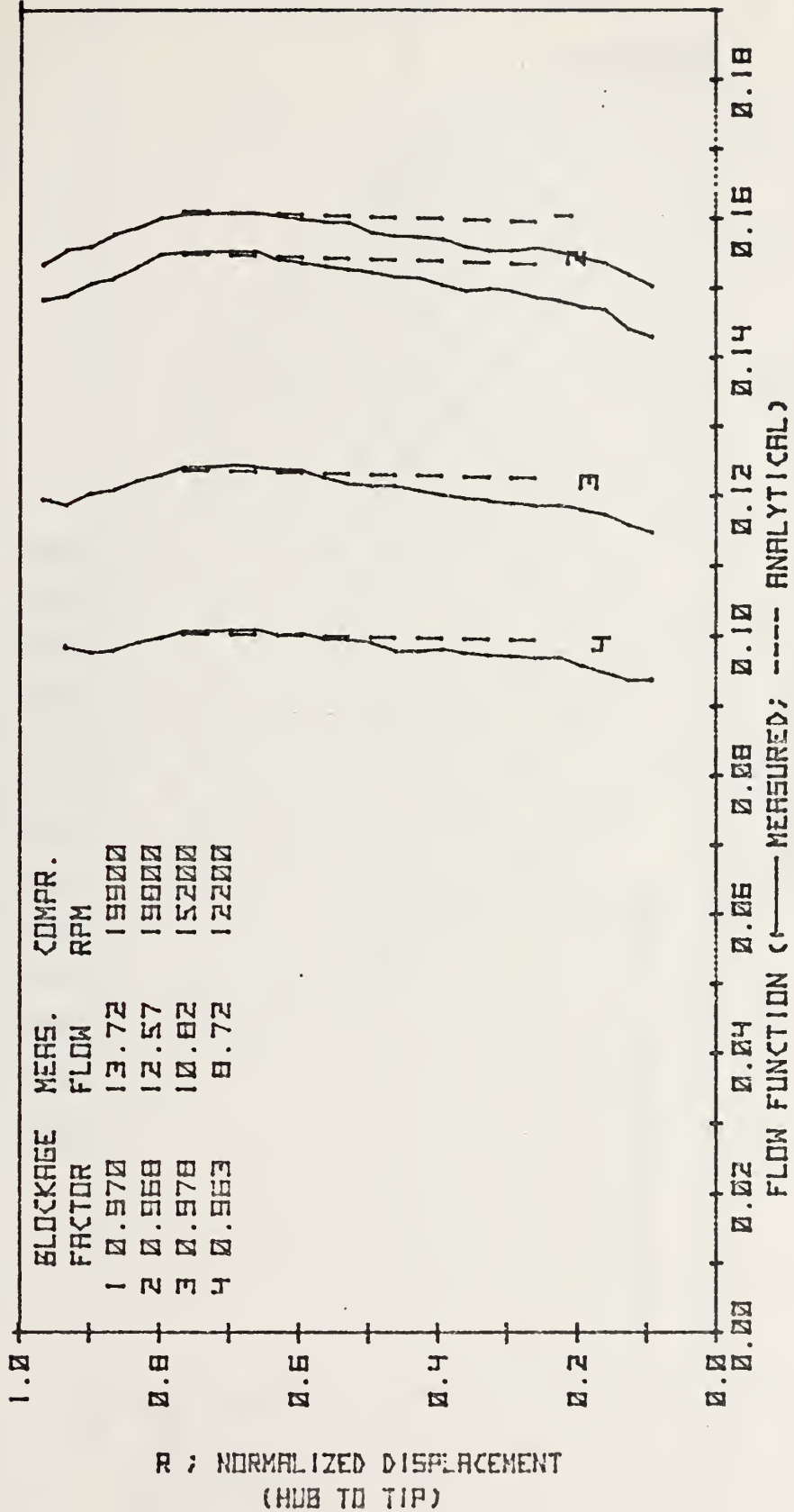
FIG. 14. DISTRIBUTION OF FLOW FUNCTION AHEAD OF THE ROTOR.
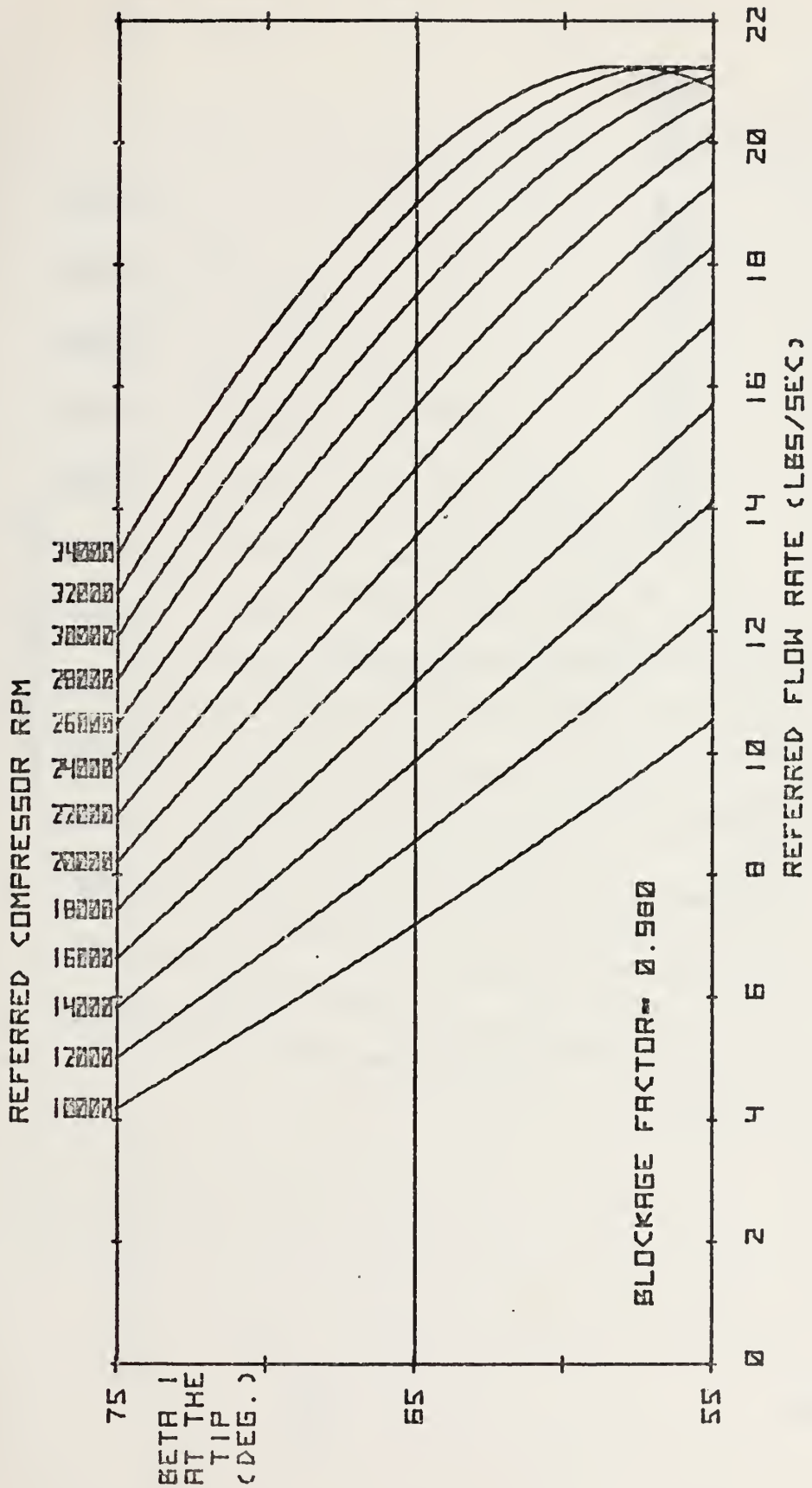
FIG. 15. TRANSONIC COMPRESSOR - CALCULATED FLOW INTO THE ROTOR
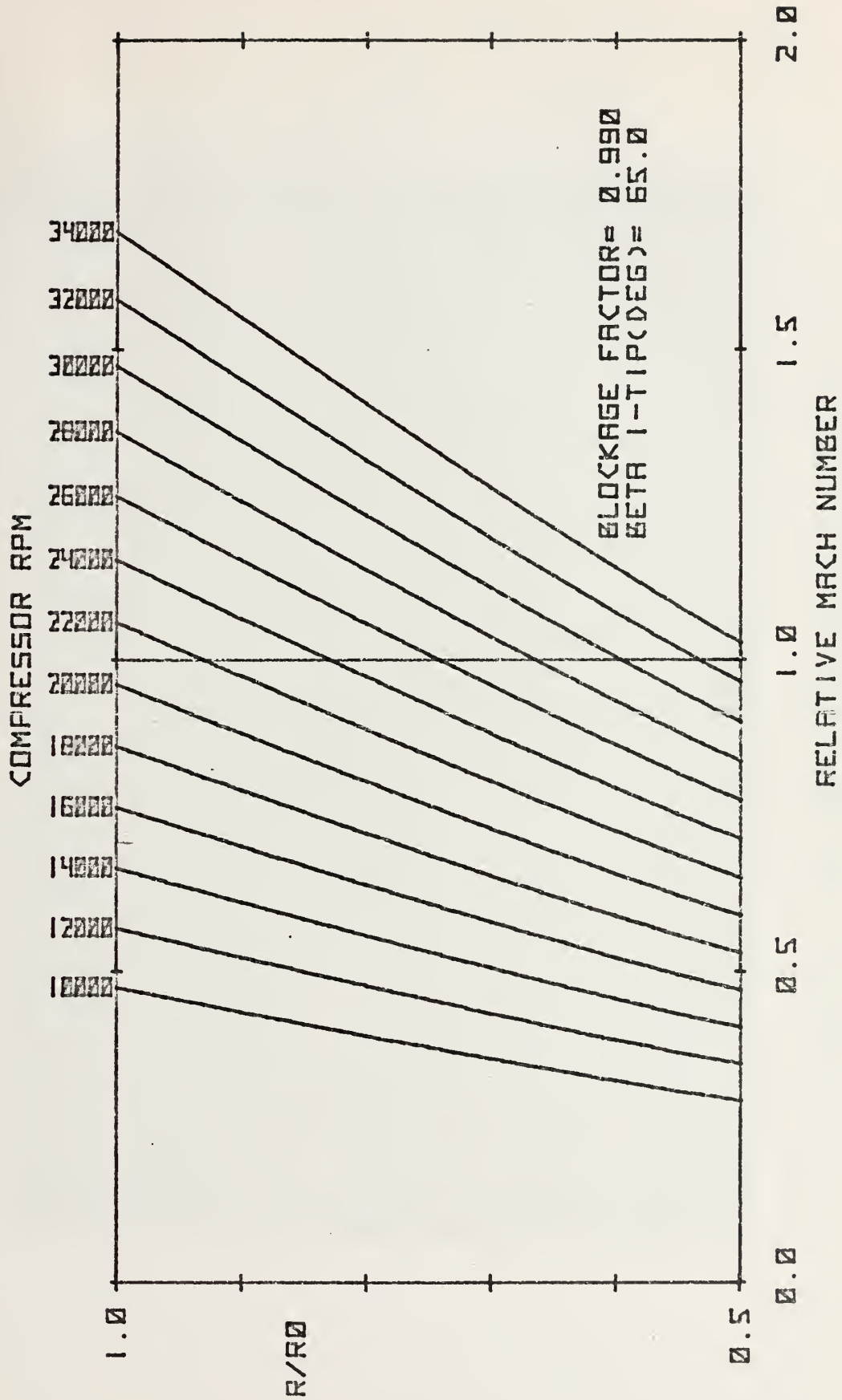
FIG. 16. TRANSONIC COMPRESSOR - CALCULATED FLOW INTO THE ROTOR
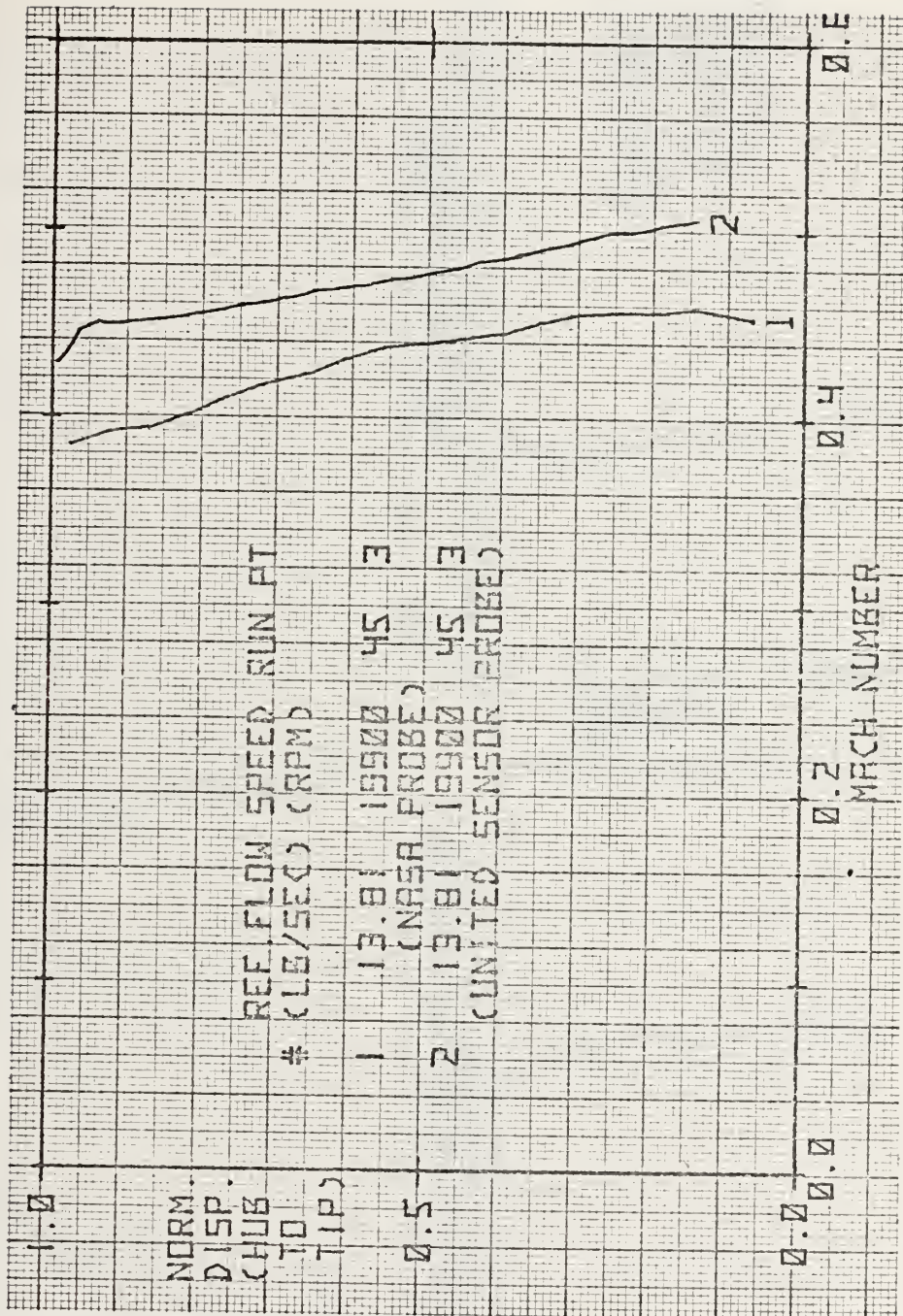
Figure 17. Mach Number Distribution Prior To
Application of the Annulus Corrections
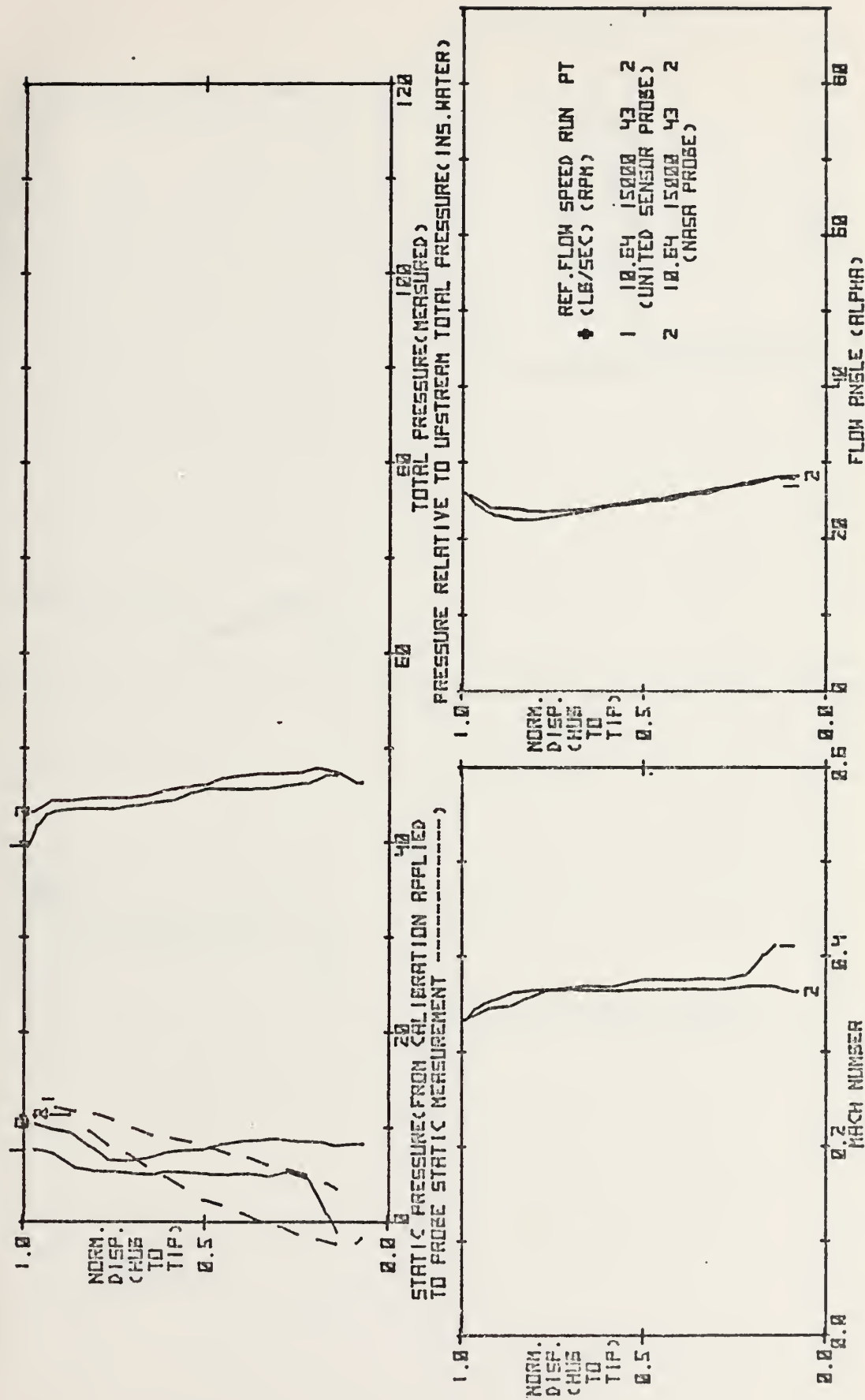
FIGURE 18. RESULTS OF PROBE SURVEYS DOWNSTREAM OF THE TRANSONIC COMPRESSOR ROTOR

49
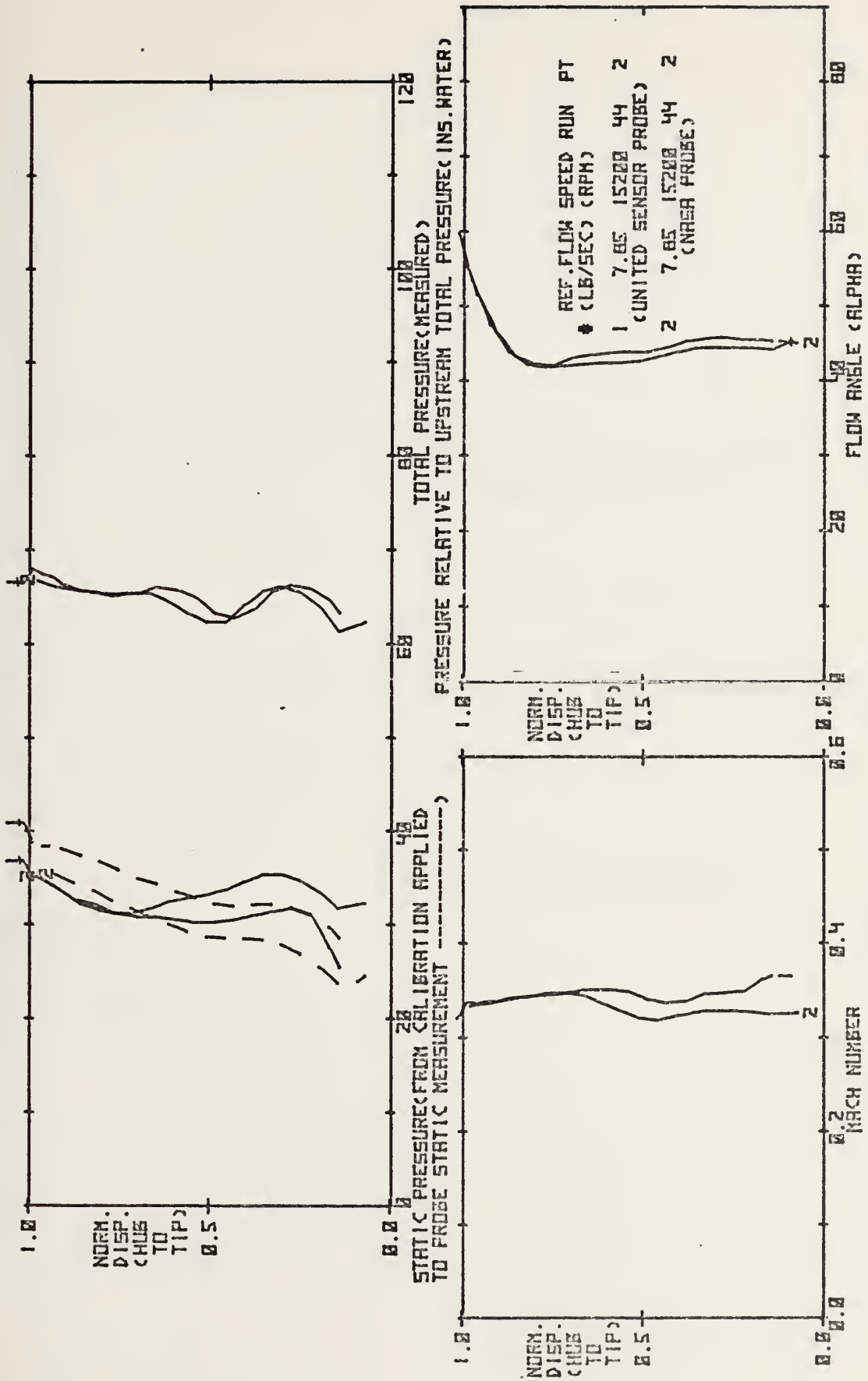
FIGURE 19. RESULTS OF PROBE SURVEYS DOWNSTREAM OF THE TRANSONIC COMPRESSOR ROTOR

50
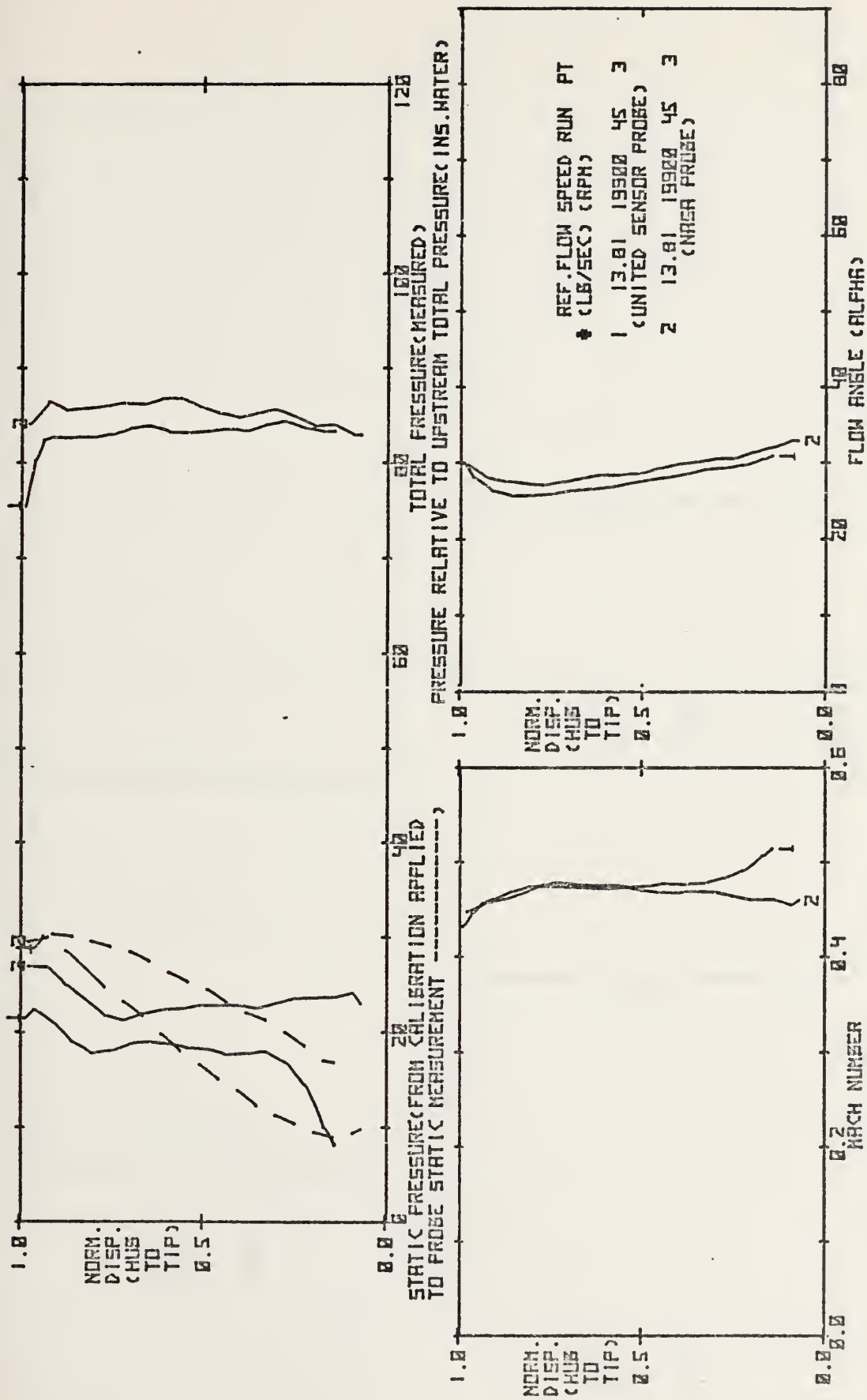
FIGURE 20. RESULTS OF PROBE SURVEYS DOWNSTREAM OF THE TRANSONIC COMPRESSOR ROTOR

51
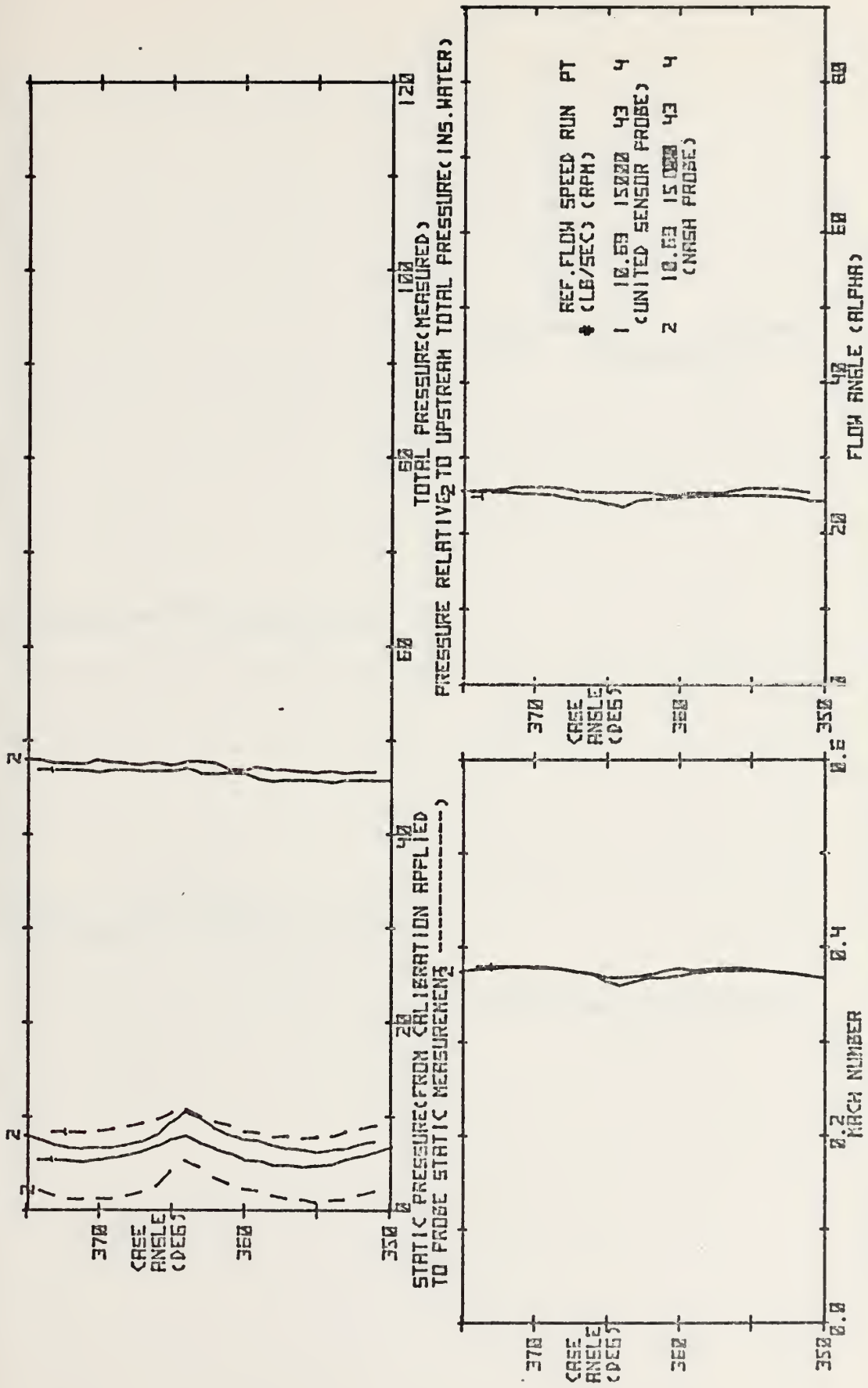
FIGURE 21. RESULTS OF PROBE SURVEYS DOWNSTREAM OF THE TRANSONIC COMPRESSOR ROTOR
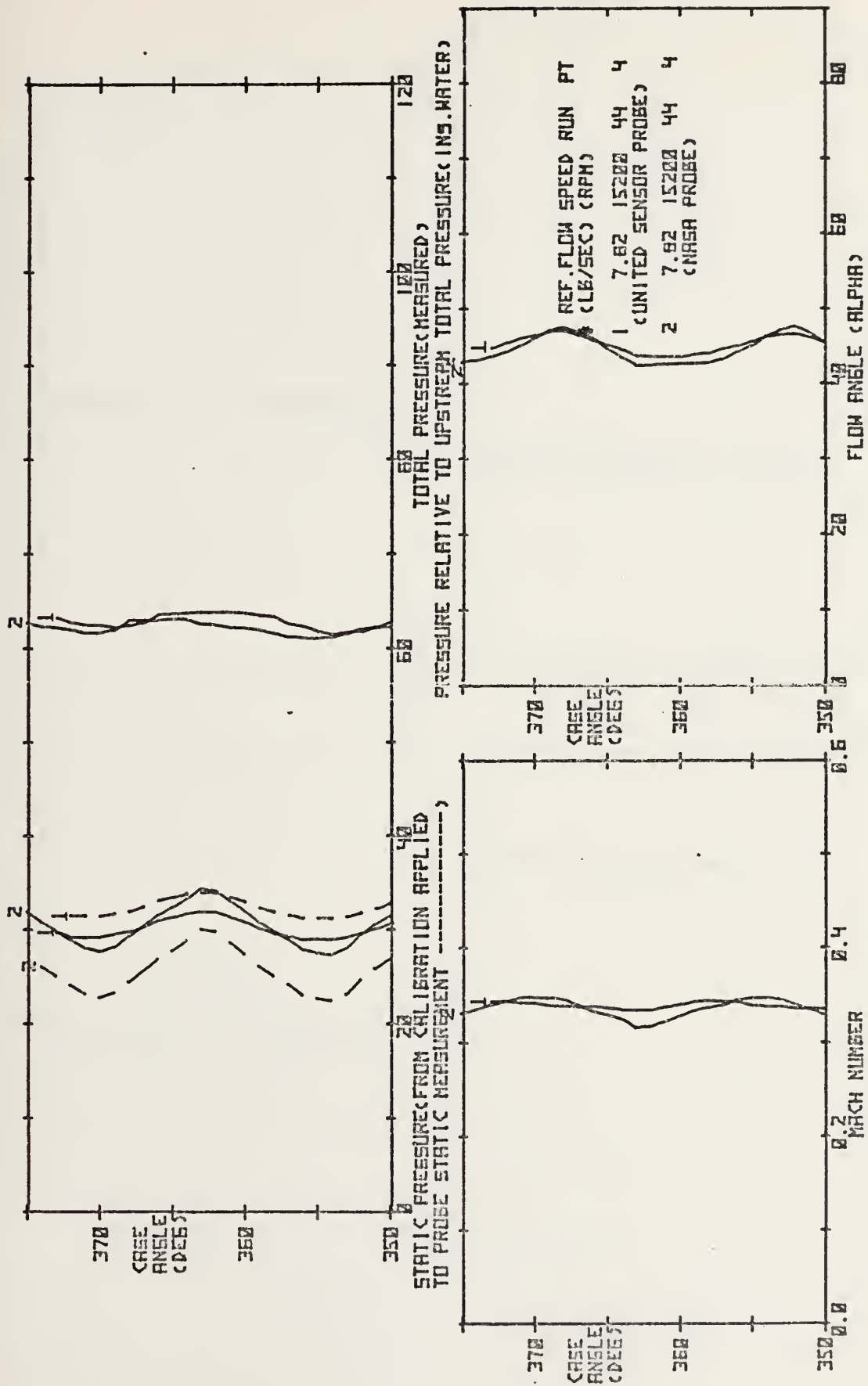
FIGURE 22. RESULTS OF PROBE SURVEYS DOWNSTREAM OF THE TRANSONIC COMPRESSOR ROTOR

53
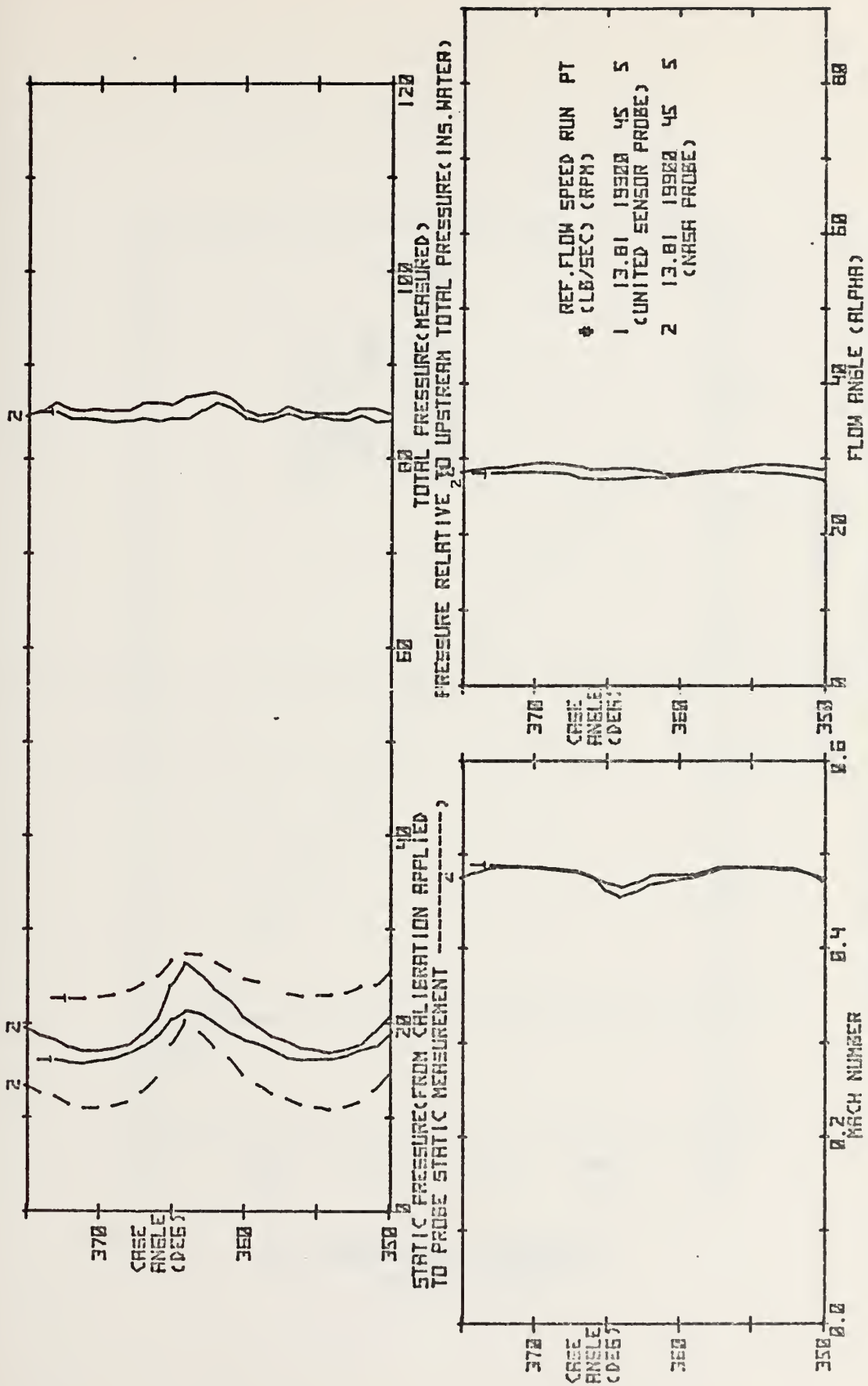
FIGURE 23. RESULTS OF PROBE SURVEYS DOWNSTREAM OF THE TRANSONIC COMPRESSOR ROTOR

54

FIGURE 24. PITCH ANGLE DISTRIBUTION BEHIND THE ROTOR.
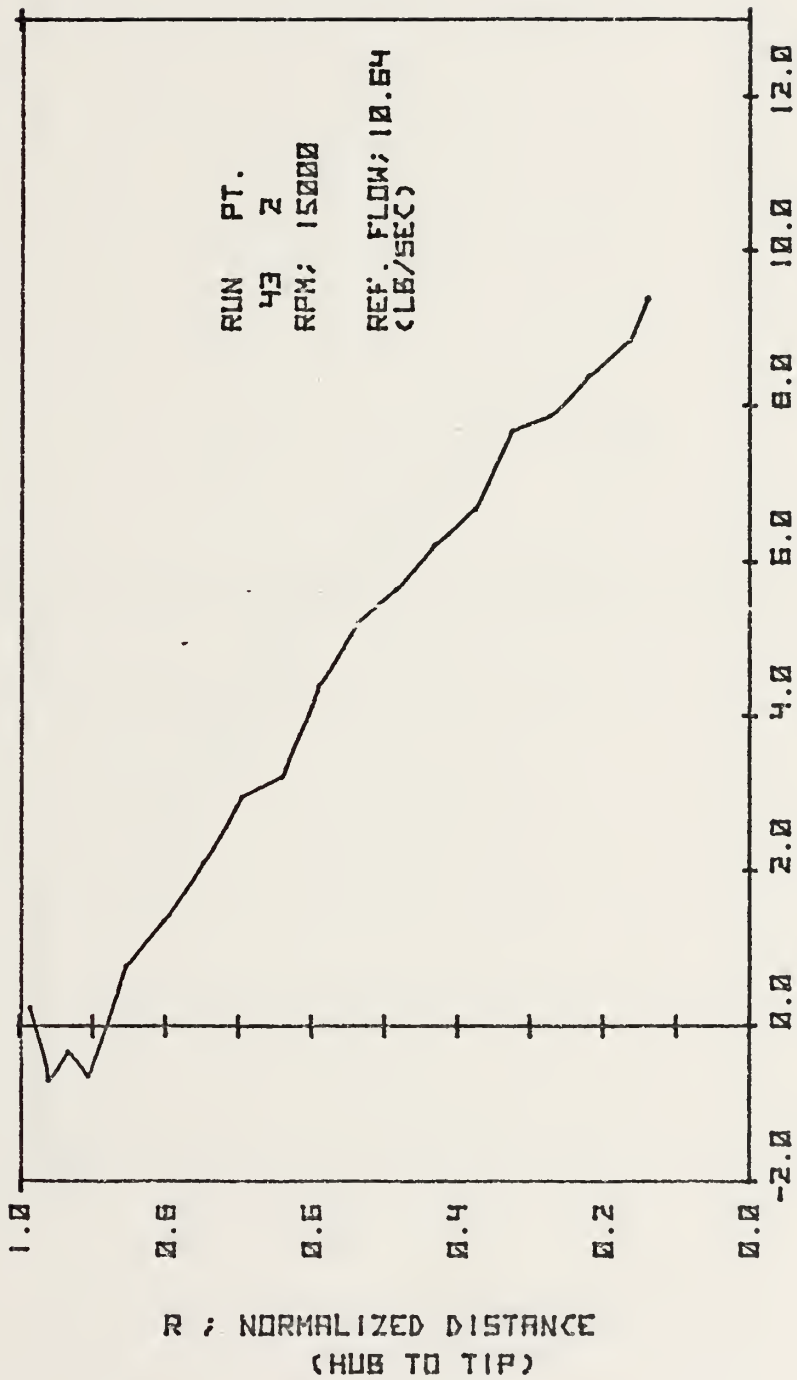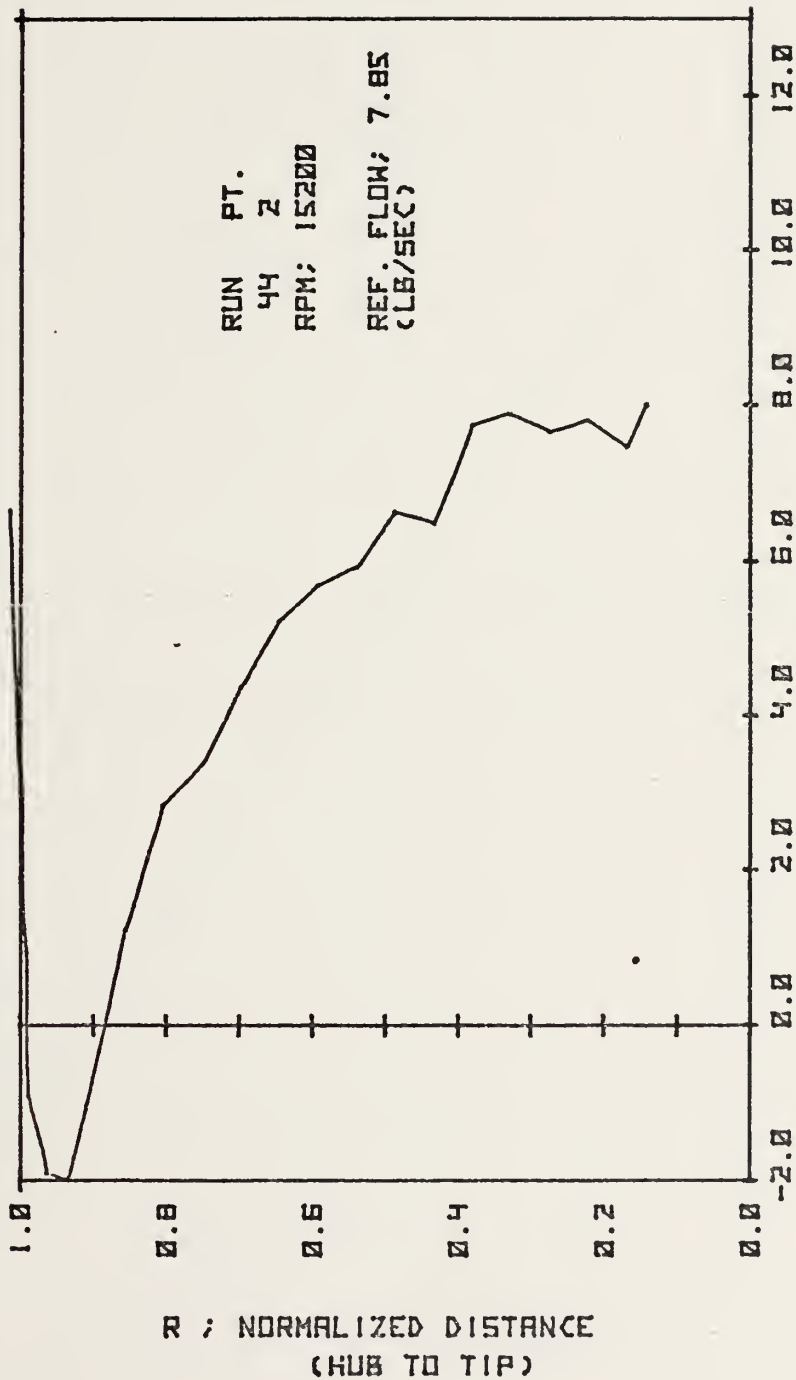
PITCH ANGLE (DEGREES)

FIGURE 25. PITCH ANGLE DISTRIBUTION BEHIND THE ROTOR.
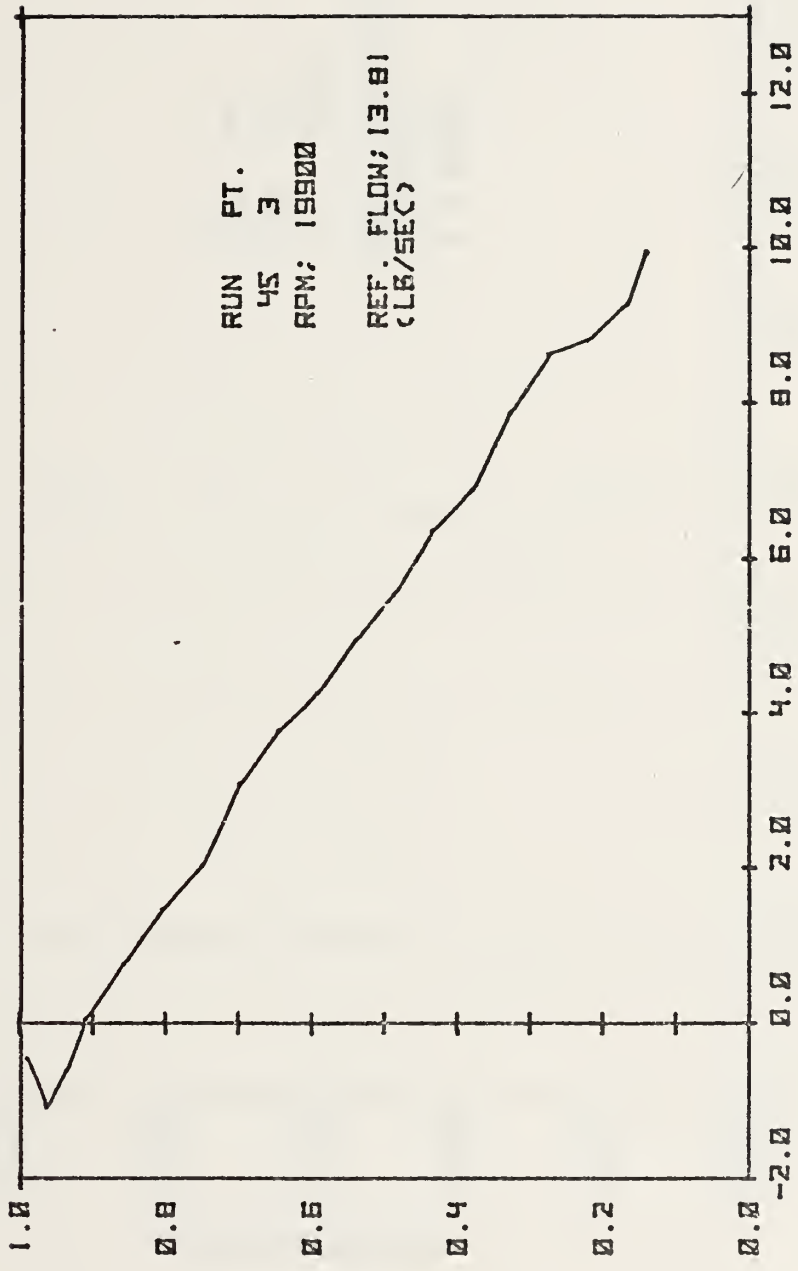
R ; NORMALIZED DISTANCE
(HUB TO TIP)

56

FIGURE 26. PITCH ANGLE DISTRIBUTION BEHIND THE ROTOR.
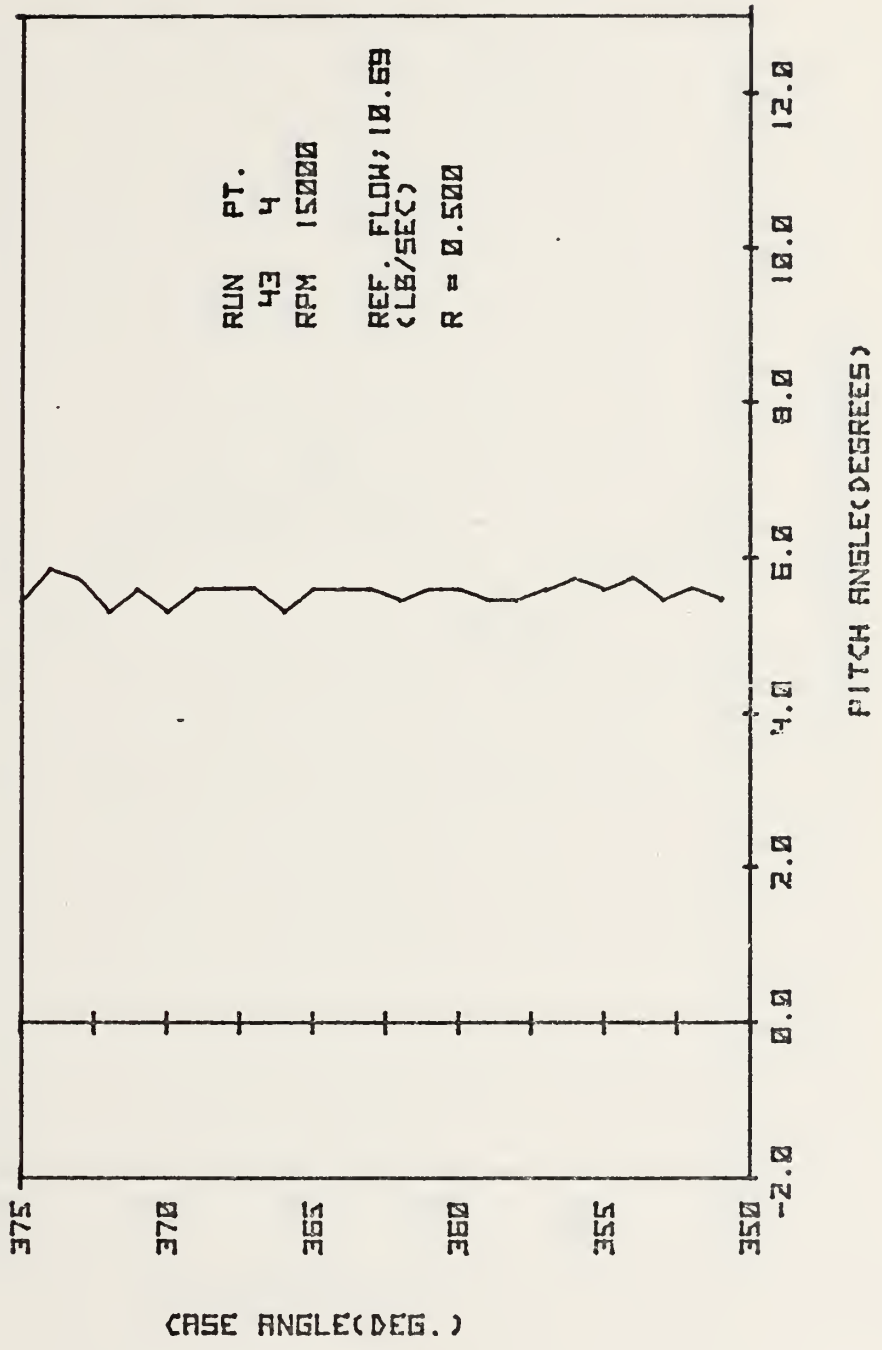
FIGURE 27. PITCH ANGLE DISTRIBUTION BEHIND THE ROTOR.

58
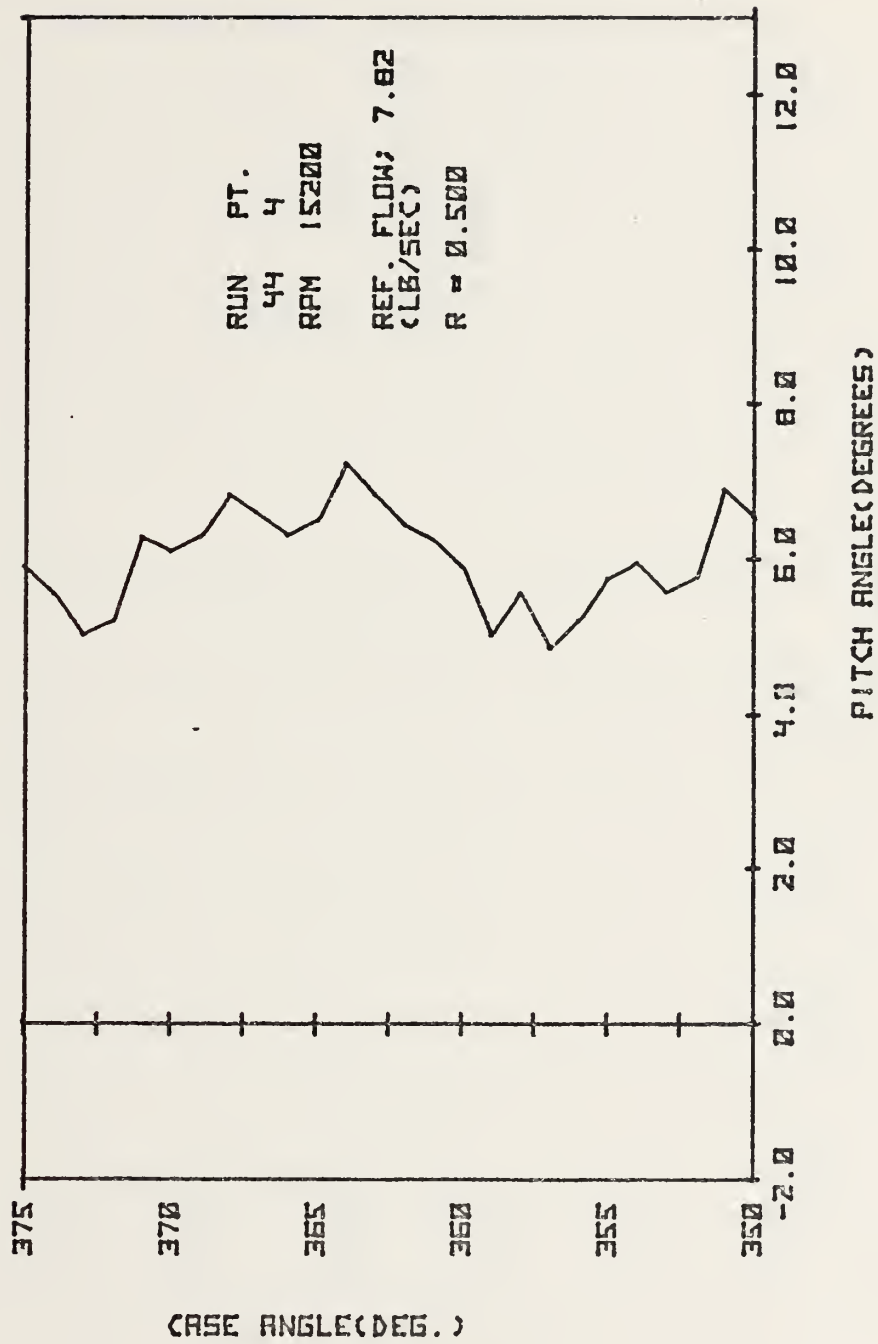
FIGURE 28. PITCH ANGLE DISTRIBUTION BEHIND THE ROTOR.

59
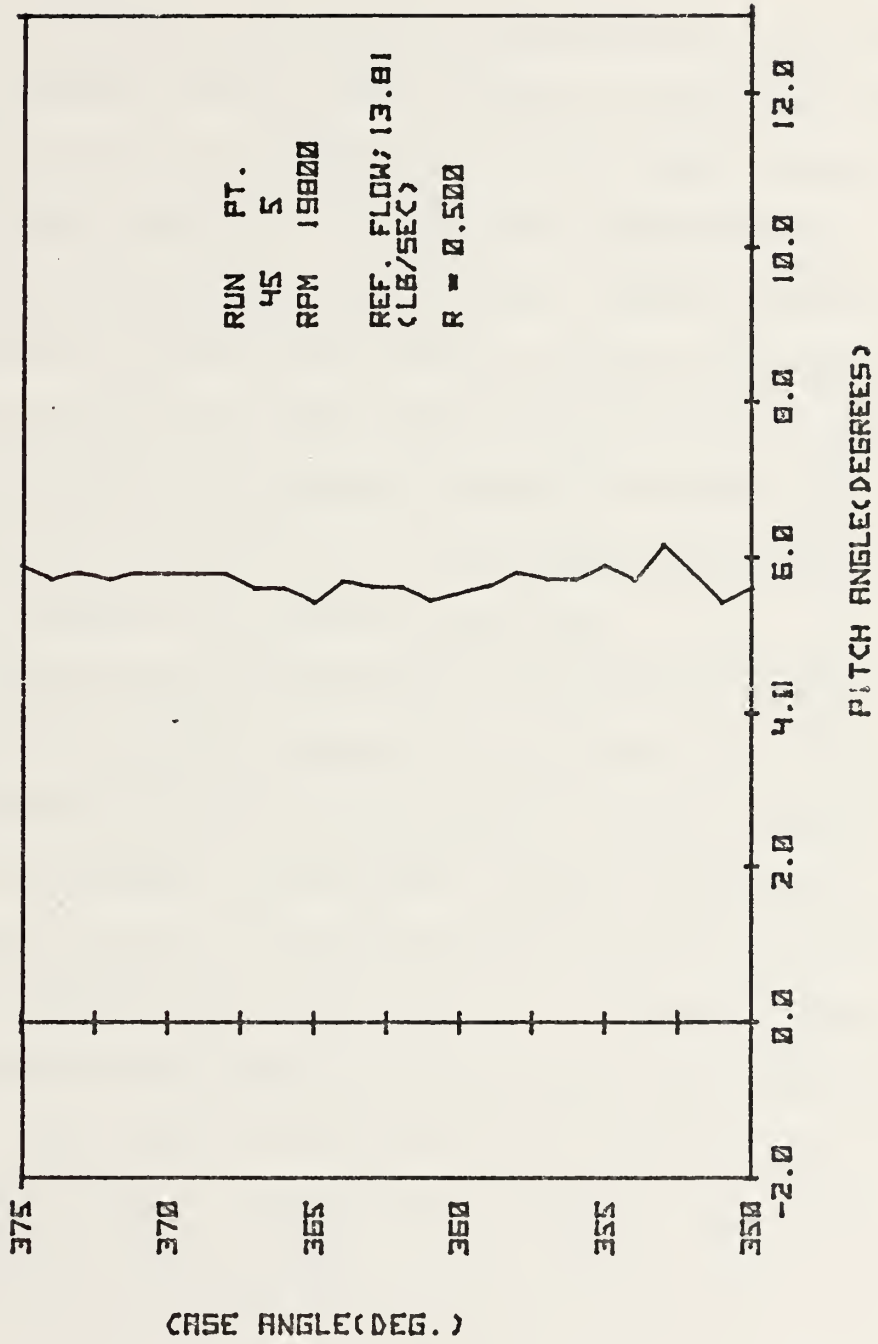
FIGURE 29. PITCH ANGLE DISTRIBUTION BEHIND THE ROTOR.

60

Appendix A: Determination of Velocity Vector From 5-Hole Pressure Probe Measurements

A.1 Method of Approach

The limited axial space available for instrumentation in most turbo-machinery flow passages severely limits the types and sizes of pressure probes which can be used. The United Sensor DA-125, 5-hole pressure probe is designed for this application. The probe, when calibrated, will measure flow velocity, yaw angle and pitch angle. A major drawback of the probe has been the tedious labor required to extract velocity and angle data from non-linear, and inter-related calibration curves. The purpose of this appendix is to document a method for calibrating the United Sensor 5-hole probe such that, in application, data reduction can be performed by computer at the time of acquisition.

Results are given here for a particular probe which was used to measure profiles in the TRANSX. compressor. It was found to be necessary to correct the measurements made in the compressor annulus for effects attributable to the passage size and shape. The method is therefore in two parts. First, the probe was calibrated with reference to a Prandtl probe in a jet contained within a larger pipe. . Analytical approximations were found which were represented as a function of the radial position in the annulus. These steps are described in section A2 and section A3 respectively, where methods of applying the calibration with and without the passage correction are also given.

A.2   Calibration and Application Free of Wall Effects

A.2.1   Probe Description and Analysis

The 5-hole probe is shown in Fig. A1. Characteristics of this and
similar probes are given in the manufacturer's catalogue (8). Briefly,
the probe is rotated in the flow until the pressure indicated by ports 2
and 3 (p_1 & p_3) are equal. The yaw angle (α) is then read on a vernier
scale attached to the top of the probe. (Fig. A2). The average of pressures
p_2 and p_3 (p_{23}, obtained pneumatically through a mixing value) is referred to
as the "indicated static" pressure of the probe. Port 1 (p_1) measures "in-
dicated total" pressure and the difference between the pressures p_4 and p_5
is a measure of the pitch angle. However, the relationship of p_{23}, and
(p_4 - p_5) to actual static pressure, total pressure and pitch angle must
be established by calibration in a known flow. Indicated static pressure is
known to be more subject to errors than total pressure, particularly when
the sensing holes are within about ten probe diameters of a boundary.

The calibration of the probe is expected to depend on flow Mach number.
It is more convenient however to non-dimensionalize the velocity using the
"limiting" velocity, $V_t = \sqrt{2C_p T_t}$ (for a perfect gas), when the stagnation
temperature is a constant in the flow. The use of limiting velocity is
discussed in Appendix A of reference 7 . The non-dimensional velocity is
given by

$$X = V/V_t \qquad\qquad A(1)$$

where V_t = 109.62 $\sqrt{T_t}$ ft/sec. for air when the stagnation temperature, T_t,
is in°R. As shown in reference 7 , the relationships between the static
and stagnation gas properties become

$$\frac{T}{T_t} = 1 - X^2$$

$$\frac{p}{p_t} = (1 - X^2)^{\frac{\gamma}{\gamma-1}} \qquad\qquad A(2)$$

$$\frac{\rho}{\rho_t} = (1 - X^2)^{\frac{\gamma}{\gamma-1}}$$

The relationship between Mach number and X is given by

$$X^2 = \frac{\frac{\gamma-1}{2} M^2}{1 + \frac{\gamma-1}{2} M^2} \qquad\qquad A(3)$$

The calibration of the 5-hole probe can be represented in the form of two functions of Mach number (or X) and pitch angle, ϕ.

If p_t and p are the true stagnation and static pressures, then define

$$F_\theta (X, \phi) = \frac{p_1 - p_{23}}{p_t - p} \qquad\qquad A(4)$$

and

$$F_\phi (X, \phi) = \frac{p_4 - p_5}{p_t - p} \qquad\qquad A(5)$$

to be the required calibration functions, where it is understood that the probe pressures are taken when $p_2 = p_3$.

The value of X is obtained from true static and stagnation pressures using Eq. A(2):

$$X = 1 - \left(\frac{p}{p_t}\right)^{\frac{\gamma-1}{\gamma}} = 1 - \left[1 - \frac{(p_t - p)}{(p_t - p_A) + p_A}\right]^{\frac{\gamma-1}{\gamma}} \qquad A(6)$$

where p_A = atmospheric pressure, and the pressure differences can be measured by manometers.

To calibrate, the probe must be placed in a flow at a known pitch angle and the true static and impact pressures measured by a reference probe. From the measured pressures, the value of X is calculated from Eq. A(6) and the values of F_θ and F_ϕ from Eq. A(4) and Eq. A(5). However, in applying the probe in an unknown flow, expressions relating only 5-hole probe measurements to the unknowns X and ϕ are required. Rearranging Eq. A(4) and using Eq. A(2),

$$\frac{p_1 - p_{23}}{p_1} = (\frac{p_t}{p_1}) \, F_\theta \, (X, \phi) \, [1 - \frac{p}{p_t}] = (\frac{p_t}{p_1}) \, F_\theta(X, \phi) \, [1 - (1-X^2)^{\frac{\gamma}{\gamma-1}}] \qquad A(7)$$

Define

$$F'_\phi \, (X, \phi) = F_\theta \, (X, \phi) \, [1 - (1-X^2)^{\frac{\gamma}{\gamma-1}}] \qquad A(8)$$

and, similarly

$$F'_\phi \, (X, \phi) = F_\phi \, (X, \phi) \, [1 - (1-X^2)^{\frac{v}{\gamma-1}}] \qquad A(9)$$

The two functions F'_θ and F'_ϕ can be tabulated as functions of X and ϕ using the values obtained in the calibration for F_θ and F_ϕ at each value of X. If, in addition, it can be shown that $p_{t/p_1} = 1.0$ to within the desired accuracy over the range of X and ϕ of interest, then, from Eq. A(7)

$$F'_\theta \, (X, \phi) = \frac{(p_1 - p_{23})}{(p_1 - p_A) + p_A} \qquad A(10)$$

and similarly

$$F'_\phi \, (X, \phi) = \frac{p_4 - p_5}{(p_1 - p_A) + p_A} \qquad A(11)$$

In using the calibration expressed by Eq. A(10) and Eq. A(11), it is necessary to interpolate in the tables established for F'_θ and F'_ϕ to find values of X and ϕ for which Eq. A(10) and Eq. A(11) are simultaneously satisfied by the measurements. Alternatively, analytical approximations can be derived for F'_θ and F'_ϕ which can be solved by iteration. The analytical approximation technique was chosen here.

A.2.2   Calibration Tests in a Jet

The 5-hole probe was calibrated as shown in Fig. A3. An A.S.M.E. flow nozzle, 7 inches in diameter, was flanged between two 36 inch lengths of 10 inch diameter steel pipe. (The internal contour of the nozzle was chrome plated and polished to a maximum roughness of 32 micro inches). Air was supplied to the 10" pipe at controlled flow rates from an industrial compressor (3) via a 4 ft. diameter settling chamber and entrance bellmouth. A 12" long bundle of $\frac{1}{2}$" diameter tubing removed any swirl remaining in the flow from the plenum. The flow from the pipe downstream of the flow nozzle exhausted into the laboratory.

A Prandtl probe was used to obtain the reference measurements of static and total pressures. The 5-hole and Prandtl probe tips were positioned on opposite sides of the flow centerline at a radius of one inch. The measuring station was 2 inches downstream of the nozzle exit face. The 5-hole probe was mounted through an aluminum block as shown in Fig. A4. The block allowed the pitch angle to be set in 5° increments from $- 10^\circ$ to $+ 10^\circ$ and in 10° increments from $- 40^\circ$ to $+ 40^\circ$ with no change in the tip location. All pressure differences were measured using U-tube water manometers. The stagnation temperature was measured using an iron-constantan thermocouple probe in the flow upstream of the flow nozzle.

The flow at the measuring plane was first surveyed using the Prandtl probe with the 5-hole probe removed. The result in Fig. A5 showed that the velocity (X) was uniform over a 4" diam core, and therefore that the flow at the reference probe tip and the 5-hole probe tip were the same to within measurement accuracy.

The procedure for the calibration tests was the following: The flow rate from the compressor was set and allowed to stabilize. The 5-hole probe was then inserted in turn at each desired value of the pitch angle. Pressure differences were recorded by hand from the manometer for the Prandtl and 5-hole probes. The thermocouple probe reading and barometric pressure were also recorded.

To cover the range required in the probe application, ϕ was varied from -5° to + 40° in 7 steps. Nine values of X were set giving dynamic pressures between 9 and 75 inches of water column. If ± 0.025 inches in the accuracy of reading each manometer column, the pressure differences are measured to ± 0.05 inches of water. However, unsteadiness in the air supply over the recording time period can be expected to reduce to overall accuracy to ± 0.1 inches water.

A.2.3 Analysis of the Results

The recorded data is given in Table A1. The ratio (p_1/p_t) was calculated to be within 0.2% of unity over the complete range of X and ϕ measured and hence was set equal to unity in representing and applying the calibration results. Using the data in Table A1, values of F'_θ and F'_ϕ were calculated using Eq. A(8) and Eq. A(9), where F_θ and F_ϕ were obtained from Eq. A(4) and Eq. A(5) and X was calculated using Eq. A(6). The remaining task was to find analytical approximations for the values of F'_θ and F'_ϕ as functions of X and ϕ, and to devise an iterative computer solution.

66

F_θ' and F_ϕ' were plotted as functions of ϕ for each value of X. The results are shown in Fig. A6 and Fig. A7. Using polynomial regression on the Hewlett-Packard 9830A calculator, F_θ' at constant X was satisfactorily fit by a 4th order polynomial in ϕ. F_ϕ' at constant X was satisfactorily fit by a 2nd order polynomial in ϕ. This representation however was found to be unsuitable in solving iteratively for X and ϕ with F_θ' and F_ϕ' given. Instead, expressions were found for

$$F_\phi' = F_\phi' \; (\phi) \; |_{x \; = \; const}$$

as in Fig. A7, and

$$X = X \; (F_\theta') \; |_{\phi \; = \; const}$$

Fig. A8 shows the results plotted in the latter form. Quadratic functions were found to represent the data satisfactorily.

Since data was taken for 9 values of X and 7 values of ϕ, the two sets of functions were expressed as

$$F_{\phi_i}' \; (\phi) = a_i(X) + b_i(X) \; \phi + c_i(X). \; \phi^2 \qquad\qquad A(12)$$

where $i = 1, 2 \;$--- 9 and a_i, b_i and c_i are coefficients which depend on the value of X, and

$$X_j(F_\theta') = f_j(\phi) + g_j(\phi). \; [F_\theta'] + h_j(\phi).[F_\theta']^2 \qquad\qquad A(13)$$

where $j = 1, 2 \;$--- 7 and f_j, g_j and h_j are coefficients which depend on the value of ϕ.

Next, the coefficients a_i, b_i and c_i from the 9 equations represented by Eq. A(12) were approximated by a polynomial expansion in X, and the coefficients f_j, g_j and h_j from the 7 equations represented by Eq. A(13) by

a polynomial expression in ϕ. Thus coefficients were found for the expressions

$$a_i \, (X) = A_1 + A_2 X_i + A_3 \, X_i^2 + - - - - -$$

$$b_i \, (X) = B_1 + B_2 X_i + B_3 \, X_i^2 + - - - - - \qquad\qquad A(14a)$$

$$c_i \, (X) = C_1 + C_2 X_i + C_3 X_i^2 + - - - - -$$

$$f_j \, (\phi) = F_1 + F_2 \phi_j + F_3 \phi_j^2 + - - - - -$$

$$g_j \, (\phi) = G_1 + G_2 \phi_j + G_3 \phi_j^2 + - - - - - \qquad\qquad A(14b)$$

$$h_j \, (\phi) = H_1 + H_2 \phi_j + H_3 \phi_j^2 + - - - - -$$

which gave the best fit to the 9 values of a_i, b_i, c_i and to the 7 values of f_j, g_j and h_j. This results in a single equation (Eq. A(12)) for $F_\phi' \, (\phi)$ in which the coefficients are analytic functions of X, and a single equation (Eq. A(13)) for $X(F_\theta')$ in which the coefficients are analytic functions of $\dot{\phi}$. The coefficients in Eq. A(14) are given in Table A3.

In application, the probe measurements give values to F_θ' and F_ϕ' through Eq. A(10) and Eq. A(11). Equation A(12) and Eq. A(13) must be solved for the unknown ϕ and unknown X. An initial estimate of the pitch angle was devised in the following way. A new function of the probe pressure differences was defined such that

$$F_\lambda' (X,\phi) \equiv \frac{F_\phi'}{F_\theta'} \equiv \frac{P_4 - P_5}{P_1 - P_{23}} \qquad\qquad A(15)$$

When ϕ was plotted as a function of F_λ' for each value of X, it was observed that the curves were nearly linear with similar slopes. Therefore the average of the 9 values of F_λ' at each value of ϕ was calculated and a third order polynomial was found to fit the 7 average values when ϕ was plotted

as a function the average F'_λ (Fig. A9). This gave

$$\phi_1 (F'_\lambda) = J + K (F'_\lambda) + L (F'_\lambda)^2 + M (F'_\lambda)^3 \qquad \text{A(16)}$$

where ϕ_1 is the desired initial estimate of the pitch angle and F'_λ is
obtained from the probe measurements using Eq. A(15). The coefficients J,
K, L & M are given in Table A4.

A2.4 Application

When applying the 5-hole probe to measure an unknown flow, the pressure
differences read when p_2 and p_3 are balanced are reduced to the three factors
F'_θ, F'_ϕ and F'_λ using Eq. A(10), Eq. A(11) and Eq. A(15). X and ϕ are evaluated
using the calibration relations derived in the preceeding section. The yaw
angle is read directly from the probe scale. The velocity is obtained from
the product of X and V_t which requires the input of the stagnation temperature.

The reduction to velocity and pitch angle was programmed for the Hewlett-
Packard Model 9830A calculator. A flow chart of the program is shown in Fig.
A10. The program first calculates the initial estimate of ϕ ($=\phi_1$) using
Eq. A(16). The initial estimate of X ($=X_1$) is calculated from Eq. A(13) using
ϕ_1 in Eq. A(14b) to evaluate the coefficients f, g and h. The coefficients
a, b and c in Eq. A(12) are then calculated using X_1 in Eq. A(14a). In
general the value of F'_ϕ which could be calculated using these coefficients in
Eq. A(12) would not be equal to the value calculated from the input data. An
iterative procedure is begun using ϕ_1 and X_1 as initial values.

In the adopted procedure, Eq. A(12) is viewed as an equation to be solved
for an unknown ϕ in terms of a known F'_ϕ and known X. Equation A(13) is treated
as an equation for X in terms of a known ϕ. Equation A(12) is solved by fixed
point iteration (9) beginning with the initial values ϕ_1 and X_1. In this

69

method, the $(i+1)^{th}$ value of ϕ in the iteration is given in terms of the ith value by rewriting Eq. A(12) as

$$\phi_{i+1} = [F'_\phi - a - c\,\phi_i^2]/b \qquad\qquad A(17)$$

For a fixed value of $X(=X_i)$, which fixes the coefficients a, b, and c, successive values of ϕ are calculated using Eq. A(17) until $|\phi_{i+1} - \phi_i| < \epsilon_\phi$ is satisfied. ϵ_ϕ is a small quantity. A new value of $X(=X_{i+1})$ is then calculated using $\phi = \phi_{i+1} = \phi_i$ in Eq. A(13) and the process repeated until $|X_{i+1} - X_i| < \epsilon_x$, where ϵ_x is a small quantity.

The steps in the solution may be summarized as follows:

1) Calculate ϕ from Eq. A(16)

2) Calculate X_1 from Eq. A(13)

3) Calculate ϕ_{i+1} from Eq. A(17)

4) If $|\phi_{i+1} - \phi_i| < \epsilon_\phi$ do step 5), otherwise go to step 3)

5) Calculate X_{i+1} from Eq. A(13) using $\phi = \phi_{i+1} = \phi_i$

6) If $|X_{i+1} - X_i| < \epsilon_x$ stop, otherwise go to step 3).

70

A.3 Corrections to the Calibration for Application in an Annulus

A3.1 Introduction

The calibration described above was carried out where the presence of flow boundaries would not be expected to influence the probe readings. A change in the calibration of the probe is expected when measurements are made within about ten probe diameters of a boundary, and when the probe size is significant compared to the flow passage area. A precise correction which would allow the use of the probe in any flow field is a difficult task and not attempted here. Instead, a calibration of the probe in an axial annular flow of similar geometry to the compressor annulus was carried out, and corrections to the "wall-free" calibration of section A2 were derived which were represented as a function of radial position. The test of the success of this proceedure was to compare measurements made in the compressor using two different types of probes. Agreement in the velocity profiles derived from the two probes would be expected if the corrections applied to each calibration were valid. Also, the distribution of true static pressure derived from the probe calibrations should be consistent with wall tap measurements on the tip and hub surfaces. In the following sections, the calibration tests are described and the derivation of corrections to the "wall-free" calibration is presented. The application of the revised calibration to compressor measurements is then given.

A3.2 Calibration Tests in an Annulus

An annular axial flow was generated as shown in Fig. A11. An axisymmetric body with a maximum diameter of 6"over 28"of its length was supported in the center of a 10" pipe. At the upstream end, four thin airfoil struts were positioned ahead of the contoured nose section which generated a smooth contraction of the flow passage to a 2" annulus. Heavy struts supported the

71

centerbody at the outlet flange where the flow exhausted into the laboratory. A view of the apparatus is shown in Fig. A12. Six equally spaced wall pressure taps were provided in the 10" pipe at each of 3 axial stations. Corresponding pressure taps were provided on the centerbody surface. Provision for radial probe surveys was made at the same three axial stations.

It was established in preliminary surveys that the wall pressures at station 1 in Fig. A11 were uniform around the periphery to ± 0.34% of the average dynamic head. The outer (tip) wall pressures were consistently lower than inner (hub) wall pressures by 0.45% of the dynamic head. The flow was measured to be axial to within the sensitivity of the 5-hole probe yaw angle measurement (± .1°). Probe calibration was therefore carried out at station 1. Static pressure was assumed to vary linearly between hub and tip values, and the pitch angle was taken to be zero.

Radial surveys were made from hub to tip at fixed flow rates using the 5-hole probe, a Kiel probe and a pitot-static probe in succession. Readings were taken at the same radial locations with each probe. Intervals of 0.2", decreasing to 0.05" near the walls, were used. Dynamic pressure was varied from 27 to 73 inches of water in 7-8 inch increments. The data for seven surveys is given in Table A2.

A3.3 Analysis of the Results

An example of the distribution of pressures measured by the three probes is given in Fig. A13. It was observed that the probes gave the same values of impact pressure at corresponding points to within the accuracy of the measurements except close to the outer wall where the velocity gradients were large. The static pressure indicated by the pitot static probe was observed to vary very little across the annulus, and was in agreement with a linear

72

variation of the true static pressure between hub and tip measurements at the wall. Also, the wall pressures at hub and tip away from the traverse station were not measurably affected by the prove movement. Consequently, the 5-hole probe indicated total presure (P_1) and a static pressure obtained by a linear interpolation between measurements at the walls were used to calculate the actual velocity (X) at the probe location. By applying the methods of section A2, the 5-hole probe pressure measurements were reduced to "wall-free" values of velocity and pitch angle, $(\bar{X}$ and $\bar{\phi})$, which in general were different from the actual values, $(X$ and $\phi)$ at the probe location.

A velocity correction factor, $\bar{K}_x$, was defined and examined as a function of position in the annulus and the indicated velocity, thus:

$$\bar{K}_x \ (H,\bar{X}) = \frac{X - \bar{X}}{\bar{X}} \qquad\qquad A(18)$$

where $H = y/h$, y is the distance outwards from the hub wall and h is the annulus depth. At each value, H_i, of the probe position the dependence of $\bar{K}_x$ on $\bar{X}$ was approximated by a polynomial

$$\bar{K}_{x_i} = q_i + r_i \ \bar{X} + s_i \ \bar{X}^2 + \qquad\qquad A(19)$$

where $i = 1, 2, --- 12$, and $H_i = 0.125, 0.15, --- 0.975$. The coefficients in Eq. A(19) are listed in Table A5.

The pitch angle at each probe position, H_i, was found to be independent of X. A pitch correction factor, $\bar{K}_\phi$ was defined which was then a function of position only: thus

$$\bar{K}_\phi \ (H) = \frac{(\phi + \beta) - (\bar{\phi} + \beta)}{(\bar{\phi} + \beta)} \qquad\qquad A(20)$$

where β is a constant angle introduced to avoid division by zero. Since

$\phi = 0$ in the calibration test, Eq. A(20) with $\beta = 180°$ becomes

$$\bar{K}_\phi(H) = - \frac{\bar{\phi}}{180}$$ A(21)

The values of $\bar{K}_\phi$ obtained for the tests in the annulus using Eq. A(21) were approximated by a 6th order polynomial,

$$\bar{K}_\phi (H) = z_1 + z_2 H + z_3 H^2 + z_4 H^3 + z_5 H^4 + z_6 H^5 + z_7 H^6$$ A(22)

to .995 root mean square. The coefficients in Eq. A(22) are listed in Table A6.

A3.4 Application

It is assumed that the corrections required to the calibration free of wall effects when the 5-hole probe is used to determine the flow field in a compressor annulus, are those established for an axial flow in the annulus of similar geometry. The probe readings are first reduced to values of $\bar{X}$ and $\bar{\phi}$ using the methods given in Section A2. Then, from Eq. A(18) and Eq. A(20) with $\beta = 180°$, the corrected velocity and pitch angle are given by

$$X = (\frac{1}{1 - \bar{K}_X}) \cdot \bar{X}$$ A(23)

and

$$\phi = (\frac{1}{1 - \bar{K}_\phi}) \cdot \bar{\phi} + 180 (\frac{\bar{K}_\phi}{1 - \bar{K}_\phi})$$ A(24)

At any probe position, H, the value of $\bar{K}_\phi$ in Eq. A(24) is given by Eq. A(22) for which the coefficients are given in Table 6.

The value of $\bar{K}_X$ in Eq. A(23) must be obtained by interpolation. The uncorrected velocity $\bar{X}$ is known at the probe position H; however, the correction factor $\bar{K}_X$ can be evaluated using Eq. A(19) only at discreet locations H_i. The method adopted is a form of quadratic interpolation for uneven

74

intervals (10). First the value of i is found such that H is located in the interval between H_i and H_{i+1} as shown in Fig. A(14). The values of $\bar{K}_{x_{i-1}}$, $\bar{K}_{x_i}$, $\bar{K}_{x_{i+1}}$ and $\bar{K}_{x_{i+2}}$ are calculated from Eq. A(19) using the coefficients given in Table A5. The coefficients of quadratics for $\bar{K}_x$ passing through each of the two sets of three points H_{i-1}, H_i, H_{i+1} and H_i, H_{i+1}, H_{i+2} are calculated and each quadratic is used to calculate a value for $\bar{K}_x$ at H. The arithmetic mean of the two values is taken for the interpolation. In the first or the last interval, or to extrapolate outside the given range, only one quadratic is used.

The data reduction with corrections was programmed for the Hewlett-Packard Model 9830A calculator. The flow chart is given in Fig. A(15). The steps are summarized as follows:

1) Input probe pressure data, probe position, flow stagnation temperature, atmospheric pressure.

2) Calculate $\bar{\emptyset}$ and $\bar{X}$ using the steps given in Section A2.4.

3) Calculate $\bar{K}_{\emptyset}$ with Eq. A(22).

4) Calculate $\bar{K}_x$ using quadratic interpolation between $\bar{K}_{x_i}$ values given by Eq. A(19).

5) Calculate X and $\emptyset$ using Eq. A(23) and Eq. A(24).

This proceedure was applied to the calibration data as described in Section A3.2 and listed in Table A2. The results for one survey are shown for illustration in Table A7. At each probe position in the annulus, H, the uncorrected indicated velocity, X(UNMOD), the measured actual velocity, X(ACTUAL), and the corrected velocity, X(MOD) are compared. The largest error between the corrected and actual values was less than 0.3% for all points in all surveys taken.

75
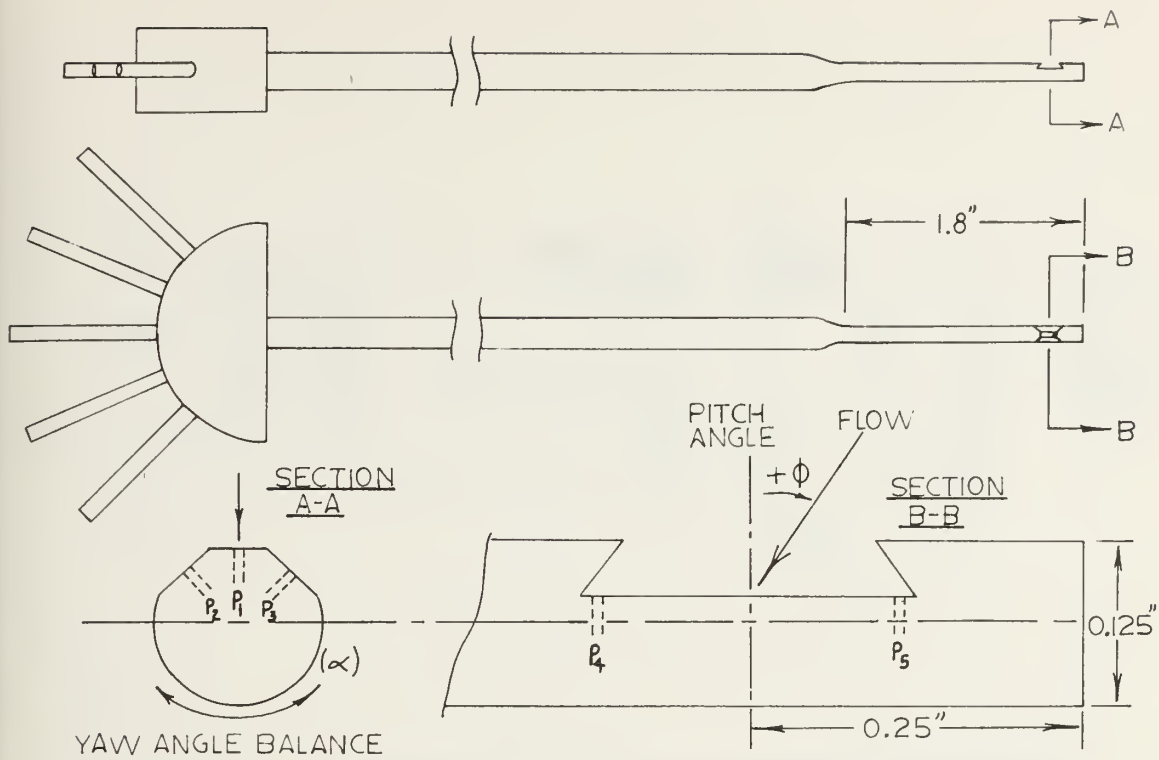
FIGURE A1. SCHEMATIC OF THE 5-HOLE PROBE
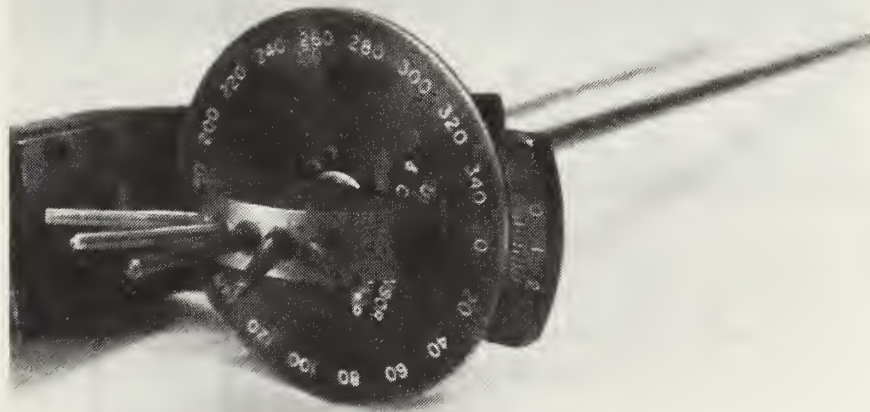
FIGURE A2. VIEW OF THE 5-HOLE PROBE SHOWING YAW

ANGLE SCALE

76
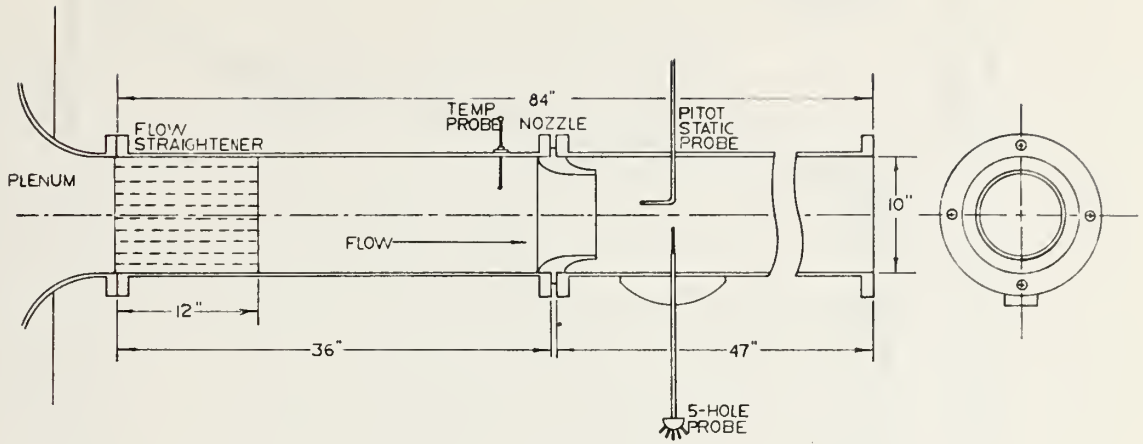
FIGURE A3.   SCHEMATIC OF THE APPARATUS FOR PROBE

CALIBRATION FREE OF WALL EFFECT
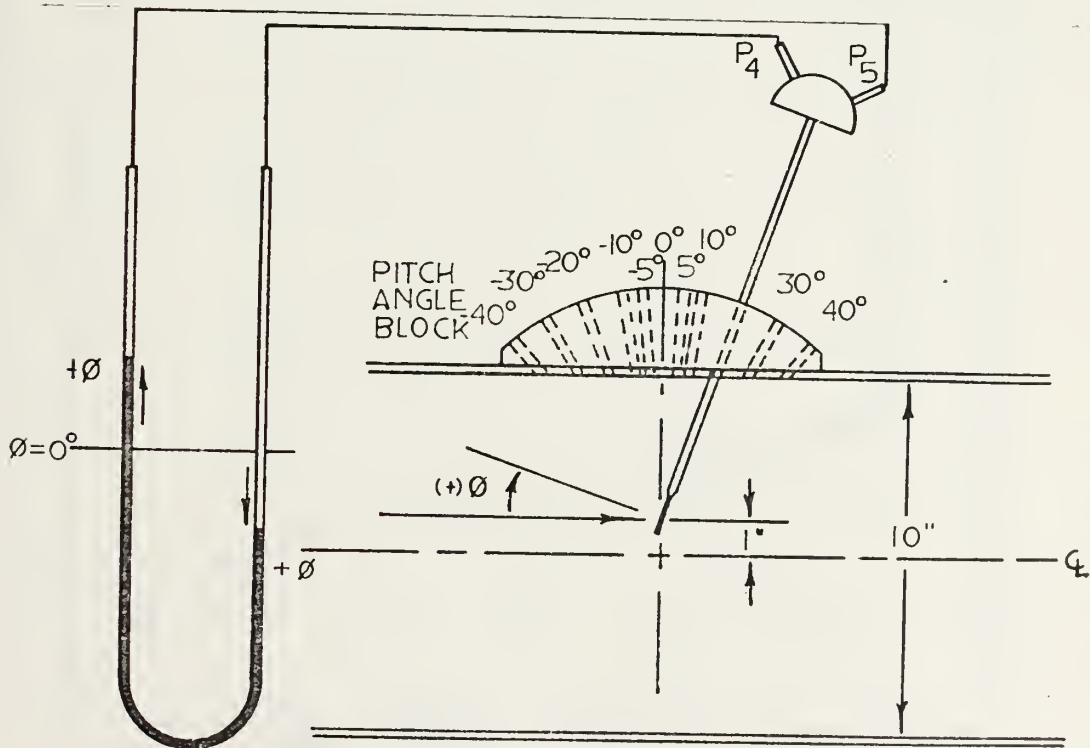
FIGURE A4.   PITCH ANGLE BLOCK
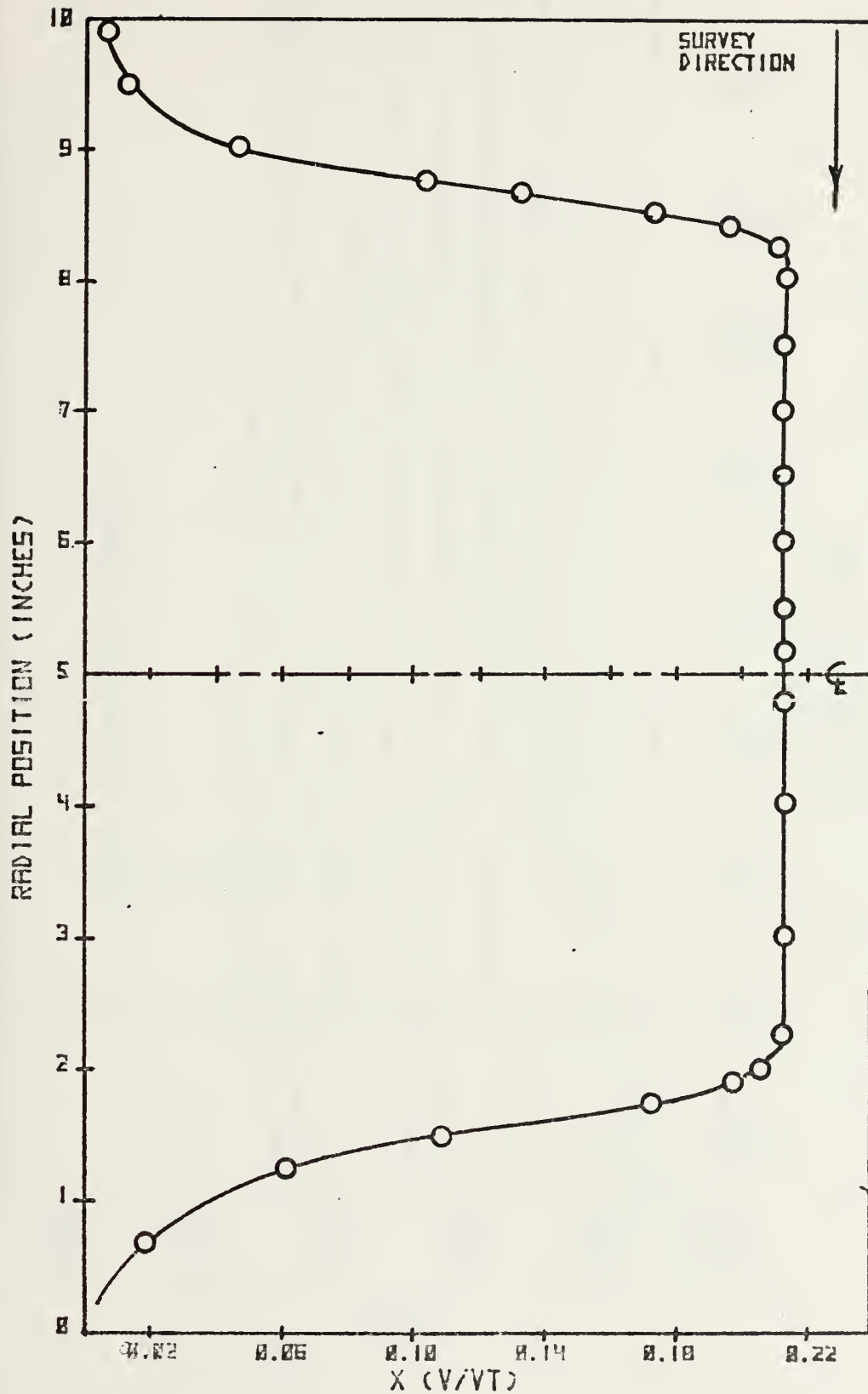
FIGURE A5. VELOCITY PROFILE IN THE
MEASUREMENT PLANE.

FIGURE A6. F'(THETA) VS. PHI DATA POINTS AND POLYNOMIAL CURVE FITS.

79
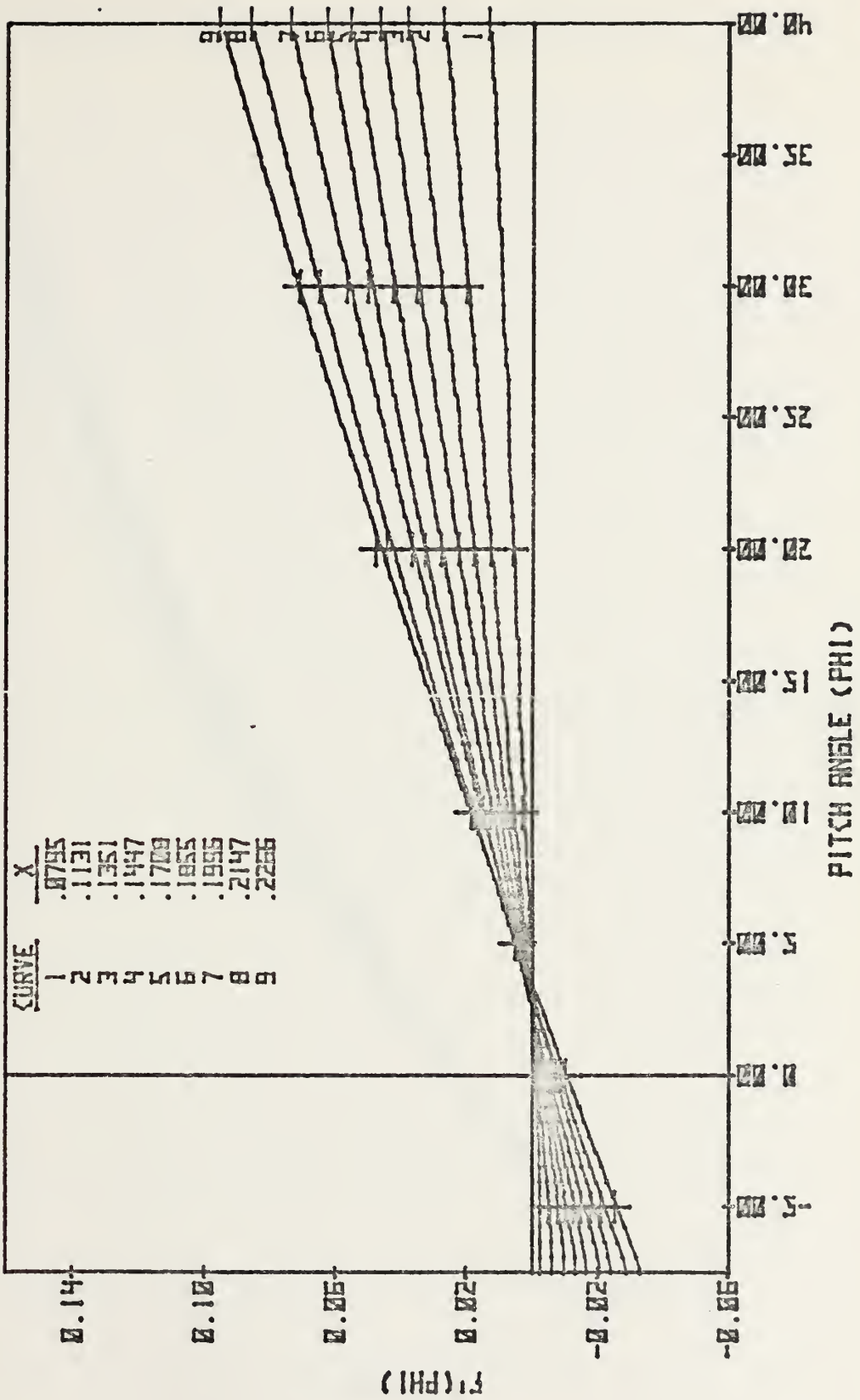
FIGURE A7. F'(PHI) VS. PHI DATA POINTS AND POLYNOMIAL CURVE FITS.

80
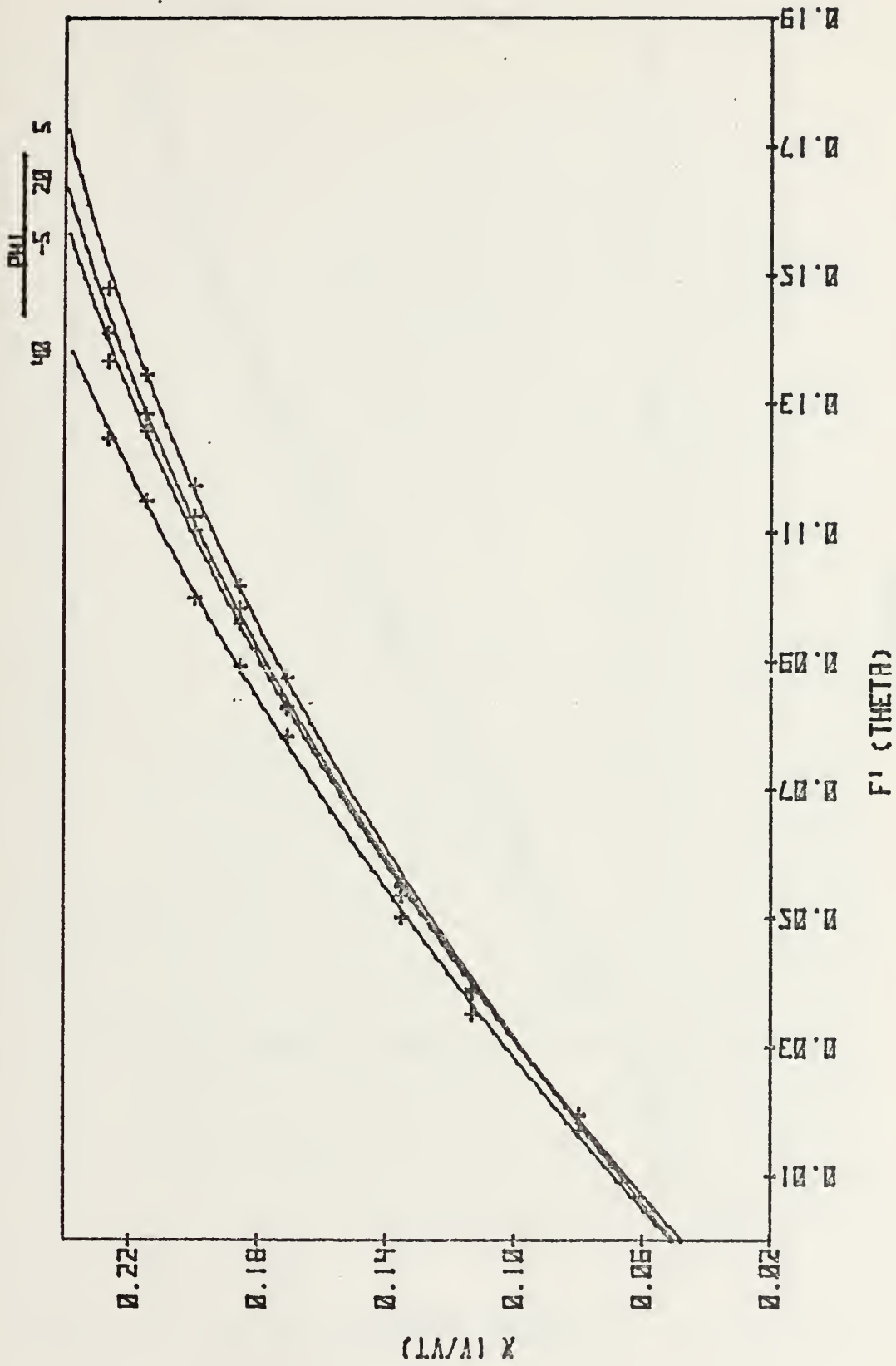
FIGURE A8. X VS F'(THETA) DATA POINTS AND POLYNOMIAL CURVE FITS.

81
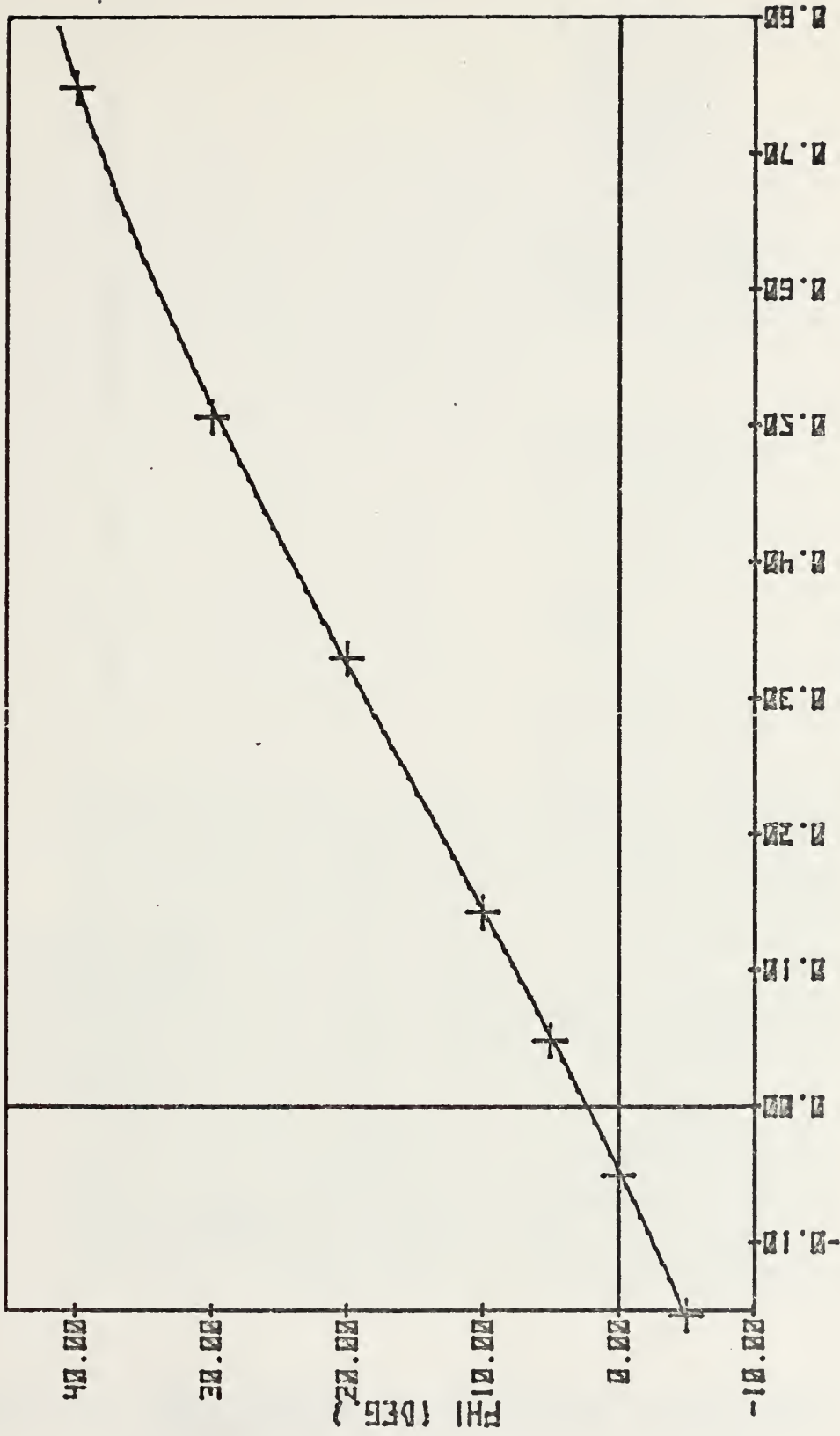
FIGURE A9. PHI VS. AVERAGE F'(LAMBDA) AND POLYNOMIAL CURVE FITS.
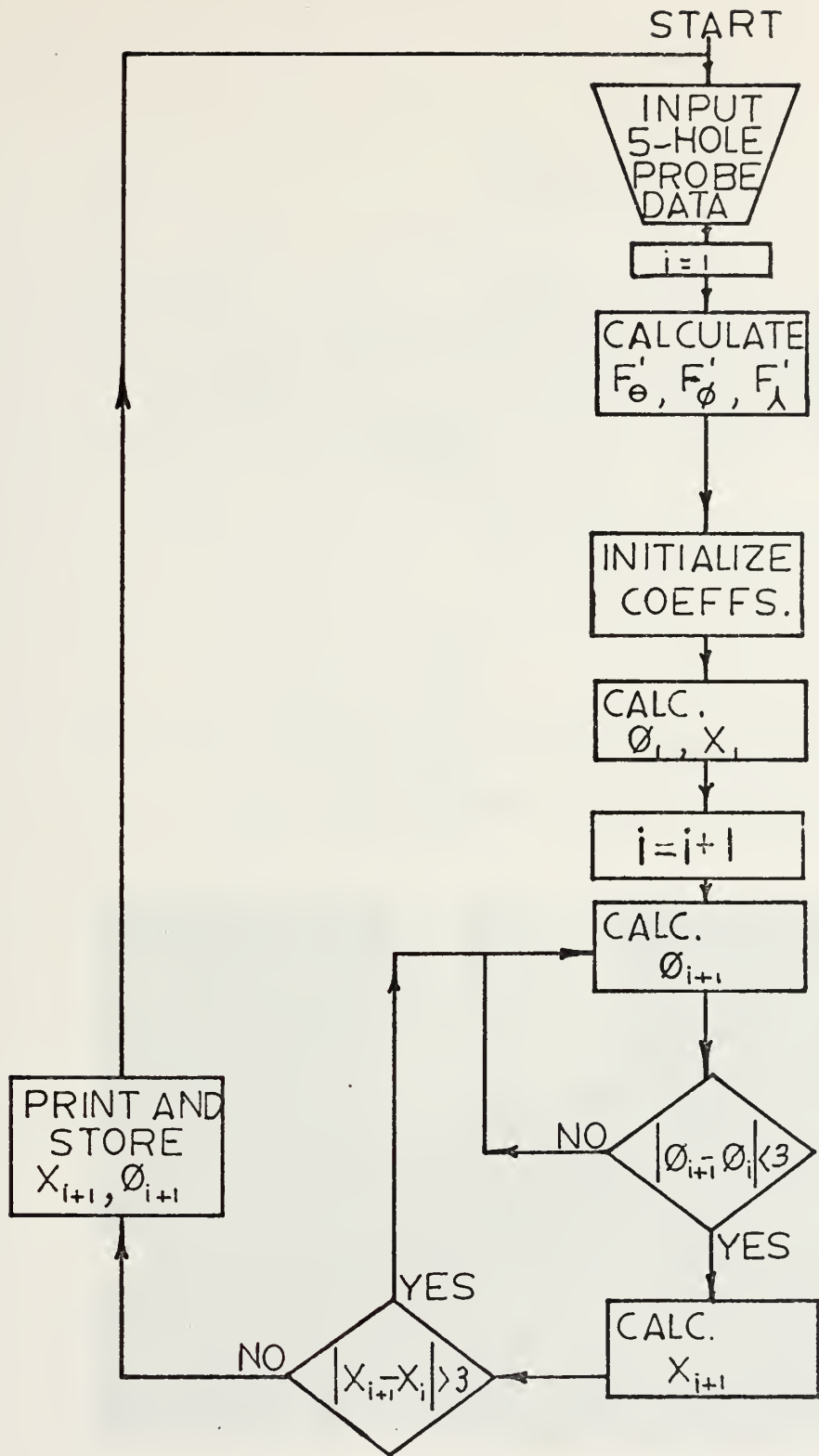
FIGURE A10. FLOW CHART FOR THE REDUCTION OF 5-HOLE PROBE
MEASUREMENTS TO VELOCITY AND PITCH ANGLE.
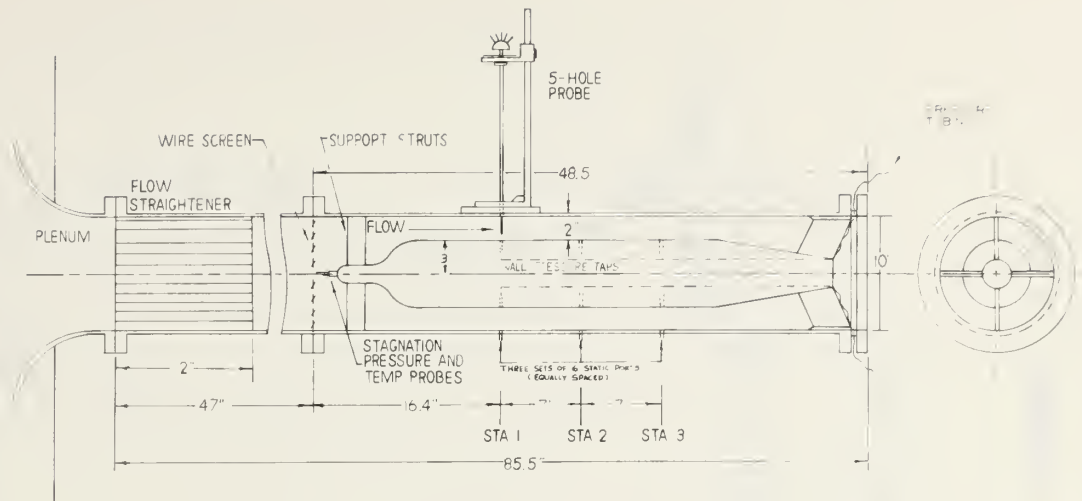
FIGURE A11.   SCHEMATIC OF THE APPARATUS FOR PROBE

CALIBRATION IN AN ANNULUS
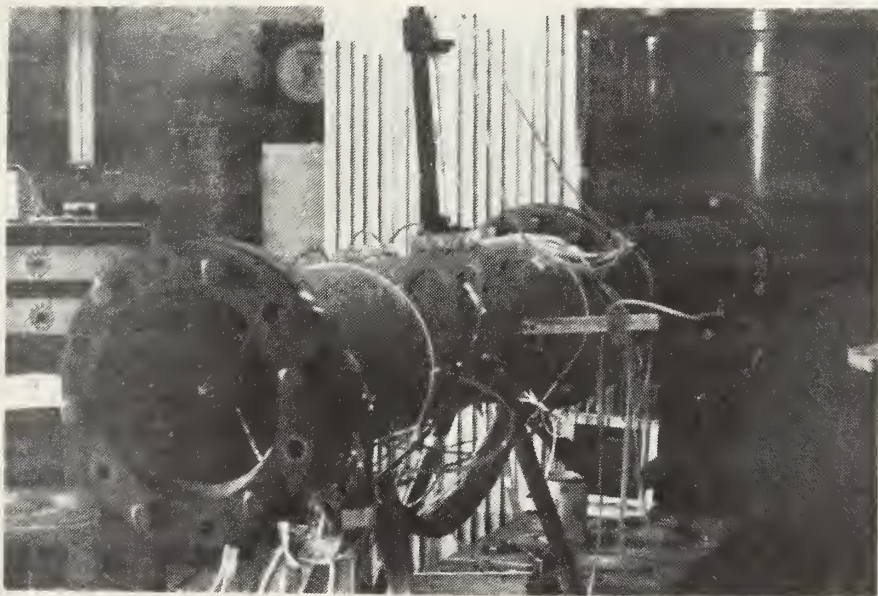
FIGURE A12.   VIEW OF THE CALIBRATION APPARATUS

84
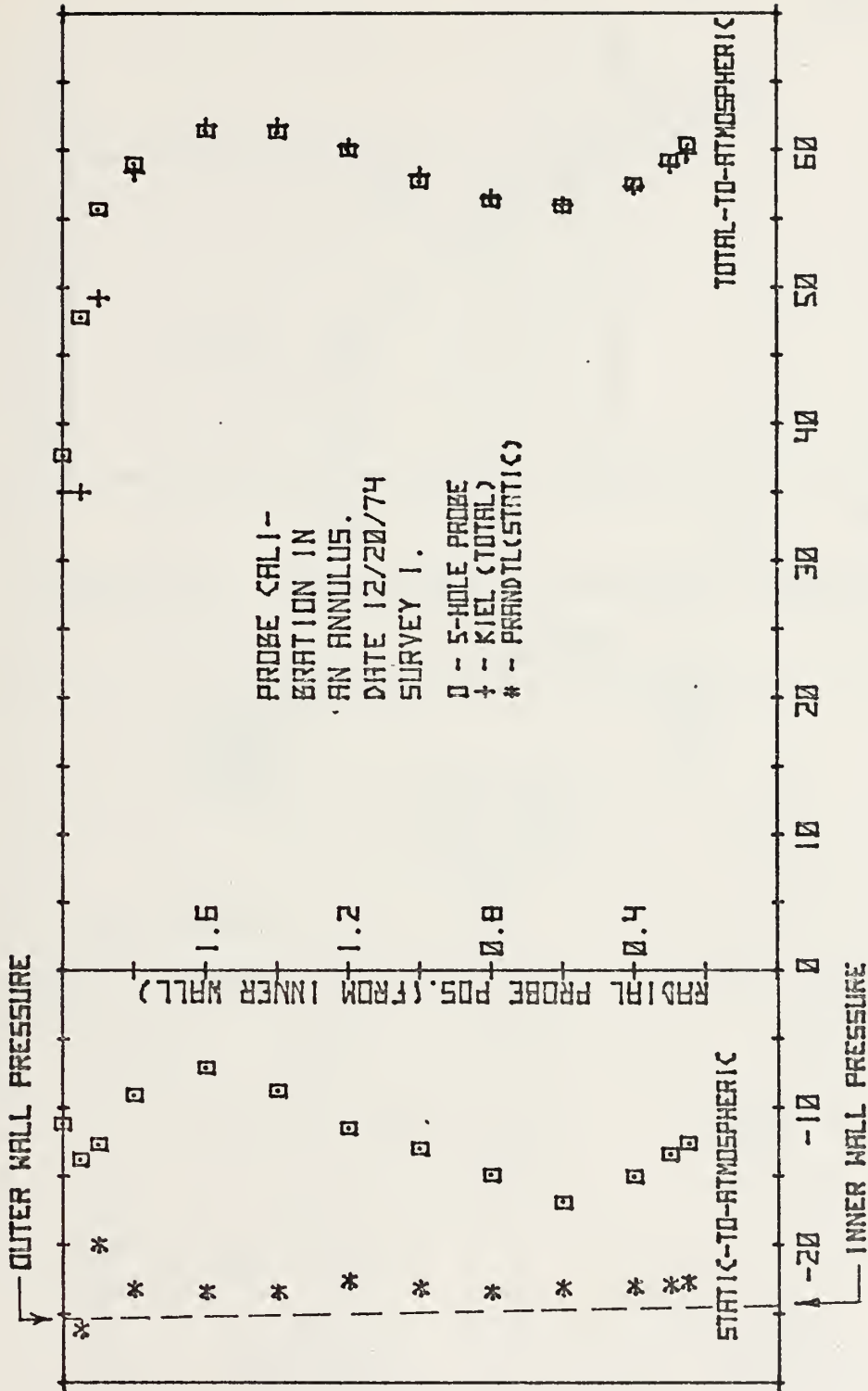
FIGURE A13. RADIAL DISTRIBUTION OF PRESSURE MEASURED IN THE
ANNULUS WITH DIFFERENT PROBES.
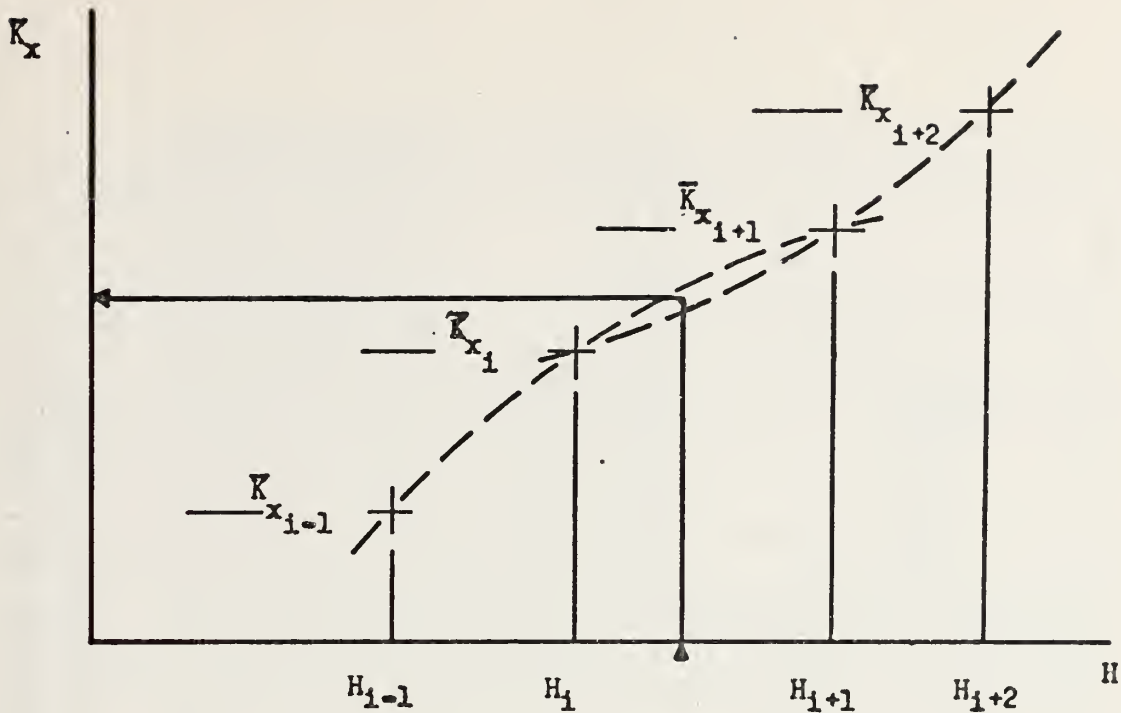
FIGURE A14. ILLUSTRATION OF QUADRATIC INTERPOLATION

METHOD
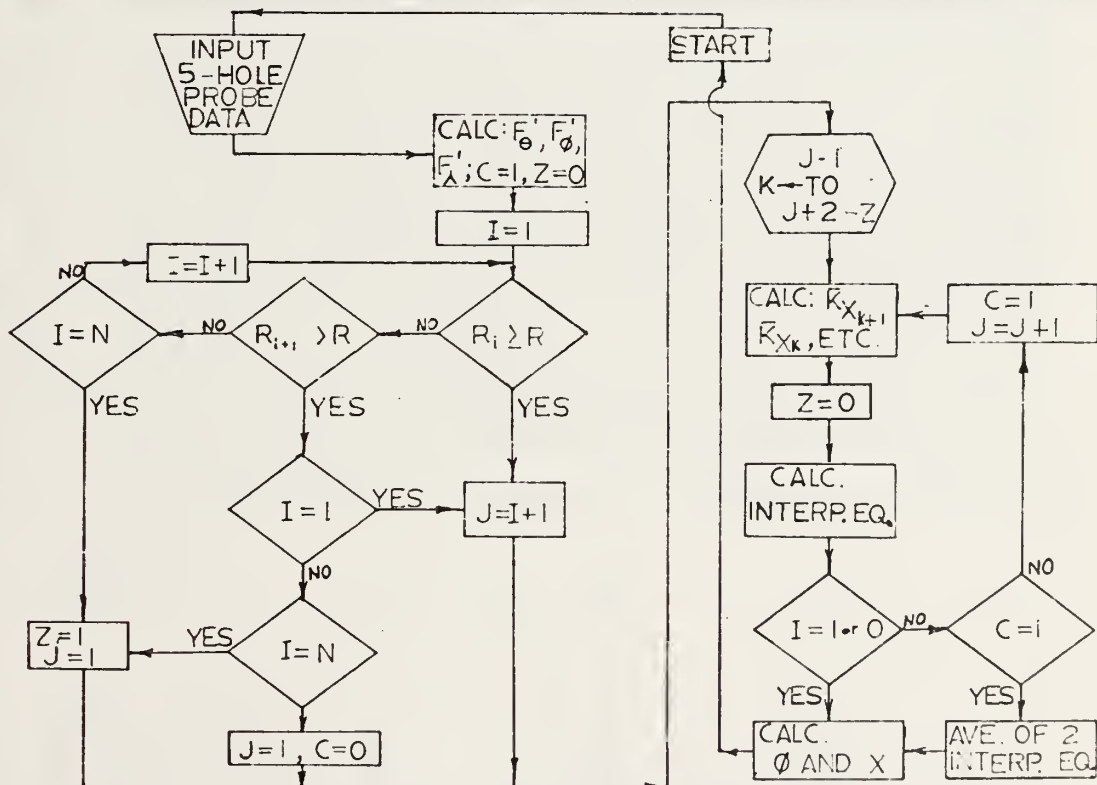
FIGURE A15. FLOW CHART TO CORRECT PROBE CALIBRATION

FOR MEASUREMENTS IN AN ANNULUS

TABLE A1. RESULTS OF PROEE CALIBRATION IN A JET.

U-TUBE WATER MANOMETER COLUMN HEIGHT IN INCHES

SURV. NO.	BAROM. (IN. Hg.)	T (°F)	∅	p_A	p_1	$p_{2/3}$	p_1	p_4	p_5	p	p_t	p_t	p_A
1	29.86	102	-5	44.20	39.45	44.30	36.30	43.30	42.20	47.15	38.30	39.60	44.70
			0	44.20	39.45	44.25	36.30	42.90	42.6	47.15	38.30	39.60	44.65
			5	44.20	39.45	44.25	36.30	42.55	43.00	47.15	38.30	39.60	44.65
			10	44.20	39.45	44.25	36.30	42.20	43.30	47.15	38.30	39.60	44.65
			20	44.15	39.50	44.30	36.20	41.55	44.00	47.10	38.30	39.60	44.65
			30	44.20	39.45	44.30	36.20	40.75	44.80	47.15	38.30	39.60	44.65
			40	44.15	39.55	43.80	36.75	40.00	45.55	47.15	38.30	39.60	44.65
2	29.86	102	-5	47.00	36.90	48.15	32.15	43.80	41.70	52.00	33.70	36.90	47.40
			0	47.00	36.85	48.40	31.85	43.00	42.50	52.00	33.70	→	→
			5	46.95	36.90	48.25	32.00	42.20	43.30	52.00	33.70	→	→
			10	46.95	36.90	48.30	31.90	41.50	44.00	52.00	33.70	→	→
			20	46.90	36.95	48.20	32.05	40.10	45.40	52.00	33.70	→	→
			30	46.80	37.00	48.30	32.00	38.55	46.95	52.05	33.65	36.95	47.35
			40	47.00	37.05	47.50	32.85	37.10	48.50	56.00	29.80	34.70	49.70
3	29.86	102	-5	49.30	34.80	51.35	28.80	44.30	41.00	→	→	34.75	49.65
			0	49.20	34.85	51.75	28.30	43.20	42.20	→	→	→	→
			5	49.20	34.80	51.65	28.35	42.05	43.35	→	→	→	→
			10	49.25	34.75	51.75	28.30	41.00	44.45	→	→	→	→
			20	49.20	34.80	51.60	28.30	39.95	46.50	→	→	→	→
			30	49.15	34.85	51.65	28.50	36.90	48.60	→	→	→	→
			40	49.05	34.95	50.60	29.50	34.70	50.85	→	→	→	→
4	29.86	102	-5	51.45	32.75	54.40	25.60	44.80	40.50	→	→	32.60	51.90
			0	51.50	32.70	55.25	24.80	43.35	42.00	→	→	→	→
			5	51.50	32.70	55.05	24.95	41.90	43.50	→	→	→	→
			10	51.50	32.70	55.15	24.85	40.45	44.95	→	→	→	→
			20	51.40	32.80	54.60	25.40	37.90	47.50	59.90	26.00	→	→
			30	51.40	32.80	55.05	25.00	35.20	50.25	59.90	26.00	→	→
			40	51.30	32.90	53.80	26.35	32.90	52.80	60.00	25.90	→	→

TABLE A1.(CONT.)

SURV. NO.	BAROM. (IN. Hg.)	T (t₁)(°F)	φ	p_A	p_1	p_2/3	p_1	p_4	p_5	p	p_t	p_t	p_A
5	29.87	100	-5	53.90	30.60	57.70	22.10	45.30	39.90	64.00	21.90	30.30	54.25
			0	53.85	30.60	58.70	20.90	49.60	41.70	64.10	21.80	30.30	54.25
			5	53.80	30.65	58.60	21.00	41.70	43.60	64.10	21.80	30.35	54.30
			10	53.75	30.70	58.25	21.45	39.95	45.40	64.10	21.80	30.40	54.20
			20	53.70	30.75	57.70	22.05	36.75	48.70	64.00	22.00	30.50	54.10
			30	53.65	30.80	58.05	21.65	33.60	51.90			30.55	54.15
			40	53.60	30.80	56.70	23.10	30.85	54.85			30.50	54.20
6	29.87	100	-5	55.90	28.55	60.50	18.90	45.80	39.40	67.80	18.10	28.20	56.40
			0	55.95	28.50	61.80	17.50	43.80	41.50	67.90	18.00	→	→
			5	→	→	61.70	17.60	41.55	43.75	→	→	25.90	58.65
			10	55.85	28.60	61.60	17.75	39.40	45.90	68.00	17.85	25.90	58.65
			20	55.85	28.60	61.00	18.40	35.50	49.80	67.95	17.90	25.80	58.70
			30	55.90	28.55	61.10	18.25	31.85	53.70			25.80	58.70
			40		26.25	61.10	20.45	29.30	56.60			25.90	58.60
7	29.87	99	-5	58.15	26.25	59.15	15.40	46.50	38.65	72.00	13.95	23.25	61.25
			0	58.20	26.15	63.70	13.55	44.20	41.00	71.90	13.90	23.20	61.25
			5	58.10	26.10	65.20	13.70	41.80	43.60	72.00	13.90	23.25	61.30
			10	58.20	26.20	65.10	14.00	39.10	46.15	71.90	13.95	23.20	61.25
			20	57.95	26.20	64.85	14.90	34.60	50.70	71.90	14.00	23.25	61.30
			30	60.65	26.40	64.15	15.00	30.40	55.25			23.10	61.40
			40	60.70	23.50	64.05	17.80	26.70	59.15			23.25	61.25
8	29.87	99	-5	60.75	23.50	61.50	11.40	47.20	37.90	76.60	9.40	21.00	63.35
			0	60.80	23.50	67.40	9.40	44.50	40.65	76.60	9.40	20.85	63.45
			5	60.55	23.55	68.85	9.35	41.50	43.70	76.65	9.30	20.80	63.60
			10	60.65	23.70	68.95	9.90	38.65	46.60	76.70	9.30	21.00	63.45
			20	60.60	23.55	68.45	10.85	32.95	52.60	76.75	9.35	21.00	63.50
			30	62.80	23.85	67.70	10.65	28.45	57.30	76.80	9.10	21.05	63.40
			40	62.60	21.50	67.90	14.10	23.95	62.20	76.70	9.25	21.05	63.35
9	29.87	100	-5	62.75	21.30	64.95	8.50	48.20	36.90	81.10	6.00		
			0	62.80	21.05	69.60	6.55	44.85	40.25	81.15	5.95		
			5	62.80	21.45	71.55	6.15	41.65	43.55	81.50	5.75		
			10	62.80	21.40	72.40	6.50	38.45	46.80	81.20	6.10		
			20	62.50	21.45	71.65	7.45	32.00	53.40	81.35	6.00		
			30		21.65	70.55	8.00	27.00	58.80	81.35	5.90		
			40			67.05	11.40	21.65	64.45	81.15	6.10		

UNITED SENSOR 5-HOLE PROBE DA-125(847-2)   BAROMETER (p_A): 30.17 IN.Hg.

SURV NO.	PRESS. DIFF. (IN.H_2O)	0.25	0.30	0.40	0.60	0.80	1.00	1.20	1.40	1.60	1.80	1.90	1.95	2.00
						DISTANCE FROM HUB (INCHES)								
1	p_1-p_A	60.4	59.2	57.5	55.9	56.3	57.7	60.0	61.3	61.4	59.0	55.7	47.8	37.7
	$p_{23}-p_A$	-12.6	-13.4	-15.0	-16.9	-14.9	-13.0	-11.5	-8.8	-7.1	-9.1	-12.7	-13.8	-11.2
	p_4-p_5	-3.6	-4.4	-5.5	-7.0	-7.2	-7.2	-6.9	-6.0	-4.1	0.4	4.7	9.2	17.9
2	p_1-p_A	52.7	51.8	50.6	49.8	50.0	51.5	53.1	53.6	53.3	51.1	49.1	42.3	33.3
	$p_{23}-p_A$	-10.7	-11.6	-13.8	-14.7	-12.9	-11.2	-9.8	-7.7	-6.1	-8.4	-10.6	-12.0	-10.0
	p_4-p_5	-2.5	-3.3	-4.5	-5.9	-6.0	-5.9	-5.5	-4.7	-3.0	1.0	3.8	7.2	14.7
3	p_1-p_A	46.2	45.7	44.5	44.0	44.4	45.8	47.0	47.4	47.1	44.8	41.5	36.5	28.7
	$p_{23}-p_A$	-9.5	-10.4	-12.7	-13.4	-11.6	-10.0	-8.9	-6.8	-5.5	-7.7	-10.0	-10.9	-9.1
	p_4-p_5	-2.0	-2.6	-3.9	-5.0	-5.1	-5.0	-4.7	-3.9	-2.4	-1.1	3.5	6.2	12.5
4	p_1-p_A	40.4	39.6	38.6	38.0	38.3	39.5	40.8	41.5	41.4	39.3	36.5	31.6	24.2
	$p_{23}-p_A$	-8.5	-9.1	-11.9	-11.9	-10.5	-9.1	-8.1	-6.3	-4.9	-6.6	-9.2	-9.5	-7.6
	p_4-p_5	-1.6	-2.2	-3.5	-4.2	-4.4	-4.2	-4.0	-3.4	-2.1	0.8	3.0	5.5	11.7
5	p_1-p_A	34.5	34.0	33.1	32.1	31.9	32.8	34.0	34.7	34.4	33.0	30.4	26.5	19.3
	$p_{23}-p_A$	-7.3	-7.7	-10.2	-10.1	-9.1	-7.9	-7.0	-5.4	-4.2	-5.2	-7.4	-7.8	-6.3
	p_4-p_5	-1.3	-1.9	-2.8	-3.3	-3.7	-3.5	-3.3	-2.7	-1.8	0.3	2.6	4.7	10.2
6	p_1-p_A	28.4	28.0	27.3	26.6	26.5	27.3	28.2	28.7	28.4	27.1	25.1	21.2	15.9
	$p_{23}-p_A$	-6.0	-6.7	-8.6	-8.4	-7.8	-6.7	-5.9	-4.7	-3.6	-4.4	-5.8	-6.4	-5.2
	p_4-p_5	-1.2	-1.6	-2.3	-2.7	-2.9	-2.8	-2.6	-2.2	-1.3	0.5	2.0	3.8	7.9
7	p_1-p_A	22.3	22.0	21.4	20.9	20.9	21.4	22.1	22.5	22.2	20.2	19.5	16.5	12.2
	$p_{23}-p_A$	-4.8	-5.3	-6.7	-6.5	-6.1	-5.3	-4.6	-3.7	-2.8	-3.7	-4.7	-5.0	-4.2
	p_4-p_5	-0.8	-1.2	-1.8	-2.1	-2.2	-2.1	-2.1	-1.7	-0.9	0.6	1.6	3.1	6.2

TABLE A2. (CONT.)

KIEL PROBE

BAROMETER (p_A): 30.17 IN.Hg.

DISTANCE FROM HUB (INCHES)

SURV NO.	PRESS. DIFF. (IN.H_2O)	0.25	0.30	0.40	0.60	0.80	1.00	1.20	1.40	1.60	1.80	1.90	1.95	2.00
1	p_t-p_A	59.8	58.9	57.3	56.0	56.5	58.2	60.3	61.8	61.8	58.4	49.2	35.0	—
	p_t-p	83.9	83.0	81.5	80.3	80.9	82.7	84.8	86.4	86.5	83.2	74.1	59.9	
7	p_t-p_A	22.3	22.0	21.5	21.0	20.9	21.5	22.2	22.5	22.3	20.9	17.4	12.6	
	p_t-p	20.2	20.3	20.4	20.6	20.8	21.0	21.2	21.4	21.6	21.8	21.9	22.0	

p=wall pressure.

PITOT-STATIC PROBE

BAROMETER (p_A): 30.17 IN.Hg.

SURV NO.		0.25	0.30	0.40	0.60	0.80	1.00	1.20	1.40	1.60	1.80	1.90	1.95	2.00
1	p_s-p_A	-22.7	-22.9	-23.0	-23.1	-23.4	-32.1	-22.6	-23.4	-23.4	-23.2	-20.0	-26.2	—
7	p_s-p_A	-7.8	-7.5	-7.4	-7.4	-7.4	-7.3	-7.3	-7.4	-7.3	-7.3	-7.7	-8.5	—

p_s = probe static pressure.

TABLE A3. COEFFICIENTS FOR EQ. A(14)

ORDER OF COEFFICIENT	EQ. 14(a)			$f(\emptyset)$	EQ. 14(b)	
	$a(x)$	$b(x)$	$c(x)$		$g(\emptyset)$	$h(\emptyset)$
ZEROTH	-0.004046	-0.0001054	5.1653×10^{-6}	0.04995	1.7027	-3.5102
FIRST	0.073024	0.0010741	-4.1165×10^{-5}	1.7255×10^{-4}	-0.00644	0.001453
SECOND	-0.43267	0.055827	-1.0657×10^{-4}	-2.17×10^{-5}	5.328×10^{-4}	1.25×10^{-4}
THIRD	0	0	0	4.6×10^{-7}	-8.0×10^{-6}	0

EXAMPLE: $a(x) = -0.004046 + (0.073024) \cdot x - (0.43267) \cdot x^2$

TABLE A4. COEFFICIENTS IN EQ. A(16)

J	K	L	M
2.389	51.013	19.813	-27.708

TABLE A5. COEFFICIENTS FOR EQ. A(19)

R(IN.)	i	q_i	r_i	s_i	t_i	u_i	v_i
0.25	1	0.2665	-3.2028	9.3584	0	0	0
0.3	2	0.2334	-2.9667	8.8060			
0.4	3	0.4412	-5.7011	16.5125			
0.6	4	0.3419	-4.4082	12.4122			
0.8	5	0.2663	-3.5527	10.3881			
1.0	6	0.2577	-3.2609	9.5088			
1.2	7	0.2860	-3.4314	9.9040			
1.4	8	0.2565	-2.9199	8.6109			
1.6	9	0.2674	-2.7889	8.1486			
1.8	10	1.5690	-38.4439	361.1053	-1510.6201	2365.1646	
1.9	11	-5.3574	124.4065	-1060.0796	3932.2165	-5356.9732	
1.95	12	9.0701	-284.4704	3543.1654	-21818.4473	66267.8659	-79303.1550

TABLE A6.   COEFFICIENTS FOR EQ. A(22)

z_1	z_2	z_3	z_4	z_5	z_6	z_7
-0.0543	0.6963	-3.5519	10.2028	-16.5283	13.9093	-4.7455

TABLE A7.   RESULTS OF APPLYING ANALYTICAL CORRECTION TO
CALIBRATION MEASUREMENTS IN AN ANNULUS.

SURVEY # 3

R/RO	X(UNMOD)	X(ACTUAL)	X(MOD)	% ERROR
0.1250	0.2048	0.2053	0.2054	0.0619
0.1500	0.2059	0.2045	0.2050	0.2470
0.2000	0.2088	0.2027	0.2028	0.0562
0.3000	0.2099	0.2018	0.2025	0.2977
0.4000	0.2073	0.2023	0.2025	0.0954
0.5000	0.2066	0.2043	0.2045	0.1033
0.6000	0.2063	0.2060	0.2063	0.1350
0.7000	0.2027	0.2065	0.2065	0.0111
0.8000	0.1990	0.2059	0.2062	0.1355
0.9000	0.1981	0.2024	0.2024	0.1339
0.9500	0.1965	0.1974	0.1974	0.0122
0.9750	0.1893	0.1894	0.1895	0.0127

93

APPENDIX B: DETERMINATION OF BLOCKAGE
FACTOR FOR FLOW INTO THE ROTOR

B.1. INTRODUCTION

The analysis in Reference 1 established a blockage factor for the flow into the TRANSX compressor rotor which was used to correct inviscid mass flow calculations. The blockage factor at station 1 was defined as,

$$K_B = \frac{\dot{w}_m}{\dot{w}} = \frac{\text{measured flow rate}}{\text{inviscid flow rate}} \qquad B(1)$$

and K_B was shown to be related to the displacement thickness of the boundary layer. Preliminary measurements were made ahead of the TRANSX compressor rotor to determine the boundary layer thickness at the outer wall [Reference 1]. From the measurements, ignoring the hub wall boundary layer, and assuming that the inviscid flow field was described correctly, the result obtained was,

$$K_{B_1} = 0.989$$

Then the flow into the rotor was described by the inviscid flow calculation for a total flow rate ($\dot{w}$) which was related to the measured flow rate ($\dot{w}_m$) by the relation

$$\dot{w} = \dot{w}_m / K_{B_1} \ .$$

The purpose of the present study of the flow into the rotor was to measure the inviscid flow

field, as well as the boundary layer region, and to
relate the measurements to the analytical descrip-
tion. It was necessary therefore to change the defin-
ition of blockage factor, from that involving only
boundary layers, to obtain the desired relationship.
In the following sections, necessary parts of the
analysis given in Reference 1 are repeated, and the
method is given for relating the analytical distribu-
tion of mass flux and flow angle to the distributions
measured using the 5-hole probe.

B.2. ANALYTICAL BACKGROUND AND METHOD

Referring to Fig. B1, and assuming that stream-
lines are axisymmetric, continuity at station 1
gives

$$\dot{w} = \int_{r_i}^{r_o} \rho V \cos\lambda \cdot (2\pi r) \, dr \qquad \qquad B(2)$$

Non-dimensionalizing Eq. B(2),

$$\overline{W}_t = \frac{\dot{w}}{\rho_t V_t \pi r_o^2} = \int_{r_i^2}^{r_o^2} \frac{\rho V}{\rho_t V_t} \cos\lambda \, d(\frac{r}{r_o})^2 \qquad B(3)$$

The definition of the total flow function is given
in Reference 7 as

$$\overline{\Phi} = \frac{\rho V}{\rho_t V_t} = X(1-X^2)^{\frac{1}{\gamma-1}}, \text{ where}$$

$$X = V/V_t \text{ and } V_t = \sqrt{2c_p T_t} \, .$$

Writing $R = r/r_o$, Eq. B(3) taken between R_1 and R_2

95

becomes

$$\overline{W} = \int_{R_1^2}^{R_2^2} \Phi \cos\lambda \, d(R^2) \, .$$

Introducing the values of the flow function and flow angle at the outer wall, indicated by a "o" subscript, the above equation becomes

$$\overline{W} = \Phi \cos\lambda_o \int_{R_1^2}^{R_2^2} \frac{\Phi}{\Phi_o} \frac{\cos\lambda}{\cos\lambda_o} \, d(R^2)$$

In the TRANSX compressor $\lambda_o = 0$, therefore

$$\overline{W} = \Phi_o \int_{R_1^2}^{R_2^2} \left(\frac{\Phi}{\Phi_o}\right) \cos\lambda \, d(R^2) \qquad\qquad \text{B(4)}$$

The assumption is then made, in Reference 1, that the pattern of streamlines does not depend on the flow rate, that $\overline{\Phi} = \Phi/\Phi_o$ is a function of R only and $\cos\lambda$ is another function of R. Based upon functions derived from a computer solution of the compressible flow, for $R_1 = R_i$ and $R_2 = R_o$, it is shown that

$$\xi = \int_{R_i^2}^{R_o^2} \overline{\Phi} \cos\lambda \, d(R^2) = 0.70836 \qquad\qquad \text{B(4a)}$$

96

where, using Eq. B(4),

$$\overline{W}_t = \Phi_o \xi .$$ B(4b)

Therefore the "theoretical" flow rate is proportional
to the value of the analytical flow function at the
outer wall.

In order to relate the analytical description of
the flow to the measured distributions of the flow
function and angle, the "theoretical" mass flux was
integrated and set equal to the integral of the
measured distribution of the mass flux over that re-
gion of the flow where the measurements were valid.
The probe measurements were considered to be free of
"immersion" or "wall" effects from 20% to 80% of the
hub-to-tip survey. Therefore, using Eq. B(4)

$$\int_{R_1^2}^{R_2^2} \Phi_m \cos\lambda_m d(R^2) = \Phi_o \int_{R_1^2}^{R_2^2} \overline{\Phi} \cos\lambda \, d(R^2)$$ B(5)

defines a value of the analytical flow function at the
outer wall which corresponds to the measured flow
conditions. Equation B(4b) then gave the "theoreti-
cal" flow rate corresponding to the measured flow rate,
and Eq. B(1) was again used to evaluate a blockage
factor.

B.3. PROCEDURE

The analytical distribution of the total flow
function [Ref. 1] is represented as

$$(1-R^2) = a_1(1-\bar{\Phi})^{n_1} + m_1(1-\bar{\Phi}), \qquad B(6)$$

where a_1, n_1, m_1 are coefficients, listed in Table B1,
which were evaluated in Reference 1 from a computer
solution using a curve fitting technique. $\bar{\Phi}$ is un-
known for a given R and must be determined as follows:

1) Choose an initial value for $\bar{\Phi}$ which does
   not exceed unity. Take
   $\bar{\Phi}_1 = 1 - .03(1-R_1^2)^2$, R_1 given.

2) Set $Y = 1-\bar{\Phi}_i$, $i=1, 2,\ldots, n$

3) Calculate $R_i^2 = 1 - a_1 Y^{n_1} - m_1 Y$

4) Test for convergence of calculated R^2;
   ? $\left| R_1^2 - R_i^2 \right| < \mathcal{E}$, $\mathcal{E} =$ convergence limit.
   If yes, the solution is complete.
   If no, continue to step 5.

5) Calculate the slope

   $$d(R_i^2)/dy = -a_1 n_1 Y^{n_1-1} - m_1, \text{ and calculate}$$

   $$\bar{\Phi}_{i+1} = \bar{\Phi}_i - \left[\frac{R_1^2 - R_i^2}{d(R_i^2)/dy} \right]$$

6) Repeat steps (2) through (5) until conver-
   gence occurs.

Using this procedure the value of $\bar{\Phi}$ could be calculated

for each probe position R.

A quantity K_o was defined such that

$$K_o = \int_{R_1^2}^{R_2^2} \bar{\Phi} \cos\lambda \cdot d(R^2) \ . \qquad B(7)$$

K_o was determined for a given R_1 and R_2 using numer-
ical integration applied over unequal intervals.
R_1 was chosen to be the first point greater than 20%
of the distance from hub to tip and R_2 was chosen
to be the last point before 80% of the distance from
hub to tip.

The analytical distribution for the flow angle
(λ) used in Eq. B(4a) was evaluated in Reference 1
as

$$\cos\lambda = a_2 (1-R^2)^{n_2} + m_2 (1-R^2) \qquad B(8)$$

where the coefficients are given in Table B1.

Using Eq. B(5), Eq. B(4b) and Eq. B(3) with
the perfect gas equation of state in Eq. B(7),

$$K_o = \frac{\xi K_{B_1} \pi r_o^2 V_t}{\bar{w}_m R_G T_t} \int_{R_1^2}^{R_o^2} p_t \Phi_m \cos\lambda_m \ d(R^2) \qquad B(9)$$

p_t, λ_m and Φ_m are given from measurements at each
point in the probe survey and all other quantities in
Eq. B(9) are constant for the survey. Since slight
variations in the flow rate were noted during the sur-
vey, a correction was introduced. The measured flow

rate, $\dot{w}_m$, in Eq. B(9) was the average of data reduced from scans of fixed instrumentation taken before and after each survey. The value of $\dot{w}_m$ corresponded to a differential pressure, Δh_r, across a flow nozzle. Since the flow rate at any time was proportional to the square root of this differential pressure, Δh, the value of Δh was recorded at each survey point. Rearranging Eq. B(9), with the correction introduced into the integration, the blockage factor is given by

$$K_{B_1} = \frac{K_o \dot{w}_m R_G T_t}{\xi \pi r_o^2 V_t} \left[\frac{1}{\int_{R_1^2}^{R_2^2} \sqrt{\frac{\Delta h_r}{\Delta h}} \, p_t \bar{\Phi}_m \cos\lambda_m d(R^2)} \right] \quad B(10)$$

Eq. B(6), B(7) and B(10) were programmed to calculate the blockage factor for flow at the rotor inlet from probe survey measurements.

The correction for slight variations in the flow rate was also included in comparing the measured and analytical distributions of the mass flux (or flow function). The left hand side of Eq. B(5) is written, with the addition of the flow correction, as

$$K_m = \int_{R_1^2}^{R_2^2} \bar{\Phi}_m \sqrt{\frac{\Delta h_r}{\Delta h}} \cos\lambda_m \, d(R^2) \quad B(11)$$

so that with Eq. B(7), Eq. B(5) becomes

$$K_m = \bar{\Phi}_o K_o.$$

The analytical flow function, which was included
on plots of the measured flow function, was obtained
from

$$\overline{\Phi}(R) = \overline{\Phi}(R) \left(\frac{K_m}{K_o} \right) \qquad\qquad B(12)$$

where $\overline{\Phi}$ was obtained from Eq. B(6), K_m was obtained
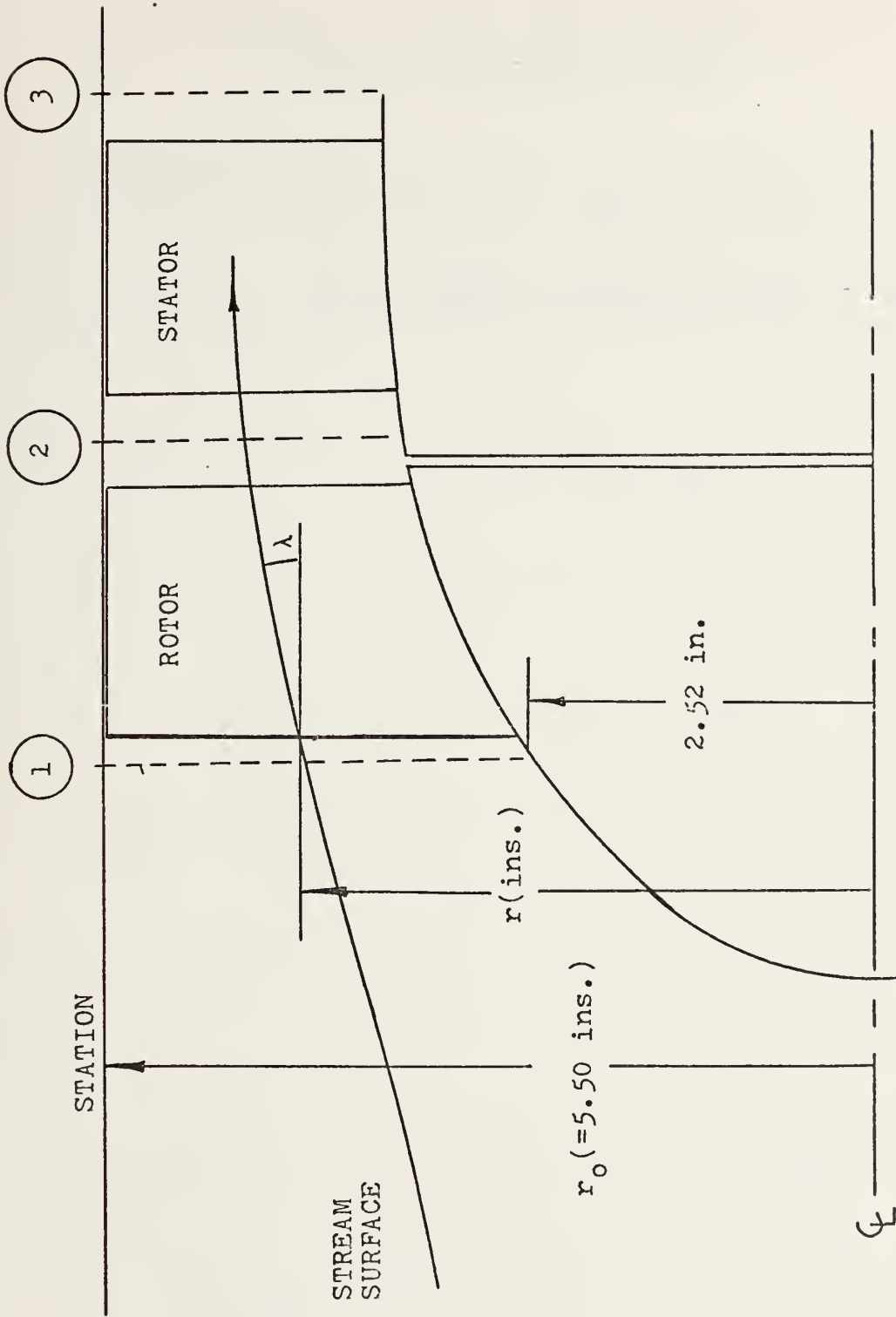from Eq. B(11) and K_o was already known from Eq. B(7).

FIGURE B1. SCHEMATIC OF COMPRESSOR GEOMETRY

102

TABLE Bl. CURVE FIT COEFFICIENTS
FOR EQ. B(6) AND EQ. B(8)

EQUATION	i	a_i	n_i	m_i
B(6)	1	1.79864	o.38582	22.3048
B(8)	2	0.98927	3.81679	0.47149

REFERENCES

1. Naval Post Graduate School Report NPS-57Sf4081, Flow Into A Transonic Compressor Rotor, Part-1 Analysis, by R.P. Shreeve, August 1974.

2. NASA Technical Note TN D-4816, A Small Combination Sensing Probe for Measurement of Temperature Pressure, and Flow Direction, by G.E. Glawe, L.M. Krause and T.J. Dudzinski, October 1968.

3. Naval Post Graduate School Report NPS-57Va72091A, A Description of the Turbopropulsion Laboratory in the Aeronautics Department at the Naval Post Graduate School, by M.H. Vavra and R.P. Shreeve, September 1972.

4. Naval Post Graduate School Report NPS-57Va73071A, Design Report of Hybrid Compressor and Associated Test Rig, by M.H. Vavra, July 1973.

5. Naval Post Graduate School Report NPS-57Sf73112A, Report on the Testing of A Hybrid (Radial-to-Axial) Compressor, by R.P. Shreeve, November 1973.

6. U.S. Army Aviation Material Laboratories Technical Report 67-30, Element Design and Development of Small Centrifugal Compressor, Volume II, by A.D. Welliver and J. Acurio, August 1967.

7. Naval Post Graduate School Report NPS-57Sf73071A, Calibration of Flow Nozzles Using Traversing Pitot-Static Probes, by R.P. Shreeve, July 1973.

8. United Sensor Corporation, Bulletin 5 "Directional Probes 3-Dimensional". United Sensor and Control Corp., Watertown, Massachusetts.

9. Conte, S.D. and deBoor, C., Elementary Numerical Analysis: An Algorithmic Approach, McGraw Hill (p. 44-49).

10. Shreeve, R.P., "Program to Calculate Non-Uniform Cylindrical Flow in a Compressor Annulus", Memo GA-RPS 7406-1, 20 June 1974 (Unpublished).

INITIAL DISTRIBUTION LIST

No. Copies

1. Defense Documentation Center   2
   Cameron Station
   Alexandria, Virginia 22314

2. Library, Code 0212   2
   Naval Postgraduate School
   Monterey, California 93940

3. Chairman, Department of Aeronautics   1
   Naval Postgraduate School
   Monterey, California 93940

4. Associate Professor R.P. Shreeve, Code 57Sf   1
   Department of Aeronautics
   Naval Postgraduate School
   Monterey, California 93940

5. Distinguished Professor M. H. Vavra, Code 57Va   1
   Department of Aeronautics
   Naval Postgraduate School
   Monterey, California 93940

6. Mr. J. E. Hammer, Code 57   1
   Department of Aeronautics
   Naval Postgraduate School
   Monterey, California 93940

7. Dr. H. J. Mueller   1
   Research Administrator, Code 310A
   Naval air Systems Command
   Navy Department
   Washington, D. C. 20360

8. Turbo-Propulsion Laboratory   10
   Naval Postgraduate School
   Monterey, California 93940

9. LT. D. J. Anderson, USN   1
   HC-6, NAS
   Norfolk, Virginia 23541